The *Swift* Gamma-Ray Burst Mission: First Results

Neil Gehrels[1], on behalf of the Swift Team

[1]*NASA/Goddard Space Flight Center, Code 661, Greenbelt, Maryland, 20771, USA*

ABSTRACT

The Swift mission is designed to discover 100 new gamma-ray bursts (GRBs) each year, and immediately (within tens of seconds) start simultaneous X-ray, optical and ultraviolet observations of the GRB afterglow. Since its launch on 20 November 2004, it has already collected an impressive database of bursts (reaching more sensitive limits than BATSE); uniform X-ray/UV/optical monitoring of afterglows; and rapid follow up by other observatories (utilizing a continuous ground link with burst alerts and data posted immediately to the GCN).

1. INTRODUCTION

Despite impressive advances over the roughly three decades since GRBs were first discovered (Klebesadel et al. 1973), study of bursts remains highly dependent on the capabilities of the observatories which carried out the measurements. The era of the Compton Gamma Ray Observatory (CGRO) led to the discovery of 2609 bursts in just 8.5 years. Analysis of these data led to the conclusion that GRBs are isotropic on the sky and occur at a frequency of roughly one per day (Briggs 1996).

The *BeppoSAX* mission made the critical discovery of X-ray afterglows (Costa et al. 1997). With the accompanying discoveries by ground-based telescopes of optical (van Paradijs et al. 1997) and radio (Frail et al. 1997) afterglows, GRBs could start to be studied within the astrophysical context of identifiable objects in a range of wavelength regimes. Successful prediction of the light curves of these afterglows across the electromagnetic spectrum has given confidence that GRBs are the signal from extremely powerful explosions at cosmological distances, which have been produced by extremely relativistic expansion (Wijers, Rees & Mesaros 1997).

The Swift mission selected by NASA in 1999 combines the sensitivity to discover new GRBs with the ability to point high sensitivity X-ray and optical telescopes at the location of the new GRB as soon as possible. From this capability Swift has the goal to answer the following questions:

1. What causes GRBs?

2. What physics can be learned about black hole formation and ultra-relativistic out- flows?

3. What is the nature of subclasses of GRBs?

4. What can GRBs tell us about the early Universe?

After five years of development Swift was launched form Kennedy Space Center on 20 November 2004. The spacecraft and instruments were carefully brought into operational status over an eight-week period, followed by a period of calibration and operation verification, which ended with the start of normal operations on 5 April 2004. A complete description of the Swift mission can be found in Gehrels et al. (2004).

As of 28 September 2005, the Swift achievements include: discovery of 77 new GRBs by the Swift BAT instrument (with a typical error region of less than 2 arcmin radius); discovery of 60 X-ray afterglows by the Swift XRT instrument (with a typical error region of less than 3 arcsec radius); and observations of 14 afterglows by the Swift UVOT instrument. More than half of the afterglow observations start within two minutes of the BAT GRB trigger (with a record of only 54 seconds!); and afterglow observations have been made of non-Swift discovered bursts within hours (with a record of 40 minutes for the GRB050408, discovered by HETE-II).

2. SWIFT HIGHLIGHTS

2.1 BAT Detected GRBs

The Burst Alert Telescope (BAT) on Swift has detected 77 GRBs since it was turned on in December 2004 to 28 September 2005. Thus in 285 days of operation, the BAT has discovered GRBs at a rate of about 98 bursts per year. This value is quite close to the rate of 100 bursts estimated prior to launch. These bursts include short bursts and x-ray flashes.

Spectral analysis of the BAT bursts show them to be consistent with the population of GRBs seen by the Compton Gamma-Ray Observatory BATSE experiment, both in the ratio of the fluxes in the 25-50 keV and 50-100 keV energy bands, and in the comparison of flux ratios to T90 values.

2.2 XRT Detected GRBs

The X-Ray Telescope (XRT) has rapidly imaged the location determined by the BAT trigger for new GRBs. In the first 60 cases, all but 3 of the BAT GRB triggers resulted in detection of an X-ray counterpart for the BAT source. In 2 cases the XRT observations started while the BAT was still detecting hard X-ray prompt emission from the GRB.

In about half of the cases, Swift started observations in less than 300 seconds after the burst. When XRT arrives this quickly it is very common to see a fast X-ray decline within the first 300 seconds. Measurement of redshift for these burst afterglows is very important. With a redshift it is possible to convert the observed fluxes into luminosities. Fifteen of the Swift GRBs have redshift determinations.

In addition to the BAT detected events, Swift can also observe GRBs discovered by other satellites. Swift has discovered X-ray afterglow emission in 2 cases each for the HETE-II and INTEGRAL satellites. In a particularly impressive case, Swift was able to respond to the ground control commands and start observations of the GRB050408 within 40 minutes of the GRB.

2.3 UVOT Detected GRBs

The Ultra-Violet/Optical Telescope (UVOT) is co-aligned with the XRT and so observes the GRB afterglows just as promptly as the XRT. Despite these prompt observations the UVOT has detected far fewer UV/optical counterparts than the XRT.

Of the first 50 GRBs observed by the UVOT, only 14 had detected emissions. The UVOT has generated important upper limits for these early times, which are lower those for bursts studied by previous missions.

Speculation on the reasons for this reduction include the possibility that the Swift bursts are farther away (higher z) than previous bursts; that a substantial number of GRBs have intrinsic dust extinction which suppresses the optical/UV emission compared to the I and R bands typically reported for earlier afterglows; or the possibility that some afterglows come from high magnetic field regions in the outflow which suppresses the optical and UV emission. These possibilities are discussed in Roming et al. (2005).

Although not every GRB produces UV or optical flux which can be detected by the UVOT, several bursts have produced early time light curves, including GRB050318 (Still et al. 2005) and GRB050319 (Mason et al. 2005).

2.4 XRT Early Light Curve Behavior

Swift has opened up a new regime for GRB afterglow studies. Never before has it been possible to study the X-ray behavior on timescales of minutes after the GRB happens. Swift has frequently started observations within a few minutes of the detection of GRBs by the BAT (with a record of only 52 seconds).

Typical Swift Lightcurve

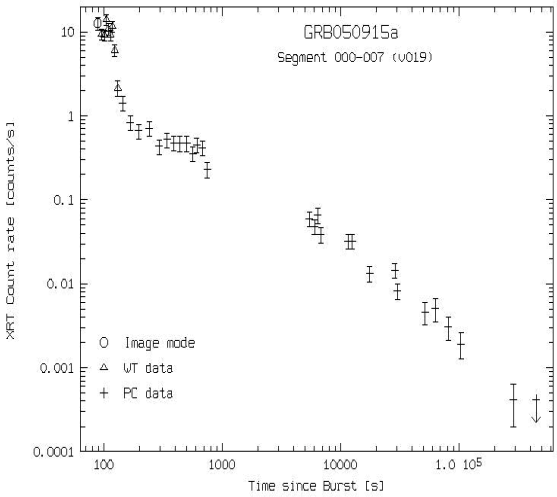

Fig. 1. Typical afterglow light curve.

These extremely prompt observations have given rise to a new phenomenology. In roughly 50% of the cases, the GRBs can be characterized by a three-part light curve (see Figure 1). First comes an extremely rapid decay of a very bright source. At these early times the decay can be fit by a power law of index in the range of 2.5 or greater. After a few minutes the decay rate flattens, and we can fit it with an index in the range of 1 (plus or minus perhaps 0.5). Finally after a delay ranging from hours to days, the decay rate will steepen again, resulting in a behavior interpreted as the jet break. Tagliaferri et al (20005) and Barthelmy et al. (2005a) each consider two early XRT afterglows. They show that the X-ray emission during the prompt phase (estimated from extrapolation of the BAT spectrum) connects the bright early XRT afterglow (see Figure 2). This suggests that the bright early afterglow is an extension of the prompt phase.

Swift also detects strong X-ray flares in afterglows at early times. In one case (GRB050502b) the X-ray flux increased by a factor of roughly 1000. The dramatic flaring events seem to be superposed on a background

which follows the multipart behavior mentioned above. Burrows et al. (2005) discuss the flaring behavior seen in GRB050502b and GRB050408.

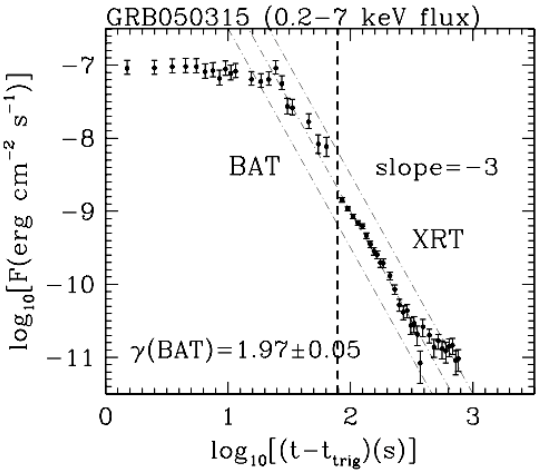

Fig. 2. From Barthelmy et al. (2005a). The BAT spectrum is extrapolated to the 0.2 – 7 keV band. The early XRT lightcurve connects smoothly to the prompt emission.

2.5 Short GRBs

As of late September 2005, the BAT has detected 4 GRBs in the short-hard class. One of them (GRB 050202 had no prompt slew and no counterparts. One (GRB 050813) had a prompt slew and XRT detection, but no identification of a counterpart or host galaxy. It did establish an important lower limit of z>0.7 for a host. From the remaining 2 events we have learned a lot. GRB 050509b (Gehrels et al. 2005) had an X-ray afterglow that gave an error circle with a bright elliptical galaxy (cD galaxy in a cluster) in it (Figure 3) GRB 050724 (Barthelmy et al. 2005b) had an XRT afterglow, plus Chandra, optical and radio detections. The sub-arcsecond positions located it once again in the outer regions of a bright elliptical. The fact that these ellipticals have very low star formation rates argues strongly against a collapsar origin like that for long bursts. Also, the redshifts for the two are in the z = 0.2 to 0.3 range, a factor of ~3 closer than typical long GRBs. The evidence to date is consistent with an origin of short burst in merging binary neutron stars.

2.6 GRB Redshifts

As of late September 2005, redshifts have been determined for 17 Swift GRBs. The average redshift (excluding short GRBs) is z=2.6. This is significantly higher than the pre-Swift average of z=1.2. The sensitivity of the Swift instruments is leading to a sampling of more distance GRBs.

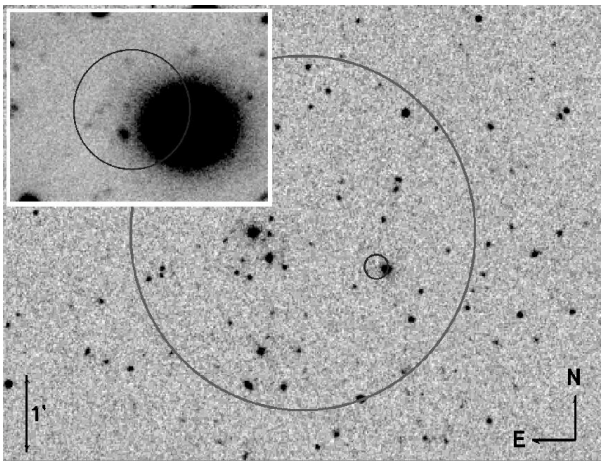

Fig. 3. Localization of short GRB 050509b. Large circle is BAT position; small circle is XRT position. The inset shows a bright elliptical galaxy in the XRT circle.

On September 4, 2005, Swift detected a long, smooth GRB (Cusumane et al. 2005). The redshift was found to be the very large value of z =6.29, one of the highest redshift objects ever seen. The light curve for this GRB is shown in Figure 4.

2.7 Giant Flare from SGR 1806-20

On 27 December 2004 the Solar System was struck by the brightest gamma-ray flux ever observed. Every orbiting gamma-ray observatory responded to the flash, produced by the soft gamma-ray repeater SGR 1806-20. Although Swift was not pointed toward the target, the flux was so high that the BAT detector was swamped by more than a billion gamma-rays passing through the structure of the spacecraft.

Palmer et al. (2005) present the Swift data on this dramatic event. Although the emitting system is located many kilo parsecs from the Earth, the received energy flux was brighter than the full Moon for the 0.2 seconds. This giant flare was more than 100 times more luminous than the two previous flares seen in 1998 from SGR1900+14 and in 1979 from SGR0526-66.

Such an event might be the cause of at least some short GRBs, in that the rapid, extremely bright flash of gamma-rays had a similar duration and energy profile to a short GRB. Had such an event been located in an external galaxy, it would have been detectable out to 40 Mpc.

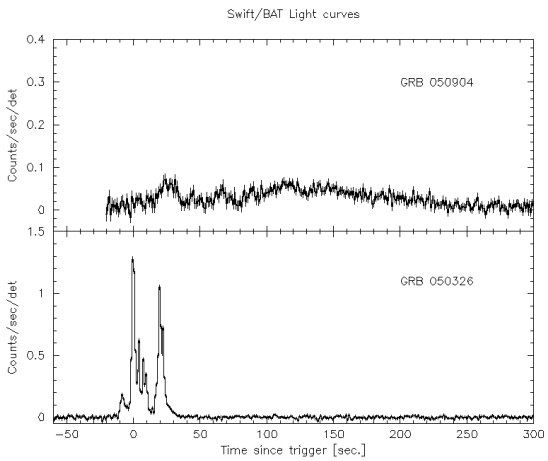

Fig. 4. Lightcurve of high-redshift GRB 050904 compared to a typical GRB. The long smooth nature of the lightcurve is due to cosmologic time dilation as the photons propagated to us from z=6.29.

2.8 UV/Optical & X-ray Observations of SN2005am

Type Ia supernovae are critically important to our understanding of the fundamental fabric of our Universe. They are the most fundamental step in our ability to measure the distances over the range in which cosmological effects become significant. Thus it is a critical astrophysical observation to study relatively nearby supernovae in the ultraviolet, because this is the wavelength regime, which becomes red-shifted into the observing windows of ground-based optical instruments.

Unfortunately nearby UV measurements require space-borne observatories with UV capability. Missions such as the *International Ultraviolet Explorer* (IUE) and the *Hubble Space Telescope* began these studies, but they were limited in the intrinsically slower operational response time than offered by Swift. Thus Swift has been an ideal observatory to start observations of nearby bright supernovae, of which SN2005am is a prime example.

Brown et al. (2005) provide ultraviolet and optical light curves for SN2005am, starting four days prior to maximum light, and extending to 69 days after peak. In addition, when the target was bright enough, Swift was able to carry out low-resolution grism UV/optical measurements. These data for SN2005am are the best sampled in time, and cover the widest range of any type Ia supernova follow-up to date.

3. CONCLUSIONS

The Swift observatory is performing excellent scientific observations at high efficiency and with important progress toward its mission objectives.

The BAT (Burst Alert Telescope) is working flawlessly, and has produced great data. The positional agreement to the XRT and ground-based detections suggests that the typical on-board positional accuracy for GRBs is roughly 65 arcsec, exceeding the pre-launch predictions.

The UVOT (UV/Optical Telescope) has demonstrated excellent UV and optical performance on GRBs and other sources.

The XRT (X-Ray Telescope) has demonstrated excellent X-ray sensitivity and rapid responsiveness. The average accuracy for the XRT positions confirmed with XMM or ground-based optical detection is 2.6 arcsec. XRT is observing afterglows at a level of 100 to 1000 times fainter than Beppo-SAX. This rapid acquisition with sensitive X-ray detection is discovering new lightcurve behaviors.

As Swift observations become more routine we expect to build up a substantial database of early (and late) X-ray and UV/optical light curves, and from these develop insights into GRB formation and GRB environments.

4. REFERENCES

Barthelmy, S., et al. 2005a, ApJ, in press.

Barthelmy, S., et al. 2005b, Nature, in press.

Briggs, M. S. 1996, ApJ, 459, 40.

Brown, P. J., et al. 2005, ApJ, in press.

Burrows, D. N., et al. 2005, Sci., in press.

Costa, E., et al. 1997, Nature, 387, 783.

Cusumano, G. et al. 2005, Nature, in press.

Frail, D. A., et al. 1997, Nature, 389, 261.

Gehrels, N., et al. 2004, ApJ, 661, 1005.

Gehrels, N., et al. 2005, Nature, 437, 851, 2005.

Klebesadel, R. W., Strong, I. B., & Olson, R. A. 1973, ApJ, 182, L85.

Mason, K., et al. 2005, ApJ, submitted.

Palmer, D., et al. 2005, Nature, 434, 1107.

Roming, P., et al. 2005, ApJ, submitted.

Still, M., et al. 2005, ApJ, accepted.
Tagliaferri, G., et al. 2005, Nature, 436, 985.
van Paradijs, J., et al. 1997, Nature, 386, 686.
Wijers, R. A. M. J., Rees, M. J., & Meszaros, P. 1997, MNRAS, 288, L51.

FIRST RESULTS FROM THE SWIFT UVOT

K. O. Mason[1], A. J. Blustin[2], and P. W. A. Roming[3]

[1]Particle Physics and Astronomy Research Council, Polaris House, North Star Ave, Swindon, Wilts SN2 1SZ, UK
[2]Mullard Space Science Laboratory, University College London, Holmbury St. Mary, Dorking, Surrey, RH5 6NT UK
[3]Department of Astronomy and Astrophysics, Pennsylvania State University, 525 Davey Laboratory, University Park, PA 16802, USA

ABSTRACT

We review some of the initial data from the UVOT telescope on the Swift observatory. Statistics based on about six months of data suggest a dark burst fraction of about 50% when combining both UVOT and ground-based observations. There is evidence that some bursts have a large gamma-ray efficiency, which may be due to strong magnetic fields in their ejecta. The bright GRB050525A shows behaviour broadly consistent with expectations from the simple fireball model for bursts, including evidence for a reverse shock component in the UVOT data, and an achromatic break in decay slope indicative of a jet break. Other bursts observed with Swift have a shallow decay initially which is difficult to reconcile with the simple model. Replenishment of the forward shock energy by continued ejection of material from the central engine, or initial injection of material with a range of velocities, offers a potential explanation. In the case of the XRF050406 an initially rising optical afterglow flux followed by a shallow decay may be due to observation of a structured jet from a significant off-axis angle.

Key words: gamma rays: bursts - shock waves - optical/UV - X-rays.

1. INTRODUCTION

The Swift observatory, launched in November 2004, is breaking new ground in the study of Gamma-ray Bursts (GRB). It is able to rapidly locate new bursts in its 1.4 sterradian field-of-view Burst Alert Telescope (BAT; Barthelmy et al. 2005) and slew to bring its narrow field X-ray Telescope (XRT; Burrows et al. 2005) and UV/Optical Telescope (UVOT; Roming et al. 2005a) to bear on that location in the sky within about 1 minute. At the same time, information on burst location and properties is immediately communicated to the ground where it is disseminated to observers world-wide via the Gamma-ray bursts Coordinates Network (GCN).

In this paper we review some early GRB results from Swift, highlighting the contribution made with data from the UVOT.

2. DETECTION STATISTICS

It is well known that not all GRB have detectable optical afterglows. However, the proportion of these so-called 'dark bursts' is debated, with estimates based on Beppo-Sax data suggesting that they comprise about 50% of the total burst population (e.g. De Pasquale et al. 2003) while HETE-II data suggest that less than 10% of bursts are optically dark (Lamb et al 2004). Possible explanations for dark bursts include a high redshift (Bromm & Loeb 2002; Fruchter 1999), absorption in a dense circumburst medium (Lazzati et al. 2002), intrinsic faintness (De Pasquale et al. 2003; Roming et al. 2005b) or a rapidly declining afterglow (Groot et al. 1998).

The Swift data offers the advantage of a sample of bursts that has been uniformly observed very soon after the initial trigger. Fig. 1 shows statistics on bursts observed by Swift using UVOT between 2005 Jan 24 (when UVOT was commissioned) and 2005 Sep 22. We distinguish between the (majority of) bursts that were observed within an hour of the trigger (and usually within a few minutes) and those that were not observed until more than 1 hour after the trigger. A delay in slewing to a new burst can occur, for example, because the burst occured in a region of the sky where pointing of the spacecraft is constrained. We divide the bursts into those that were detected with UVOT, those that were detected using ground-based telescopes only (which usually means that the burst was too red to be detected with UVOT, which has a long wavelength cut-off of about 650nm), and those that were not detected in the optical/IR by any means. These simple statistics suggest that the dark burst fraction among the Swift sample is 48% for the sample of 48 bursts that were observed using UVOT within one hour.

Fig. 2 shows the detection statistics for bursts as a func-

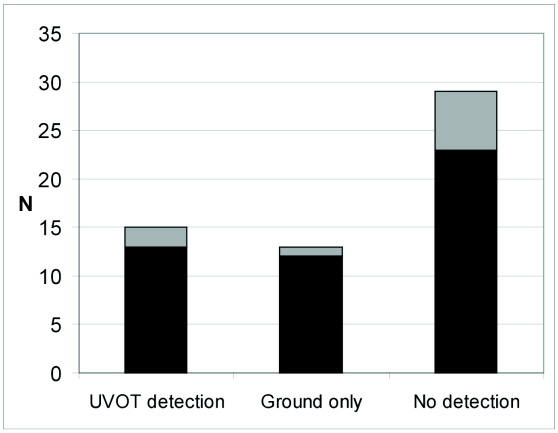

Figure 1. Detection statistics for Swift bursts between 24 Jan 2005 and 22 Sep 2005. Shown are the number of bursts detected with UVOT (column 1), detected with ground-based telescopes but not UVOT (column 2) and not detected in the optical/IR by any means (column 3). For each category, we distinguish the number of bursts that were observed with Swift within 1 hour of the BAT trigger (black area) from those that were not observed until greater than 1 hour after the trigger (grey area).

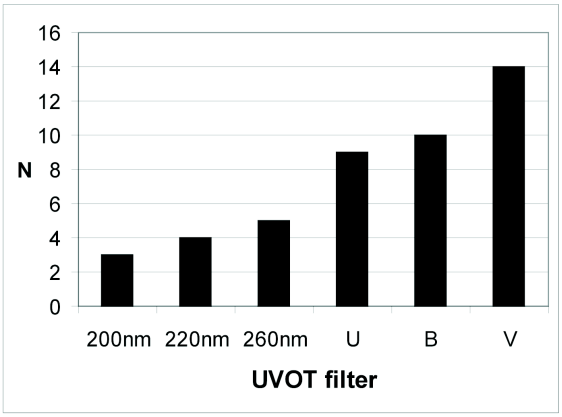

Figure 2. Detection statistics for UVOT-detected bursts between 24 Jan 2005 and 22 Sep 2005 as a function of UVOT filter.

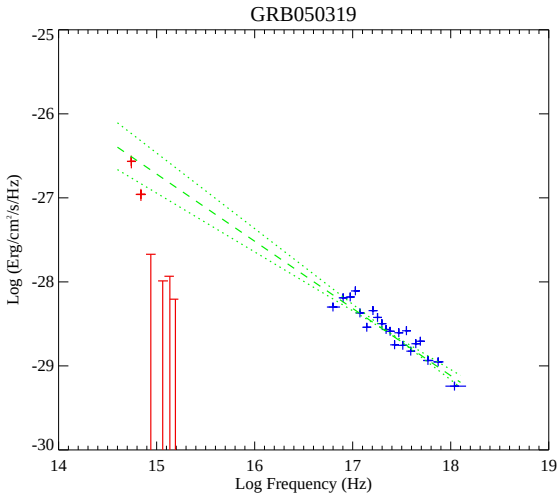

Figure 3. The multiwavelength spectrum of GRB050319 plotted as $F\nu$ vs log frequency in the observer frame, and averaged over the interval between 240s and 930s after the burst trigger. Measurements with the UVOT taken through its six broad-band filters, centered on 200nm, 220nm, 260nm, U, B abd V, are shown together with the spectral distribution inferred by fitting the count-rate as a function of energy recorded with the XRT. The best power law fit to the XRT data is illustrated as the dashed line. The 1σ bounds on the slope are indicated by the dotted lines. The XRT flux points have been corrected for Galactic absorption equivalent to $N_{\rm H} = 1.17 \times 10^{20}$ cm^{-2}.

tion of UVOT filter. Unsurprisingly, the highest rate of detection occurs in the reddest filter and the detection frequency declines monotonically towards the blue. This presumably reflects the distribution of dust reddening and/or redshift amongst the bursts. Reddening will occur due to dust, either in the rest frame of the burst or in our Galaxy, while the effects of rest-frame dust reddening and absorption due to the Lyman edge, or the Lyman forest, will be seen at progressively longer wavelengths as the redshift increases. An example is shown in Fig. 3, which shows the combined X-ray and UV/Optical spectrum of GRB050319 measured using Swift during a specific time interval (Mason et al. 2005). The V-band measurement taken with UVOT lies on an extension of the power-law that models the X-ray spectrum. However, the B-band detection, and the upper limits to the flux measured in the UVOT filters blueward of B, all lie substantially below the extrapolated power law. Interpreting this deficit as being due to the Lyman absorption edge redshifted into the UVOT band suggests a redshift for the burst of about 3.8. In fact, Fynbo et al. (2005) report an absorption line system in the source at a redshift of 3.24 which is probably the host galaxy. This is consistent with the Swift broad-band spectrum if there is also significant line opacity in the spectrum, due for example to the Lyman forest.

Roming et al. (2005b) have discussed the detectability of GRB in more detail. They consider the X-ray and op-

tical flux of GRB afterglows at a set time, 1 hour, after the burst, and compare these with the Gamma-ray fluence. The Gamma-ray fluence is a natural measure of the radiated energy of the GRB, while the X-ray flux is a proxy for the kinetic energy of the fireball's blast-wave. They find that there is a large spread in the ratio of Gamma-ray fluence to X-ray flux one hour after the burst. They highlight three bursts in particular, GRB050223, GRB050421, and GRB050422, which have a high Gamma-ray to X-ray ratio, none of which are detected in the optical band. This implies Gamma-ray efficiencies as high as 90%, which is difficult to account for in the standard fireball model. They suggest that the flows in these bursts may be highly magnetised, and that a large fraction of the energy in the ejecta is locked up in the magnetic field, at least in the early phases of the expansion.

3. THE BRIGHT BURST GRB050525A

GRB050525A was a relatively bright burst at a spectroscopic redshift of 0.61 that was followed by both the XRT and UVOT instruments from soon after the BAT trigger (Blustin et al. 2005). The data on the X-ray and optical afterglow decay are shown in Fig. 4. The data taken through the various UVOT filters are normalised together in this plot (there is no evidence of a colour dependent decay), while the relative normalisation of the X-ray data is arbitrary and chosen for display clarity.

The X-ray afterglow of GRB050525A decays initially with a power-law slope (α) of -1.2. After about 300s, the X-ray flux exhibits an excess with respect to this power-law, which persists until there is a gap in coverage due to Earth-occultation of the source. After the occultation gap the X-ray data again lie on the original power-law, suggesting that the excess flux was part of a relatively short-lived flare. There is a break in the power-law after about 10^4s to a new, steeper slope of -1.62.

The optical decay has a distinctly different form. It is initially steeper than the X-ray curve, before flattening to a shallower slope. Once again, after about 10^4s the slope steepens to a value that is consistent with the X-ray data in the same time interval. The optical decay before the 10^4s break can be represented by a combination of two power-laws. This fits naturally with the idea that there is an initial steep drop due to the fading of a reverse shock component, which is only seen in the optical band, combined with a flatter decay component from the forward shock. The behaviour of the source is clarified when one looks at the behaviour of the multiwavelength spectrum with time. This is shown in Fig. 5, which shows the X-ray and optical/UV spectrum of GRB050525A at three epochs in the decay, 250s, 800s and 25000s after the BAT trigger. A single power-law spectrum is consistent with both the X-ray and optical/UV data at 25000s after the burst, but not at the earlier epochs, where the optical/UV flux is suppressed relative to an extrapolation of the X-ray spectrum. The 'recovery' of the optical/UV emission relative to the X-ray flux in both the spectral and time domain suggests that we might be seeing the migration of the synchrotron cooling frequency through the optical/UV band. This migration is somewhat faster the prediction $\nu_c \propto t^{0.5}$ of the simple fireball model (e.g. Zhang & Mészáros 2004), possibly due again to the liberation of energy locked up in magnetic fields. The sense of the spectral evolution favours expansion into a constant density (interstellar) medium rather than the $1/r^2$ density dependance of a stellar wind.

The best-fit slope of the pre-break forward shock component is somewhat shallower than the $\alpha = -0.9$ expected from a simple fireball model. However the fitted value is sensitive to the exact form of the 'reverse shock' component. We also note that Klotz et al (2005) suggested that the optical decay suffered a 're-brightening' episode about 2000s after the burst, during the gap in UVOT coverage. If we include such a re-brightening in our model fits, the overall forward shock decay slope steepens to about $\alpha = -1$, though the quality of the fit is marginally worse. The fit parameters for the smooth ('best fit') and re-brightening ('step fit') models, together with the predictions of the fireball model are summarised in Table 1. The fitted slope of the reverse shock component is also sensitive to whether we include a re-brightening, and ranges between $\alpha = -1.5$ without re-brightening to $\alpha = -2.1$ with.

The steepening of both the X-ray and optical/UV decay slope after about 10^4s can be interpreted as a jet break. This is supported by the fact that the break is achromatic, i.e. the break occurs at the same time in both the X-ray and optical/UV range, and the post-break slope is consistent in the two bands. The best fit to a single broken power-law model yields a break time of about 14000s. However the post-break slope ($\alpha = -1.6$) is shallower than the $\alpha = -2.2$ predicted by simple fireball models. This could be due to the details of how the jet evolves, or the break might actually be more gradual than the simple model would suggest. In this case a slope of $\alpha = -2.2$ is reached at a later time. Such a model could be consistent with the data (but is not required) and yields an effective break time at about 50,000s-60,000s. A break at 14000s, combined with the measured isotropic-equivalent energy emitted in the burst, suggests a jet opening angle of about $3.2°$, assuming a uniform jet. The opening angle increases to about $5°$ if we adopt the later time implied by a gradual break.

In all, the properties of GRB050525A show good agreement with expectations based on the standard fireball model (Zhang & Mészáros 2004). There is evidence for a reverse shock component in the optical/UV decay curve, and for migration of the synchrotron cooling frequency through the optical/UV band. There is also evidence for a light curve 'jet' break, which is expected when the fireball Lorentz factor decreases to the point where the beaming angle of the emitted radiation exceeds the collimation angle of the jet (Rhoads 1999; Sari, Piran & Halpern 1999).

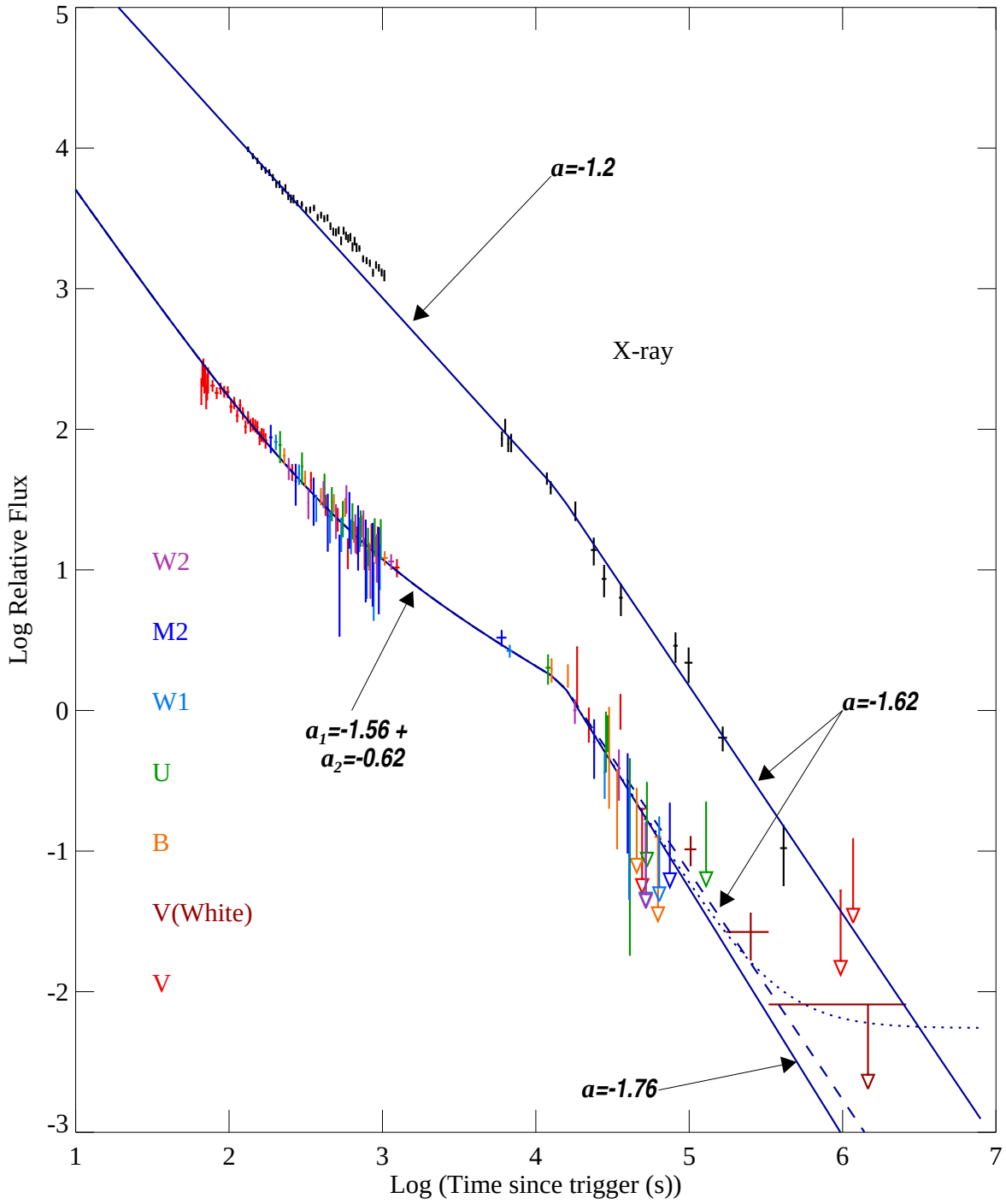

Figure 4. Comparison of flux decay of GRB050525A in the X-ray and UVOT bands. The UVOT data through different filters have been normalised in the interval up to T+1000s, and the data taken through the different filters are plotted together. The relative normalisation of the X-ray and optical/UV data is arbitrary. The best fit broken power law model is plotted through the X-ray data. The best fit double power law with break is plotted through the UVOT data (see text). The dashed line has the same post break slope as the X-ray data. The dotted line is the best fit model with a constant flux added corresponding to the value measured by Soderberg et al. (2005) using HST/ACS.

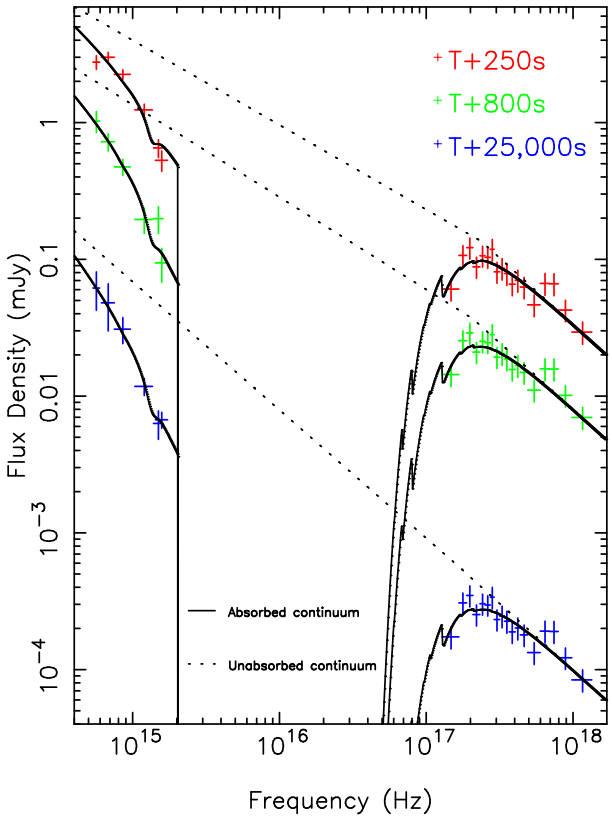

Figure 5. UVOT and XRT data on GRB050525A interpolated to the epochs T+250s, T+800s and T+25,000s, together with best spectral fit models (solid lines). The dotted lines represent the intrinsic continuum of the source, before extinction and absorption from gas and dust in both the Milky Way and the host galaxy.

Table 1. Comparison of model fits to the GRB050525A data with expectations from the fireball model.

	Fireball model[1]	Best fit	Step fit
X-ray decay	-1.15	-1.2	
Optical decay[2]	-0.9	-0.62	-1.04
X-ray spectral slope	-1.1	-0.97	
Optical spectral slope	-0.6	-0.60	

[1] For p=2.2, ISM slow cooling model
[2] Forward shock

4. GRB DIVERSITY

GRB050525A may not be a typical Swift burst in behaving broadly in line with the standard fireball model. In the case of GRB050319, the decay of both the optical and X-ray flux is much shallower than predicted, with a slope of about $\alpha = -0.5$ (Mason et al. 2005; Cusumano et al. 2005). This behaviour persists until at least 3×10^4s after the burst, before the X-ray slope, at least, steepens to a value of $\alpha = -1.1$ (Cusumano et al. 2005). This behaviour is not unique. For example De Pasquale et al. (2005a) find a similar initial slope in the X-ray decay of GRB050401, persisting for a few thousand seconds after the burst, before steepening to a value $\alpha = -1.5$. One explanation for this phenomenon is that the central engine continues to inject energy into the afterglow, at a decreasing rate, for some time after the initial burst (Zhang & Mészáros 2004). The decay rate steepens once the injection has ceased. A similar effect can be produced by ejecta that has a range of Lorentz factors, with the shock being 'refreshed' as it decelerates by initially slower moving shells that catch up with it (see De Pasquale et al 2005a, and Stanek et al. 2001, Bjornsson et al. 2002 in the context of GRB010222). Even more extreme behaviour is seen in GRB050712 (De Pasquale et al. 2005b) where the optical flux is flat, or even rises, during the first few hundred seconds following the burst. This is a case where the XRT data shows continued flaring during the same interval.

Another interesting case is the Swift data on the X-ray flash XRF050406 (Schady et al. 2005), which represent the earliest observations yet made of the optical emission of an X-ray flash, starting 88s after the BAT trigger. The optical emission is faint, but consistent with a rising flux in the first 200s of the afterglow, decaying thereafter with a shallow slope $\alpha \sim -0.7$. Schady et al. argue that both the soft X-ray spectrum of the initial burst emission, and the initially rising flux and shallow decay are consistent with observation of a structured jet viewed slightly off axis. In this case the Lorentz-beamed emission of the main jet core is not within the line of sight when the burst first goes off, and we see only fainter and softer emission from the outer portions of the jet. As the jet core decelerates, the beaming angle widens and we seen enhanced emission along our line of sight.

5. CONCLUSIONS

The Swift observatory is gathering unique data on the prompt and early afterglow emission of GRB. Data from the UVOT are providing an unprecedented glimpse of the early optical afterglow emission, which can be combined with the X-ray data taken simultaneously with XRT to study the behaviour of the afterglow across a range of frequencies and constrain physical models. Multi-filter data from the UVOT provides a valuable indicator of redshift, to supplement ground-based spectroscopy. The Swift data have already revealed considerable diversity in

behaviour among GRB, and we look forward to building up larger samples as the mission progresses, with which to investigate the full range of GRB phenomenology.

ACKNOWLEDGMENTS

We are greatful to the entire Swift team for their excellent and dedicated work in operating this challenging mission.

REFERENCES

Barthelmy, S. et al. 2005 Space Sci Rev (in press).

Blustin, A. J. et al. 2005 ApJ, (in press; astro-ph/0507515)

Bjornsson, G. et al. 2002, ApJ, 579, 62L.

Bromm V. & Loeb A. 2002 ApJ, 575, 111.

Burrows, D. et al. 2005a Space Sci Rev (in press).

Cusumano G. et al. 2005 ApJ (in press).

De Pasquale, M. et al. 2003, ApJ 592, 1018.

De Pasquale, M. et al. 2005a, A&A (in press; astro-ph/0507708).

De Pasquale, M. et al. 2005b (in preparation).

Fruchter A. S. 1999, ApJ, 512, L1.

Fynbo, J. P. U. et al. 2005 GCN Circ 3136

Groot et al. 1998, ApJ, 502, L123.

Lamb, D. Q. et al. 2004 NewAR 48 423.

Lazzati D. et al. 2002 A&A, 410, 823.

Mason, K. O. et al. 2005 ApJ, (in press).

Rhoads, J. E. 1999, ApJ, 525, 737

Roming, P. et al. 2005a Space Sci Rev (in press).

Roming, P. et al. 2005b Science (in press; astro-ph/0509273).

Sari, R., Piran, T. & Halpern, J. P. 1999, ApJ, 519, L17.

Schady, P. et al. 2005 (in preparation).

Soderberg, A. 2005, GCN Circular 3550.

Stanek K., et al. 2001 ApJ, 563, 592.

Zhang, B. & Mészáros, P. 2002, ApJ, 566, 712.

Zhang, B. & Mészáros, P. 2004, IJMPA, 19, 2385

THE X-RAY TELESCOPE ON BOARD *SWIFT*: STATUS AND MAIN RESULTS

G. Tagliaferri[1], S. Campana[1], G. Chincarini[1,2], P. Giommi[3], G. Cusumano[4], D.N. Burrows[5], J.E. Hill[5,6], J.A. Kennea[5], J.A. Nousek[5], J.P. Osborne[7], P.T. O'Brien[7], A. Wells[7], L. Angelini[6], and on behalf of the XRT team[1]

[1]INAF-Osservatorio Astronomico di Brera, Via Bianchi 46, 23807 Merate, Italy
[2]Università degli Studi di Milano-Bicocca, P.za delle Scienze 3, 20126 Milano, Italy
[3]ASI Science Data Center, Via G. Galilei, 00044 Frascati, Italy
[4]INAF-IASF Palermo, Via U. La Malfa 153, 90146 Palermo, Italy
[5]Pennsylvania State University, 525 Davey Lab, University Park, PA 16802, USA
[6]NASA Goddard Space Flight Center, MD 20771, USA
[7]University of Leicester, Department of Physics and Astronomy, Leicester, LE 17 RH, UK

ABSTRACT

The X-ray Telescope (XRT), on board the *Swift* satellite, provides: automated source detection and position with few arcsecond accuracy within few seconds from target acquisition; CCD spectroscopy and imaging capability (0.2-10 keV), with the capability of detecting a milliCrab source in about 10 seconds; automatic adjusting of the CCD readout mode to optimize the science return as the source fades. *Swift* main scientific goal is the study of gamma-ray burst (GRBs). XRT can observe GRB afterglows over several orders of magnitude in flux. The first results obtained during the first ten months of operation confirm that XRT is fully compliant with the requirements and is providing excellent results. In particular it is detecting a very steep decay in the early X-ray light curve of many afterglows. Often there are also strong flares superimposed to the X-ray light curve, probably related to the continued internal engine activity. XRT is also localising for the first time the X-ray counterparts to short bursts.

Key words: GRB; X-rays, Instrumentation.

1. INTRODUCTION

The first detection by the *Beppo*SAX satellite of a X-ray afterglow associated with GRB 970228 (Costa et al. 1997) revolutionised the study of the Gamma Ray Bursts (GRBs). It was finally possible to study the counterparts of these elusive sources. Optical and radio afterglows also were soon discovered (Van Paradijs et al. 1997; Frail et al. 1997). These studies showed that the afterglows associated with GRBs are rapidly fading sources, with X-ray and optical light curves characterised by a power law decay $\propto t^{-\alpha}$ with $\alpha \div 1 - 1.5$. Moreover, while most of the GRBs, if not all, had an associated X-ray afterglow only about 60% of them had also an optical afterglow, i.e. a good fraction of them were dark–GRBs. For a general review on these topics see Zhang & Meszaros (2004) and Piran (2005). Therefore, it was clear that to properly study the GRBs, and in particular the associated afterglows, we needed a fast-reaction satellite capable of detecting GRBs and of performing immediate multiwavelength follow-up observations, in particular in the X-ray and optical bands. *Swift* (Gehrels et al. 2004) is designed specifically to study GRBs and their afterglow in multiple wavebands. It was successfully launched on 2004 November 20, opening a new era in the study of GRBs (see also N.Gehrels this conference). *Swift* has on board three instruments: a Burst Alert Telescope (BAT) that detects GRBs and determines their positions in the sky with an accuracy better than 4 arcmin in the band 15-350 keV (Barthelmy et al. 2005a); an UV-Optical Telescope (UVOT) capable of multifilter photometry with a sensitivity down to 24th magnitude in white light and a 0.3 arcsec positional accuracy (Roming et al. 2005); an X-Ray Telescope (XRT) that provides fast X-ray photometry and CCD spectroscopy in the 0.2-10 keV band with a positional accuracy better than 5 arcsec. Here we will briefly describe the XRT overall properties, provide its in-flight performance and outline its main scientific results. For a more detailed description of the XRT characteristics see Burrows et al. (2004, 2005a).

2. XRT DESCRIPTION

A grazing incidence Wolter I telescope provides the XRT imaging capabilities, focusing the X-rays onto a CCD at a focal length of 3.5 meters. The mirror module is made of 12 nested gold-coated electroformed Ni mirrors. To prevent temperature gradients that would degrade the image quality, two thermal baffles in front of the mirror main-

tain the mirror temperature at a constant value of about 20 C. The focal plane camera houses an XMM/EPIC MOS CCD, a 600×600 array of 40μm$\times 40\mu$m pixels, that corresponds to 2.36 arcseconds in the sky. Four calibration sources illuminate the CCD corners continuously, allowing us to monitor any CCD response degradation during the mission life time. A thin Luxel filter mounted in front of the CCD blocks the optical light. A thermo-electric cooling (TEC) system is capable of maintaining the CCD temperature at -100 C, with the heat dumped to a radiator sitting at a temperature between -85 C and -45 C, depending on orbital parameters and spacecraft orientation. The XRT structure is provided by an optical bench interface flange (OBIF) and a telescope tube, composed of two sections mounted on the OBIF; the forward telescope tube that supports the star trackers and the telescope door, and the rear tube that supports the focal plane camera. The mirror module, which is inside the front tube, is mounted directly on the OBIF through a mirror collar. Electron deflection magnets are placed behind the rear face of the OBIF to prevent electrons that pass through the mirror from reaching the detector. A telescope alignment monitor provides an accurate measurement of the alignment between the XRT boresight and the star trackers that are directly mounted on the XRT forward tube (see Burrows et al. 2004, 2005a).

The main science requirements that drove the design of XRT are: rapid, accurate positions (better than 5 arcsec in less than 100 seconds after the burst), moderate resolution spectroscopy (better than 400 eV at 6 keV after three years of operation) and accurate photometry for sources spanning up to seven order of magnitude in flux with high time resolution. A final requirement is that XRT must be able to operate autonomously in order to provide the afterglow X-ray position very rapidly and efficiently follow the afterglow decay. To reach these goals, four observing modes have been implemented: an Image Mode (IM), Photo Diode mode (PD), Window Timing mode (WT) and Photon Counting mode (PC). In IM the CCD operates like an optical CCD, providing only imaging information without event recognition (i.e. no spectral capability). This mode is used as soon as *Swift* slews to the position of a new GRB just detected by the BAT. The XRT starts to accumulate images in IM, looks for the new source and determines its coordinates. These are sent down via TDRSS and distributed immediately to the community through the GCN network. Meanwhile, the XRT switches between the other operating modes depending on the source count rates. The PD mode provides fast timing resolution of about 0.14 milliseconds, but no imaging information. The entire field of view, including the corner calibration sources, will end up as a single pixel image. This mode is used for very bright sources, brighter than 2-3 Crabs. When the source flux goes below few Crabs, the XRT switches to WT mode, that provides 1.8 ms time resolution with spatial resolution along one direction (1-D image). Finally, for sources with fluxes below 1 mCrab, the XRT will operate in PC mode, that provides the full imaging and spectroscopic information with a time resolution of 2.5 seconds. This is the standard mode in which XRT operates most of the time.

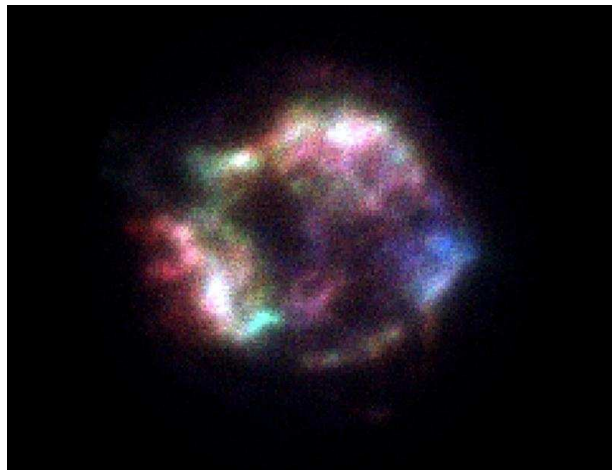

Figure 1. This colour coded XRT image of the supernova remnant Cas A immediately shows the good image quality that XRT provides.

To establish the XRT performance an end-to-end calibration campaign was performed in September 2002 at the Panter X-ray calibration facility in Munich. This allowed us to verify that the XRT Point Spread Function has a HEW of 18 arcsec at 1.5 keV (22 arcsec at 8.1 keV) and it is quite uniform over the entire field of view. The total effective area of XRT is of $\sim 135\ \mathrm{cm}^{-2}$ at 1.5 keV. The Panter tests also demonstrated that XRT can localise a source with the required accuracy and can autonomously and correctly change its readout mode accordingly to the varying source flux.

After the *Swift* launch, the XRT was turned on 2004 November 23. However, during the complete activation phase of XRT the TEC system stopped functioning, leaving the temperature control of the CCD detector only under the passive radiator system. Thus, in order to prevent the CCD from getting too hot and loosing sensitivity due to increased thermal noise, more stringent pointing constraints have been implemented to keep the CCD temperature below -50 C (this guarantees that XRT performs as expected). Since then *Swift* has been successfully operated maintaining the CCD temperature below this value for most of the time and XRT is delivering very good quality data with a high degree of observational efficiency (Kennea et al. 2005). The first light occurred on December 11, when *Swift* was pointed to the bright supernova remnant Cas A. XRT provided a superb image that shows structures and filaments at different temperatures (see Fig. 1). After the first light observation the calibration campaign started and various known X-ray targets were observed to verify: the PSF as a function of the off-axis angle; effective area; timing capability; spectral energy resolution and source location capability (e.g. Hill et al. 2005a; Moretti et al. 2005a, Romano et al. 2005a, Osborne et al. 2005). These measurements confirm the perfect functioning of XRT (see e.g. Fig. 2).

On May 28, 2005 a micrometeorite shower hit the CCD damaging various pixels. As a result a few hot columns

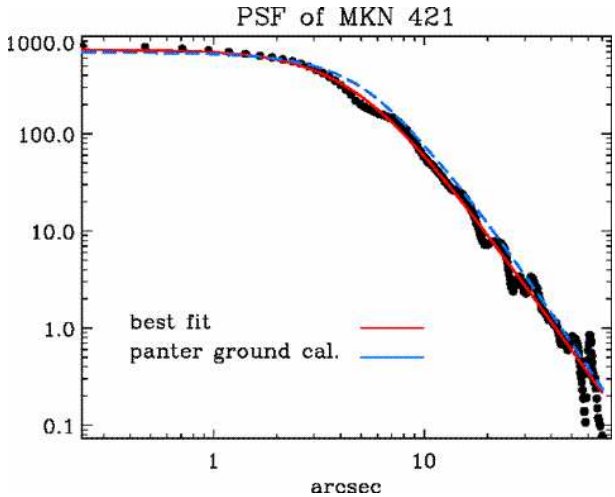

Figure 2. This figure shows the XRT PSF as measured in-flight on the bright source MKN 421. Note how the in flight PSF (continuous line) agrees perfectly with the one measured on ground (dashed line).

had to be vetoed otherwise they would saturate the telemetry. This can be done in WT and PC modes, but not in PD mode. Therefore, the latter mode has not been used since then and the XRT, after the IM mode exposures switches to WT mode. It is still possibile to recover the PD, by changing the electronic set-up of the focal plane camera. The balance between the impact on the *Swift* operations implied by these changes and the scientific loss due to the missing PD mode are currently under evaluation (for a more complete discussion on this topic see T.Abbey this conference). So far the scientific loss due to the lack of the PD mode seems to be negligible. In any case we have a few CCD columns that are off and 3 of them are quite in the center of the field of view, therefore when the source lies on top or near these columns one has to correct for the sensitivity loss in order to derive the correct source count rate. This is now automatically done by the XRT pipeline software distributed by the *Swift* consortium.

3. XRT OBSERVATIONS

Due to its low orbit and pointing constraints, a source can not be observed continuously by *Swift*. Typically three to four targets are observed during each 96 minutes orbit. Depending on its intensity and fading behaviour the X-ray afterglow of a GRB is monitored with XRT up to a few days–weeks. Therefore, on some GRBs the XRT total exposure can be as long as few hundred kiloseconds. This, together with the good PSF of XRT, that is almost flat on the central 8 arcminutes radius of the field of view, and its low background, due to the low orbit, allow us to obtain very deep X-ray images (e.g. Fig. 3) that can be use to study the cosmic X-ray background and derive its LogN-LogS. Clearly, we can not go as deep as the Chandra deep fields, but still can reach a sensitivity limit of

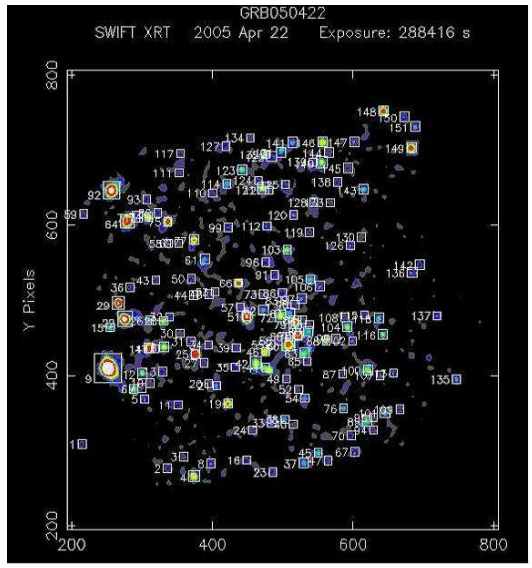

Figure 3. A 258 ks XRT exposure on the field of GRB 050422. At the sensitivity limit reached in this exposure we expect to have about ~ 1000 sources/sqdeg. Therefore, hundreds of sources will be detected in the XRT deep exposures, allowing us to investigate the LogN-LogS of the X-ray sources making up the cosmic X-ray background.

$\sim 3 \times 10^{-16}\,\mathrm{erg\,cm^{-2}\,s^{-1}}$ in the 0.5-2.0 keV band. We estimate that in a two years life time of the *Swift* mission we will cover 2 to 3 square degree of the sky at this limit, nicely complementing the Chandra and XMM-Newton surveys (Giommi et al. in preparation, see also Fig. 4). Although the goal of XRT is to study the X-ray sources associated to GRBs, still this is a nice serendipitous result that XRT will provide.

Up to the end of September 2005, the XRT observed the field of 70 GRBs, always detecting a X-ray source associated with the GRB, except in 5 cases. Of the 65 X-ray afterglows detected, 41 were detected by XRT within 200 s of the burst trigger, and 20 in less than 100 s. This immediately shows how well *Swift* is operating and how efficiently XRT is working. For the five XRT non-detections, in three cases the XRT observation started 86, 14 and 9 hours after the burst, respectively. Therefore it is not surprising that we did not found an X-ray afterglow. In another case the XRT observation started 1.6 hours after the burst. Again this non-detection is compatible with a weak X-ray afterglow that was not any more detectable. The last non-detection case corresponds to a short GRB and now we know that the X-ray (and optical) afterglow associated to the short GRBs are usually weaker than those og long GRBs (see below). Therefore, we can conclude that so far we always found a X-ray source associated to long GRBs, provided that we observe the GRB field on a timescales of a few minutes. This is a further confirmation that the X-ray observations are the most efficient way to study the afterglows associated to GRBs. The accuracy with which XRT is localising the X-ray afterglow is of ~ 4 arcsec (90% confidence, Moretti et al. 2005b).

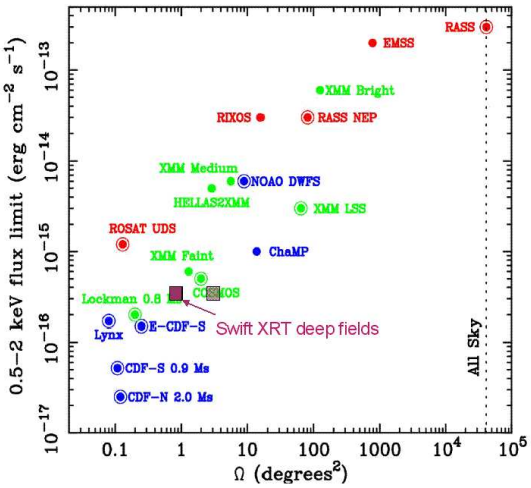

Figure 4. Comparison of the XRT sky coverage at the sensitivity limit of $\sim 3\times10^{-16}$ *erg s*$^{-1}$ *cm*$^{-2}$ *in the band 0.5-2.0 keV with those of other X-ray surveys (adapted from Brandt & Hasinger 2005). The two XRT points (filled squares) correspond to the XRT sky coverage calculated at the beginning of September 2005 and that one estimated after two years of operations.*

In spite of this good positional accuracy that allow deep follow-up searches for the optical counterpart, about 50% of the XRT afterglows are without an optical counterpart. This lack of an optical counterpart can either be due to intrinsic absorption in the GRB environment or to a very high redshift GRBs. We will now outline some of the most exciting results so far achieved by XRT.

The early X-ray light curves of GRBs and afterglows: steep-flat-steep or flat-steep shape. The first GRBs observed with XRT is GRB 041223. In this case *Swift* was on target after 4.6 hours, because the automatic repointing of *Swift* was still not allowed during this checking phase. Therefore, a command from ground was issued and the satellite repointed. A new bright and rapidly fading X-ray source was immediately discovered and soon after also the optical counterpart was identified (Burrows et al. 2005b). The automatic slewing of the satellite was enabled on January 2005 with the XRT observations starting from a few tens to a few hundred seconds after the burst (e.g. Campana et al. 2005, Hill et al. 2005b). The first unexpected results was the detection of a very steep decay of the X-ray flux ($\mathrm{F(t)} \propto \mathrm{t}^{-\alpha}$ with $\alpha \gtrsim 3$), that breaks to a flatter slope in the first few hundred seconds (Tagliaferri et al. 2005a, see Fig. 5). From the lack of a spectral evolution of the X-ray spectrum of the afterglow across this break, the clear difference of the prompt spectrum measured by BAT from that one of the afterglow measured by XRT and the discontinuity of the BAT and XRT light curves, Tagliaferri et al. (2005a) concluded that, at least for the well studied case of GRB 050219A, the early steep decay detected by XRT was not due to the prompt emission. However, a different situation was found for subsequent GRBs. In particular for GRB 050315 and GRB 050319, a spectral change across the break, with the spectrum evolving from a softer to harder shape, was detected with XRT. In these cases the XRT and BAT light curves seem to joint smoothly (Cusumano et al. 2005a; Vaughan et al. 2005). It is now believed that the early steep decay, seen by XRT in most cases, is the tail of the prompt emission, due to photons emitted at large angle with respect to the observer line of sight (see also P.O'Brien this conference). The different behaviour of GRB 050219A could be explained by the presence of a strong flare that it is only partially detected by XRT, that sees only the decaying part. In fact, strong flares have now been seen by XRT in the early phases of various GRBs (see below).

The study of the X-ray light curves of various GRBs on time scales from a few seconds to hours-days shows that two common behaviours are emerging, where the light curve consists of either three or two power law segments (Chincarini et al. 2005; Nousek et al. 2005). In the first case, which seems to be the most common, there is an initial very steep decay ($\propto \mathrm{t}^{-\alpha}$ with $\alpha \gtrsim 3$), followed by a flattening (with $\alpha \div 0.2 - 1.0$) and then by a further steepening ($\alpha > 1.0$). The first break occurs in the first one thousand seconds and the second one, usually before the first 10 ks. In the second case, the initial very steep part is not seen, although the observations start few tens of seconds after the burst explosion (e.g. GRB 050128, GRB 050401, GRB 050525A). In general, during these transitions the X-ray spectrum remains constant within the observational errors (with just a couple of exceptions during the early steep decay, see above). Finally by studying seven bursts for which the redshift was known, Chincarini et al. (2005) showed that the energy emitted during the afterglow phase correlates with the one emitted by the prompt and that the afterglow flux emitted in the 0.2-10 keV band goes from few $\%$ up to $\sim 40\%$ of the flux emitted during the prompt phase in the 15-350 keV band.

The X-ray flares seen in the XRT light curves. On April 6, 2005, a new GRB was detected by BAT and thanks to the *Swift* prompt slew the XRT started imaging the field around the BAT position 84 s after the trigger. The XRT detected a weak decaying X-ray source, that however a few tens of seconds later started to brighten. Its flux increased by a factor of 6 peaking at 213 s and then start decaying again, the flare ended at ~ 300 s after the burst, then the X-ray light curve followed again. The power law decay showed before the flare (Burrows et al. 2005c; Romano et al. 2005b). After this first detection, a very bright flare was detected in the XRT light curve of GRB 050502B, with a total fluence that exceeded that one of the prompt burst seen by BAT (Burrows et al. 2005c, Falcone et al. 2005). The spectra during these and other flares are significantly harder that those measured before and after the flare, in particular they are harder at the flare onset and then get softer while the flare evolves. After these first detections, many other flares have been detected (see also D.Burrows and G.Chincarini this conference). Here we will only mention two other notable cases, those of GRB 050724 (Barthelmy et al. 2005b), a short GRB with a very bright X-ray afterglow

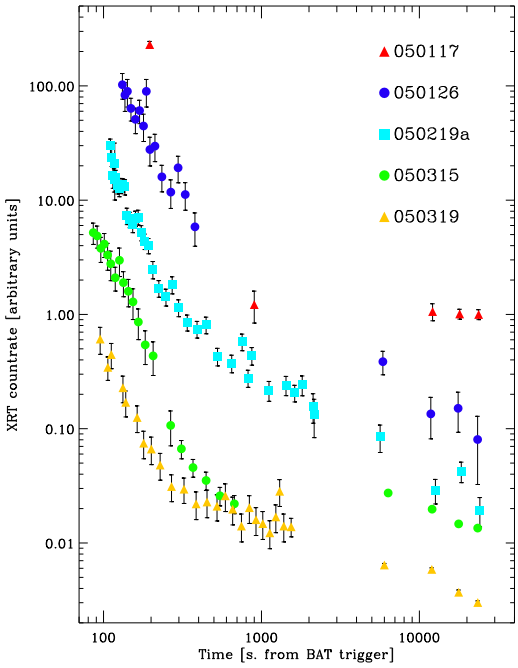

Figure 5. The steep early X-ray light curves of five GRBs observed by XRT up to March, 2005. For each GRB the XRT count rates are rescaled by an arbitrary constant factor for clarity.

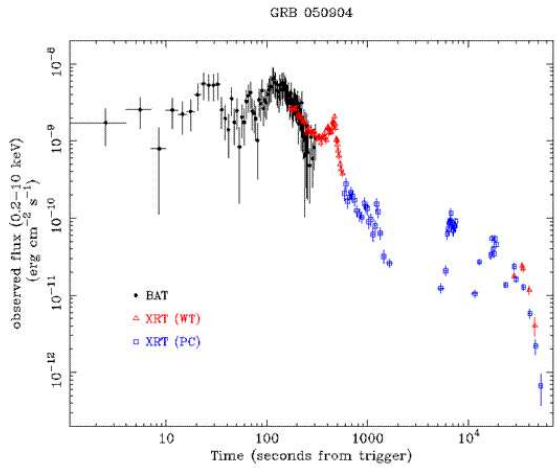

Figure 6. BAT and XRT light curve of the high redshift GRB 050904. Note that the 0.2-10 keV observed flux corresponds to the flux emitted in the 1.4-73 keV energy band and that the time along the X axis is also stretched by an amount of (1+z) in the source rest frame, allowing us to better follow the flares evolution.

(see below), and GRB 050904, a very high redshift GRB (z=6.29, Kawai et al. 2005; Tagliaferri et al. 2005b) whose X-ray light curve (see Fig. 6) shows strong and complex flare activity (Cusumano et al. 2005b; Watson et al. 2005). All of the evidence we have so far suggests that these flares, at least the ones occurring in the first few hundred seconds, are related to continued internal engine activity.

The detection of the first counterpart to the short GRBs. The discoveries that have been made in the recent years have established that long GRBs probably originate from core-collapse explosion of massive stars. On the other hand no clues were found on the origin of short GRBs. In fact, while since 1997 astronomers have been able to study the afterglows associated with long GRBs, for the short GRBs this has not been possible up to May 9, 2005, when the BAT detected a short burst, GRB 050509B. This burst was promptly pointed at by *Swift*, the XRT started imaging the field 62 s after the burst and detected an uncataloged weak X-ray source (11 counts in total) inside the BAT error circle, providing the first accurate position of a short GRB (Gehrels et al. 2005). The X-ray afterglow quickly faded below the detection limit and no optical afterglow was detected, in line with the past failure in localising short GRBs. The X-ray afterglow lies near a luminous non-star-forming elliptical galaxy with z=0.225. After the localisation of the short burst GRB 050709 by HETE-2 (Villasenor et al. 2005), that lead to the identification of an optical counterpart in a nearby galaxy (z=0.1), BAT localised another short GRB on July 24. Again *Swift* reacted promptly and the XRT started to observe the GRB field 74 s after the burst, this time detecting a very bright and flaring X-ray afterglow (Barthelmy et al. 2005b). The accurate XRT and subsequent Chandra X-ray position allowed also to identify the optical (see Fig. 7) and radio counterpart (Barthelmy et al. 2005b; Berger et al. 2005). Also in this case the burst is localised off-center in an elliptical galaxy at z=0.258. These results are consistent with the hypothesis that short GRBs originate from the merger of neutron star or black hole binaries. Also the isotropic energy emitted in the prompt phase of these short GRBs are 2-3 orders of magnitude lower than that emitted by the long bursts, again supporting the idea that short and long GRB have a different origin.

4. CONCLUSIONS

In conclusion the first ten months of operations have shown that the XRT provides excellent quality X-ray images with low background and that the overall calibration is in good shape. Thanks to this, the XRT is delivering spectacular results, maybe somewhat different from those expected. There seem to be two types of X-ray afterglow light curves: steep-flat-steep (more common) and flat-steep. On top of these light curves, various bright flares episodes are detected. There is strong evidence that, at least the flares detected in the first few hundred seconds, are related to continued internal engine activity. The XRT is providing arcsec localisation for the X-ray counterpart of short burst, allowing us to investigate the origin and properties of these, so far, elusive sources.

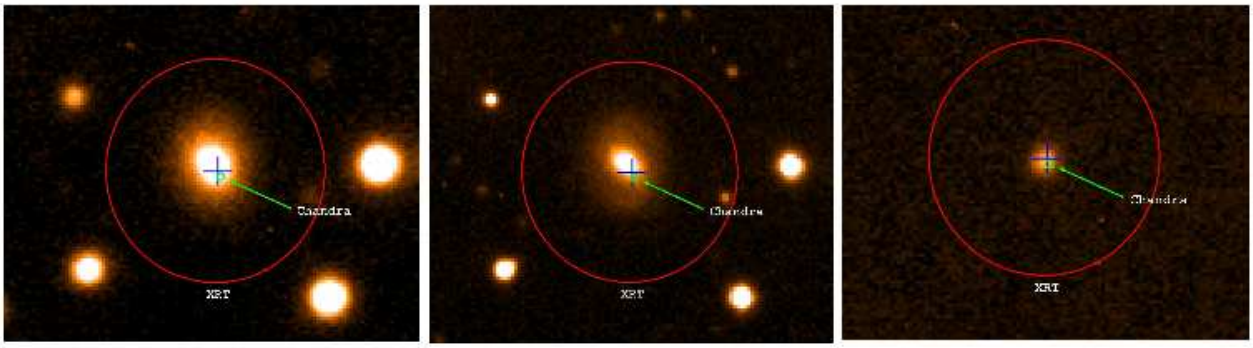

Figure 7. VLT optical images showing the position of GRB 050724, a short burst detected by BAT. The red circle shows the XRT error box of 6 arcsec radius, the green circle provides the Chandra position. while the blue cross gives the position of the optical transient (from Barthelmy et al. 2005b). The left panel shows the VLT image taken on the first night and the panel in the middle shows the VLT image taken on the second night. The panel on the right shows the result of the image subtraction, clearly showing the optical transient coincident with the X-ray afterglow.

ACKNOWLEDGMENTS

These activities are supported in Italy by ASI grant I/R/039/04, at Penn State by NASA contract NAS5-00136 and at the University of Leicester by PPARC grants PPA/G/S/00524 and PPA/Z/S2003/00507.

REFERENCES

Barthelmy S., Barbier L.M., Cummings J.R., et al. 2005a, Sp. Sci. Rev., 120, in press (astro-ph/0507410)

Barthelmy S., Chincarini G., Burrows D.N., Barbier L.M., et al., 2005b, Nature, submitted

Brandt W.N, Hasinger G. 2005, ARA&A 43, 827

Burrows D.N., et al. 2004, SPIE, 5165, 201

Burrows D.N., Hill J.E., Nousek J.A., et al. 2005a, Space Sci. Rev, 120, in press (astro-ph/0506130)

Burrows D.N., et al. 2005b, ApJ, 622, L1

Burrows D.N., Romano P., Falcone A., et al. 2005c, Science, 309, 1833

Campana S., Antonelli L.A., Chincarini G., et al. 2005, ApJ, 625, L23

Chincarini G., Moretti A., Romano P., et al. 2005, A&A submitted, (astro-ph/0506453)

Costa E., et al. 1997, Nature, 387, 783

Cusumano G., Mangano V., Angelini L., et al. 2005a, ApJ, in press (astro-ph/0509737)

Cusumano G., Mangano V., Chincarini G., et al. 2005b, Nature, submitted (astro-ph/0509737)

Falcone A.D., et al. 2005, ApJ submitted

Frail D.A., et al. 1997, Nature, 389, 261

Gehrels N., Chincarini G., Giommi P., et al. 2004, ApJ, 611, 1005

Hill J.E., et al. 2005a, SPIE, 5898, in press

Hill J.E., Morris D.C., Sakamoto T., et al. 2005b, ApJ, in press, (astro-ph/0510008)

Kawai, N., et al. 2005, GCN 3937

Kennea J.A., et al. 2005, SPIE, 5898, in press

Moretti A., et al. 2005a, SPIE, 5898, in press

Moretti A., Perri M., Capalbi M., et al. 2005b, to be submitted to A&A

Nousek J.A., Kouveliotou C., Grupe D., et al. 2005, ApJ submitted (astro-ph/05083332)

Osborne J.P., et al. 2005, SPIE, 5898, in press

Piran T., 2005, Rew. of Modern Physics, 76, 1143

Romano P., et al. 2005a, SPIE, 5898, in press

Romano P., Moretti A., Banat P.L., et al. 2005b, A&A submitted

Roming P.N., Kennedy T.E., Mason K.O., et al. 2005, Space Sci. Rev, 120, in press (astro-ph/0507413)

Tagliaferri G., Goad M.R., Chincarini G., et al. 2005a, Nature, 436, 985

Tagliaferri G., Antonelli L.A., Chincarini G., et al. 2005b, A&A, 443, L1

Van Paradijs J., et al. 1997, Nature, 386, 686

Vaughan S., Goad M.R., Beardmore A.P., et al. 2005, ApJ, in press (astro-ph/0510677)

Watson, D., et al. 2005, ApJ subm. (astro-ph/0509640)

Zhang, B., Mészáros, P. 2004, Int. Journ. Mod. Phys. A, 19, 2385

XRT Light curves:
Morphology, Flares and Energy

Guido Chincarini[1,2],
Vanessa Mangano[3], Alberto Moretti[2], Matteo Perri[4], Patrizia Romano[2],
Sergio Campana[2], Stefano Covino[2], GianpieroTagliaferri[2], Lorella Angelini[5],
David Burrows[6], Paolo Giommi[4,7], Julian Osborne[8] and Swift Team

[1] *Università degli Studi Milano – Bicocca, P.za delle Scienze 3, 20126 Milano, Italy*
[2] *INAF – Osservatorio Astronomico di Brera,Via Bianchi 46, 23807 Merate (LC), Italy*
[3] *INAF – IASF Palermo, Via U. La Malfa 153, 90146 Palermo, Italy*
[4] *ASI Science Data Center, Via G. Galilei, 00044 Frascati (RM), Italy*
[5] *Department of Astronomy & Astrophysics, Pennsylvania State University, University Park, PA 16802, USA*
[6] *Department of Physics & Astronomy, University of Leicester, Leicester LE1 7RH, UK*
[7] *Agenzia Spaziale Italiana, Unità Osservazione dell'Universo, Viale Liegi 26, 00198 Roma, Italy*
[8] *NASA/Goddard Space Flicht Center, Greenbelt, MD 20771, USA*

ABSTRACT

Following a brief introduction we show that the observations obtained so far with the Swift satellite begin to shed light over a variety of problems that were left open following the excellent performance and related discoveries of the Italian – Dutch Beppo SAX satellite. The XRT light curves show common characteristics that are reasonably understood within the framework of the fireball model. Unforeseen flares are however detected in a large fraction of the GRB observed and the energy emitted by the brightest ones may be as much as 85% of the total soft X ray emission measured by XRT. These characteristics seems to be common to long and short bursts.

1. INTRODUCTION

As discussed by Gehrels in these proceedings the Swift satellite (Gehrels et al. 2004), is giving us the answer to many of the questions that remained unsolved following the Beppo-SAX mission. The soft X_ray light curves (0.2 – 10 keV) have been observed with great detail and temporal resolution for very long periods, the record being detained by GRB050408 that was observed over a period of 38 days (Capalbi et al. 2005). More important the rapid pointing capabilities of the spacecraft allows the re-pointing of the target in some cases in less than 60 seconds after the alert to immediately start the observation in the X ray band and in the optical (1700 Å to 6500 Å). The accurate determination of the X ray position with the X ray Telescope (XRT) allowed also the localization of the short Gamma Ray Bursts. We have discovered that these occur on the outskirt of rather evolved galaxies, early types or E_m+A galaxies, and are accompanied by an isotropic emission that is about a factor 100 – 1000 smaller that the isotropic energy emitted by the long bursts. The shorts were all detected in the proximity of nearby galaxies with z < 0.5. The low redshift of the sample may in part be due to the lower energy emitted and to the difficulties of the follow up observations but mainly related to the star formation history of the Universe (Guetta & Piran 2005). In some cases the afterglow could also be absent if the event is located at the very outskirt of the galaxy where the ISM has an extremely low density. These observations are also opening our research toward a better understanding of the stellar evolution of massive stars and merging of relativistic stars.

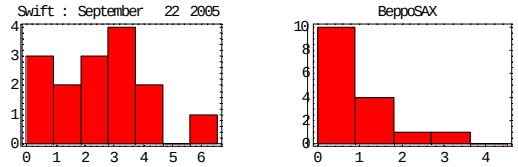

Fig. 1. The distribution of the redshifts of the GRB discovered by the Swift and by the Beppo SAX satellites. While the statistics is still small we have a strong indication that Swift tends to detect a larger number of high z objects.

Perhaps the most unexpected feature, this is not yet fully understood, is the capability of Swift to detect objects at high redshifts. As illustrated in Fig. 1 the mean redshift of the sample so far observed by Swift is quite larger than the mean redshift observed by other missions. This may be due to the fact that in the past the faint tail of the distribution or the rapid decaying afterglows were missed and to the band pass and high sensitivity of BAT. But most important the hope to detect objects at very high z was satisfied with the detection of GRB050904 for which z = 6.29

(Cummings et al., 2005, Cusumano et al. 2005, Tagliaferri et al. 2005). This detection is of paramount importance since it shows that the fast evolution of a massive star producing a GRB occurs also at epochs where stars and galaxies have very low metal abundance. More interesting we now know that we have the capability to detect these objects near the re-ionization epoch soon after the Universe exits from the Dark Age and likely we may get the possibility to learn about the formation and evolution of the early stars assuming a gamma ray burst can still occur when the composition is more or less primordial. This detection gave new impetus toward more ambitious goals and toward the developments of new strategies and computations. We believe, therefore, that the discoveries made by Swift opened up a very broad spectrum of research supplying a unique data base and new perspectives.

Previous work carried out with Beppo SAX and other satellites already evidenced that the basic model as proposed by Meszaros and Rees (1993), see however also alternative models which have been proposed, was satisfactory. For details see the excellent reviews by Piran (1999), Hurley et al. (2002), Zhang and Meszaros (2004). The observations by Swift confirmed the validity of the models and however the main challenge now is the estimate of whether or not there are constant patterns in the light curve indicating that not only we are dealing with the same kind of physics but that the evolution and magnitude of the phenomenon follows

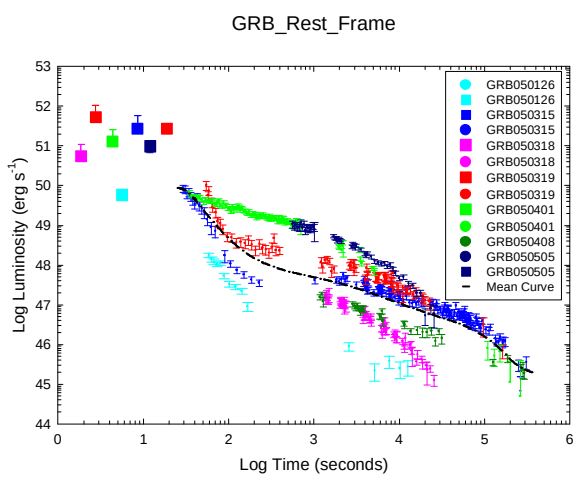

Fig. 2. The light curves have been plotted in the rest frame of each single burst. For the origin of time we used the trigger time as given by the BAT instrument. Squares refer to the mean flux observed by BAT during the burst and converted via the BAT spectrum to the energy band of XRT, circles refers to the observed flux in the band 0.2 – 10 keV. The dot dashed line is the mean curve as described in the text.

certain well understood patterns. In this context the shape of the light curves in the rest frame, their characteristics and the energy balance, especially when compared to the energy related to the prompt emission, are highly significant in refining the models. In section II we are dealing with the first set of rest frame GRB light curves, and related energy, that we observed before May 15 this year. In section III we deal with the morphology of flares and the energy involved. In particular we show that long burst flares, short bursts flares, low z flares and high z flares have all some common characteristics in the light curve. Flares that are visible during the late phases of the light curve give evidence of long lasting activity of the central engine. Turning around the problem it remains to explain, among other things, why the flares are not present in all the bursts. Unless otherwise stated we use H_0 = 65 km s^{-1} Mpc^{-1}, $\Omega_m = 0.3$ and $\Omega_\Lambda = 0.7$.

2. REST FRAME LIGHT CURVES.

By the 15th of May 2005 we had a set of only 7 XRT light curves for which also the redshift was available and none of these had flares (see section III). Flares had been already detected however in GRB050406 and in GRB050502B (Burrows et al. 2005, Romano et al. 2005 and Falcone et al. 2005). From these no flare light curves (Chincarini et al. 2005), it was immediately clear that we had at least two types of basic morphology. The first type consisting of light curves presenting a very sharp decay (power law exponent generally between -3 and -2), at the very beginning of the observations (about 30 seconds after the BAT trigger in their rest frame) followed by a mild slope (power law exponent around -0.6 with rather large variations) that would later steep (power law exponent < -1). The second type, vice versa , would start with a mild slope and later steep in a way similar to the last variation observed in the previous type (note however that GRB050401 likely shows one mini-flares). The flares observed in many light curves in the following months are simply superimposed to this basic morphology. The findings of the early sample have been confirmed, see also Nousek et al. (2005). The expected relation between the temporal decay index and spectral index is universal for synchrotron emission from spherical fireballs (or jets with an opening angle much larger than the relativistic beaming scale), and is given by $\alpha=2+\beta$ (Kumar and Panaitescu 2000) where $F_\nu \propto t^{-\alpha} \nu^{-\beta}$. The typical value of β is about 0.5 -1. , the maximal decay index could be $\alpha \sim 3$. If the decay is steeper than 3, as it may be the case for GRB 050319, we possibly have to argue for a highly collimated jet, and however in this case the time adopted for the trigger may be wrong (Chincarini et al. 2005, Barthelemy et al. 2005).

The prompt emission by GRB050319 is characterized by two bursts separated by about 137 seconds (see Fig. 2) while in GRB050401 we observe two burst

separated however only by a few seconds. Likely the true trigger [T_0] for the afterglow of GRB050319 is related to the second burst since the effects due to the first burst had enough time to decay and be overshadowed by the afterglow of the second burst.
This may not be the case for GRB050401 since the two bursts detected by BAT are one immediately after the other. In this case however note that the formal BAT zero time is more or less half way of the first burst, and this matter must be clarified as well. An other possibility exists that the steep decay of the first phase (30 to 100 seconds in the rest frame) is due to the

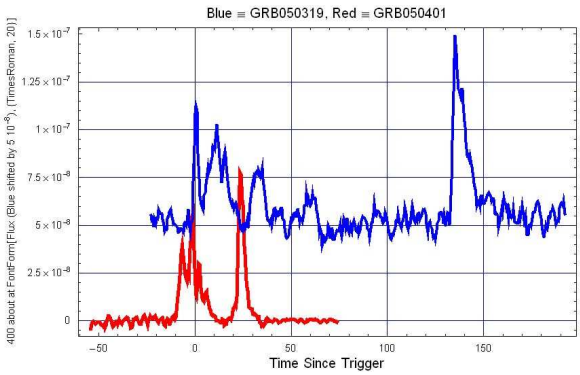

Fig. 3. The BAT light curve of GRB050319 and GRB050401 with the background of GRB050401 shifted up by 5 10^{-8} (erg cm^{-2} s^{-1}) for clarity.

decay curve of a flare whose peak was missed. This possibility can not yet be completely excluded. However it seems unlikely due to the nearby similat slope shown by most GRBs. Flares, on the contrary, show decay slopes that differ largely from flare to flare. Likewise it is unlikely that the type II is the consequence of a missed flare or of a missed phase I type I curve. In the case of GRB050401, but now we have a much larger sample, the XRT observations started about 30 seconds (rest frame) after the BAT trigger and we should have seen the sign either of a late prompt emission or of a flare. We conclude, base on the evidence we have today, that the X-ray light curves of GRB are divided mainly in two types. In addition many GRB show flare superimposed to the light curve.
For each light curve we measured both the mean spectrum and the spectrum before and after the light curve breaks to look for spectral variations. The energy index of the spectrum does not change much (the error of the mean is larger however that the error of a single estimate) from burst to burst and does not change crossing the break. We measure a mean value of the Energy Index (EI) = 1.12 ± 0.31. The rather large error is due mainly to GRB050319 that shows variation in the EI as a function of time. The hardness ratio in general changes during the flares in a way that is similar to the flare light curve but with a phase lag (this work is in preparation).

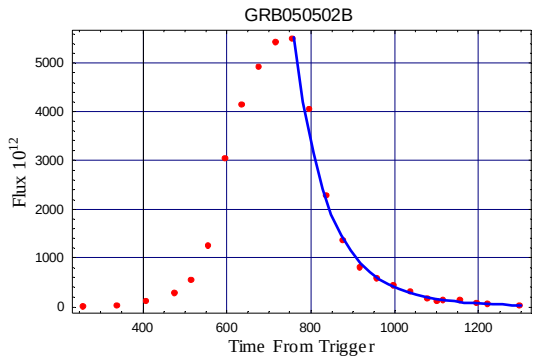

Fig. 4. Profile of the GRB050502B giant flare. The flux is expressed in 10^{-12}erg cm^{-2} s^{-1} units and after subtraction of the "background" light curve. The slope of the decay changes from -9.58 to -7.12 if rather than using for the origin of time the trigger by BAT we use the beginning of the flare itself.

The ratio of the energy emitted during the afterglow (or the Total Fluence) to the energy emitted during the prompt emission changes considerably from Burst to Burst and is in the range, for the sample of Fig. 2, from 0.016 to 0.40. For the long bursts we observe in the soft X ray afterglow at most 40% of the energy emitted during the prompt emission. An other interesting and more accurate way to compute the relation between prompt emission and afterglow is to use well defined time interval of the afterglow and compute the rest frame Fluence. Using the rest frame intervals 50 – 200 seconds and 1300 – 12600 seconds we find a tight correlation between the prompt emission and the rest frame afterglow emission indicating a rather tight correlation between the energy injected in the ISM, within the external shock scenario, and the energy emitted in the soft X ray during the afterglow.

3. FLARES: MORPHOLOGY AND ENERGETIC

The morphology of the flares, likely the direct consequence of secondary bursts, have a rather simple morphology at least in those cases where the flares are not clustered and the signal to noise is high. Subtracting the "background" decaying light curve, that in the cases we considered has the morphology described in section II, the shape is characteristic of the emission due to the clash between to relativistic shells as described in Kobayashi et al. (1997), that is a rapid rising power law followed by a very rapid power law decay. In the computation of the flare decay slope rather than using the BAT trigger time we should use an origin of time coincident with the beginning of the flare. In the case of GRB050502B the exponent of the power law decay changes, by shifting the origin of time by about 350 seconds, from -9.58 to -7.12. The change

is highly significant even if it does not cause any change that could drastically modify the possible models. The energy emitted during the flare is comparable, in some cases, to the energy emitted during the whole XRT afterglow and a rather large percentage of the prompt emission energy. The prompt emission fluence as measured by BAT is F_{BAT} = 4.7 10^{-7} erg cm^{-2} while F_{XRT}= 1.7 10^{-6} erg cm^{-2}, F_{Flare} (750 s) = 1.43 10^{-6} erg cm^{-2} and F_{Flare} (75000 s) = 2.21 10^{-7} erg cm^{-2} The first big flare has a Fluence that is about 85% of the whole XRT light curve Fluence and larger than that of the prompt emission. The flares can not be a consequence of the initial trigger but rather due to new bursts in the central engine.

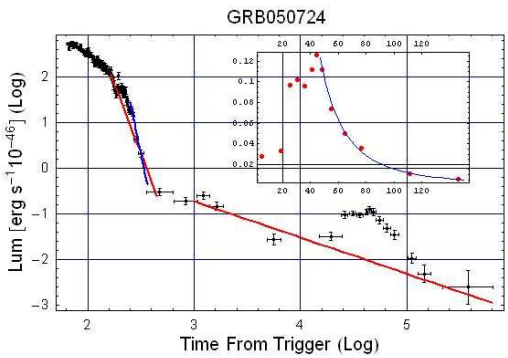

Fig. 5. The morphology of the late flare in the short GRB050724 is exactly the same as the morphology of the flare observed in long bursts and characteristics of the clash of relativistic shells. The slope of the decaying part of the flare, after subtracting the main light curve – red line in the figure, is α = -2.75 where the time is referred to the BAT trigger time. Note that in the inset graph, linear coordinates, the time is given in seconds/1000 and the Luminosity (ordinates) in 10^{-46} erg s^{-1}. The following data refer to the rest frame: BAT (15 -350 keV, Δt = 0.79 s) emission = 1.1 10^{50} erg; XRT (0.2-10 keV, Δt = 65 – 376456 s)=4.1 10^{50} erg, first flare at about 220 s RF_Fluence = 1.47 10^{49} erg, large flare at about 50000 s RF_Fluence = 6.03 10^{49}. For more details see Campana et al. in preparation.

What is striking is that the same flare structure has been observed in the long burst at high z, GRB050904 (Tagliaferri et al. 2005, Cusumano et al. 2005 and references therein) and in the only short burst, GRB050724, for which we were able to observe a detailed X ray light curve. In Fig. 5 we show in the inset the late flare with its power law decay. These observations show that flares may occur in any type of burst at any time along the light curve. This flare at about 40000 seconds (about ½ a day) clearly show that in the short bursts (as we have seen in the long bursts) the central engine must remain active for a long time and that a similar mechanism must be at work. The decay time is rather long.

This is striking if we consider the differences between the progenitor and the parent population of short and long bursts. While long bursts are the end result of the fast collapse of a very massive star (Woosley S.E. 1993), and these are generally located in star forming late type galaxies, Bloom et al. (2002), Le Floch et al. (2003) evidence is now building up that the progenitors of the short bursts are merging relativistic binaries clearly generated by an older parent population. The break through came with the Swift observations of GRB050509B (Gehrels et al. 2005), since for the first time it has been possible to get an accurate position, based on a total of 11 photons we got in the first 1640 seconds of integration time, with the XRT telescope which started to acquire data 62 seconds after the trigger. The observations we obtained with the VLT (but we had also unpublished images with the TNG), see Fig. 1 in Gehrels et al. (2005), had in the XRT error circle the outskirt of a E1 galaxy (likely the host of the short GRB) and a large number of faint background galaxies. The E1 being the II brightest galaxy of a cluster of galaxies. This interpretation seemed to fit with the coalescence model of relativistic stars (NS-NS, NS – BH). GRB050724 fully confirmed this interpretation with the detection of the afterglow near a rather bright elliptical galaxy (Barthelemy et al. 2005, Berger et al. 2005).

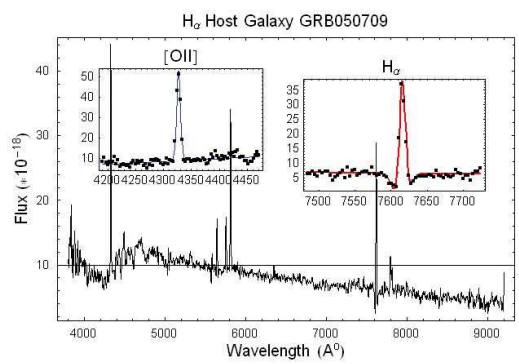

Fig. 6. Spectrum of the Host Galaxy of GRB050709. The star formation rate derived from H_α emission: SFR=0.13 $M_\odot$ / yr. The Balmer line clearly show the emission in the center of a rather broad absorption line. The [OII] nebular doublet is shown here only for comparison.

GRB050709 has been detected by HETE and the optical afterglow imaged by Hijorth et al. (2005) and later by Covino et al. (2005) with the ESO VLT. In this case the host galaxy is a blue dwarf irregular (Fox et al. 2005), and the spectrum (Covino et al. 2005), shows evidence of star formation activity, emission lines are clearly detected. Most interesting there is also evidence of a stellar population of type A as clearly indicated by the Balmer absorption line visible in the spectrum, Fig. 6. This means that the galaxy had a starburst about 5 10^9 ago. It is misleading to associate the presence of the short GRB to a star forming galaxy but rather it is associated with an old starburst the

galaxy had long ago. In other words we do not expect in the galaxy population of the GRB050709 the presence of very massive stars. We conclude that the long and short bursts have different progenitors and different parent population and occur in different environments.

The high z GRB050904 has been observed with XRT immediately after the trigger and, as shown in Fig. 7,

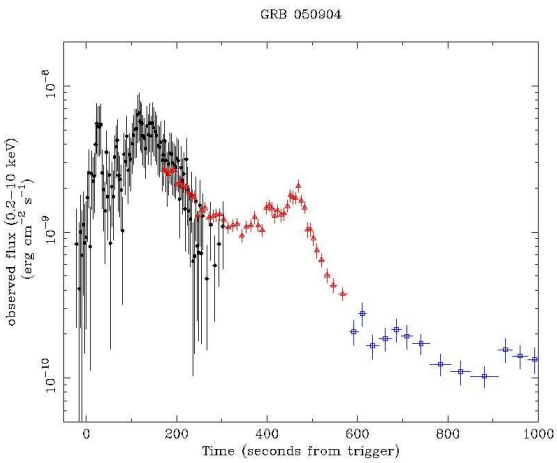

Fig. 7. The first set of observations have been obtained with the BAT telescope while the flare, second burst, has been detected by the XRT Telescope. The slope of the power law decay in the rest frame is $\alpha = -2.14$.

we have an important overlap between the data obtained by BAT and those obtained by XRT. It may clarify, but we will have more statistics in the following months, the morphology of the Type I light curves. The BAT light curve continue smoothly into the XRT light curve and the rest frame slope is in agreement with the slope generally observed in the soft X ray afterglow, $\propto t^{-2.14}$ in the rest frame. There is continuity between BAT and XRT (BAT is sensitive

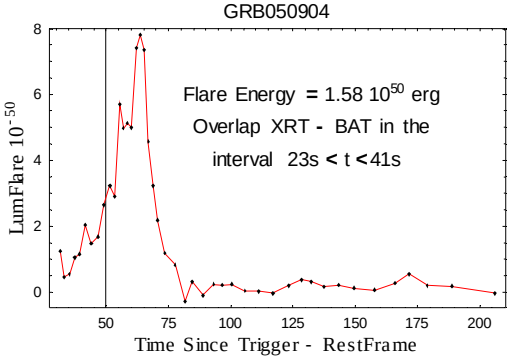

Fig. 8. The First Flare, Luminosity versus time, of the XRT light curve of GRB050904, see Fig. 6, in rest frame coordinates. Note also in this case the rapid decay and however a less rapid rise to maximum that could be due irregular energy injection however.

down to the 15 – 25 keV band, what we generally call the soft channel band) and simply shows how the internal shock decays and continue with the emission of the afterglow (external shock). On the other hand it is not clear when exactly is the external shock emission beginning.

For completeness we also show in Fig. 8 the GRB050904 flare. Whether or not the flare activity is different in high z flares, at z > 6 we expect to have stars and ISM with a very low metal abundance, as to be determined. For this only GRB we observed at very high z a peculiarity my be the very high flare activity we observe during the mild decay following the first phase of the light curve where the slope is sensibly higher.

To summarize the morphology we discussed for long bursts, morphology that seems to be similar to that of the light curves of short bursts, referring to GRB050724 that however is the only case observed and has a type I morphology and missed break, we reproduce the light curve of GRB050822 that include all of the characteristics we have described.

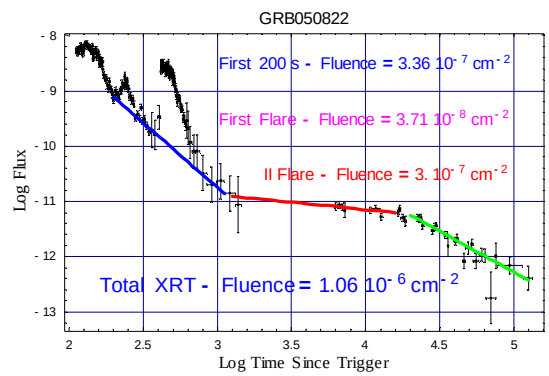

Fig. 9. Following the early maximum the light curve shows a first phase, slope -2.34, followed by a milder decay, slope -0.27 steeping to a -1.48 slope in the late phase. Superimposed to this type I light curve we have two big flares.

ACKNOWLEDGMENTS.

We would like to thank Dino Fugazza for helping with the manuscript. The work is supported in Italy by funding from ASI on contract number I/R/039/04, at Penn State by NASA contract NAS5-00136 and at the University of Leicester by PPARC contract number PPA/G/S/00524 and PPA/Z/S/2003/00507. We acknowledge in particular all those member of the Swift Team at large who made this mission possible. This goes from the building of the hardware, the writing of the software, the operation at the Mission Operation Centre and the performance of the ASI ground segment at Malindi, Kenya.

REFERENCES

Barthelemy, S.D., Cannizzo, H.K., Gehrels, N., et al. 2005 in preparation
Bartyhelemy, S., Chincarini, G., Burrows, D.N., et al. 2005 Submitted to Nature
Berger, E., Price, P.A., Cenko, S.B., et al. 2005, Astro-ph
Bloom, J.SD., Kulkarni, S.R. and Djorgovski, S.G., 2002, Ap. J. 123, 1111
Burrows, D.N., Romano, P., Falcone, A. Et al. 2005, Science, 309, 1833
Capalbi, M., Perri, M., Malesani, D., et al. In preparation
Chincarini, G., Moretti, A., Romano, P., et al. 2005, astro-ph 0506453
Falcone, A.D., Burrows, D.N., Lazzati, D., et al., 2005, submitted ApJ
Fox, D. B., Frail, D. A., Price, P. A., et al. 2005, Astro-ph 0510110
Gehrels, N., Chincarini, G., Giommi, P., et al. ApJ, 611, 1005
Gehrels, N., Sarazin, C.L., O'Brien, P.T. et al., 2005, Nature 437, 851
Guetta, D. & Piran, T., 2005, A&A, 435, 421
Cummings, J., Angelini,L., Barthelemy, S., et al. 2005, GCN3910
Cusumano,G., Mangano, V., Chincarini, G., et al. 2003, Nature submitted (astro-ph 0509737)
Hijorth, J., Watson, D. , Fynbo, J.P.U. et al. 2005, Nature 437, 859
Hurley, K., Sari, R., Djorgovski,S. G., 2002, Astro-ph 0211620
Kobayashi, S., Piran, T. And Sari, R., 1997, ApJ 490, 92
Kumar, P. And Panaitescu, A., 2000, Ap.J., 541, L51
Le Floch, E., Duc, P.-A., Mirabel, I.F. 2003, A and A 400, 499
Meszaros,P. & Rees, M. J. 1993, ApJ 405, 278
Nousek, J. Kouveliotou, C., Grupe, D. et al. 2005 ApJ submitted (astro-ph 0508332)
Romano, P., Moretti, A., Banat, P.L. et al. 2005, submitted to A&A
Piran,T., 1999, Physics Reports, Volume 314, Issue 6, p. 575-667.
Tagliaferri, G., Antonelli, L.A., and Chincarini, G. et al., 2005, A&A 443, L1
Villasenor, J.S., Lamb, D.Q., Richter, G.R. et al. 2005, Nature and Astro-ph 0510190
Woosley, S. E., 1993, ApJ 405, 273
Zhang, B. and Meszaros, P., 2004, IJMPA, 15, 2385

SWIFT XRT OBSERVATIONS OF X-RAY FLARES IN GRB AFTERGLOWS

David N. Burrows[1], P. Romano[2], O. Godet[3], A. Falcone[1], C. Pagani[1,2], G. Cusumano[4], S. Campana[2], G. Chincarini[2,5], J. E. Hill[1,6], P. Giommi[7], M. R. Goad[3], J. A. Kennea[1], S. Kobayashi[1,8], P. Mészáros[1], J. A. Nousek[1], J. P. Osborne[3], P. T. O'Brien[3], K. L. Page[3], G. Tagliaferri[2], B. Zhang[9], and the Swift XRT team[10]

[1]Department of Astronomy & Astrophysics, 525 Davey Lab., Penn. State University, University Park, PA 16802, USA
[2]INAF-Osservatorio Astronomico di Brera, Via Bianchi 46, 23807 Merate, Italy
[3]Department of Physics and Astronomy, University of Leicester, Leicester LE1 7RH, UK
[4]INAF-Istituto di Astrofisica Spaziale e Fisica Cosmica, Via Ugo La Malfa 153, 90146 Palermo, Italy
[5]Università degli studi di Milano-Bicocca, Dipartimento di Fisica, Piazza delle Scienze 3, I-20126 Milan, Italy
[6]NASA-Goddard Space Flight Center / Universities Space Research Assocation
[7]ASI Science Data Center, via Galileo Galilei, 00044 Frascati, Italy
[8]Astrophysics Research Institute, Liverpool John Moores University, Birkenhead CH41 1LD, UK
[9]Department of Physics, University of Nevada, Box 454002, Las Vegas, NV, 89154-4002, USA

ABSTRACT

The Swift XRT has been observing GRB afterglows since December 23, 2004. Three-quarters of these observations begin within 300 s of the burst onset, providing an unprecendented look at the behavior of X-ray emission from GRB afterglows in the first few hours after the burst. While most of the early afterglows have smoothly declining lightcurves, a substantial fraction has large X-ray flares on short time-scales. We suggest that these flares provide support for models with extended central engine activity producing late-time internal shocks.

Key words: GRBs; Swift; X-rays; afterglow.

1. INTRODUCTION

The Swift Explorer mission (Gehrels et al., 2004) was launched on November 20, 2004. It is detecting two bursts per week on average, and following these up with detailed optical/UV and X-ray observations. In 75% of the bursts, the spacecraft can slew immediately to the field and observations with the X-ray Telescope (XRT; Burrows et al., 2005a) begin within 5 minutes of the GRB trigger (in the remaining cases the source is too close to the Earth, Moon, or Sun and XRT observations are delayed). While early X-ray observations are available for a handful of previous bursts (e.g., see Piro et al., 2005), the large number of these observations made available by Swift is revolutionizing our knowledge base of early GRB X-ray afterglows. At the time of this writing (31 October 2005), the XRT has detected 67 X-ray afterglows of GRBs (exceeding the total pre-Swift afterglow sample), 51 of which were observed within 300 s of the trigger.

Here we discuss the discovery of X-ray flares, commonly seen during the first several hours after the burst. These flares are seen in approximately 50% of all GRBs, and cover a range of time-scales and intensities. This paper will highlight some of the key findings that led us to the conclusion that the flares are produced by extended central engine activity producing X-rays from internal shocks at times long after the cessation of hard X-ray/gamma-ray emission.

2. GRB 050406

Although in retrospect, the first flare observed by the XRT was probably in GRB 050219A (Tagliaferri et al., 2005; Goad et al., 2005), the first clear-cut example was GRB 050406 (Romano et al., 2005; Burrows et al., 2005b). The X-ray light curve of GRB 050406 is shown in Figure 1. There is a strong flare peaking at about 210 s after the BAT trigger, which rises above the underlying power-law decay by a factor of 6. The rapid power-law decay in the first 1000 s has a decay index of 1.58 ± 0.17. At about 4400 s the light curve breaks to a flatter decay index of $0.50^{+0.14}_{-0.13}$ (Romano et al., 2005). When the underlying decay is subtracted, the flare itself peaks at 213 s and has rise/fall rates (expressed as power-law indices) of ± 6.8. The flare can also be fitted as a Gaussian, in which case the width is $17.9^{+12.3}_{-4.6}$ s, and $\delta t/t_{peak} \sim 0.2 \ll 1$, where we take δt = FWHM of the Gaussian = $42.2^{+29.0}_{-10.8}$ s.

The light curve of the flare can be obtained in two energy

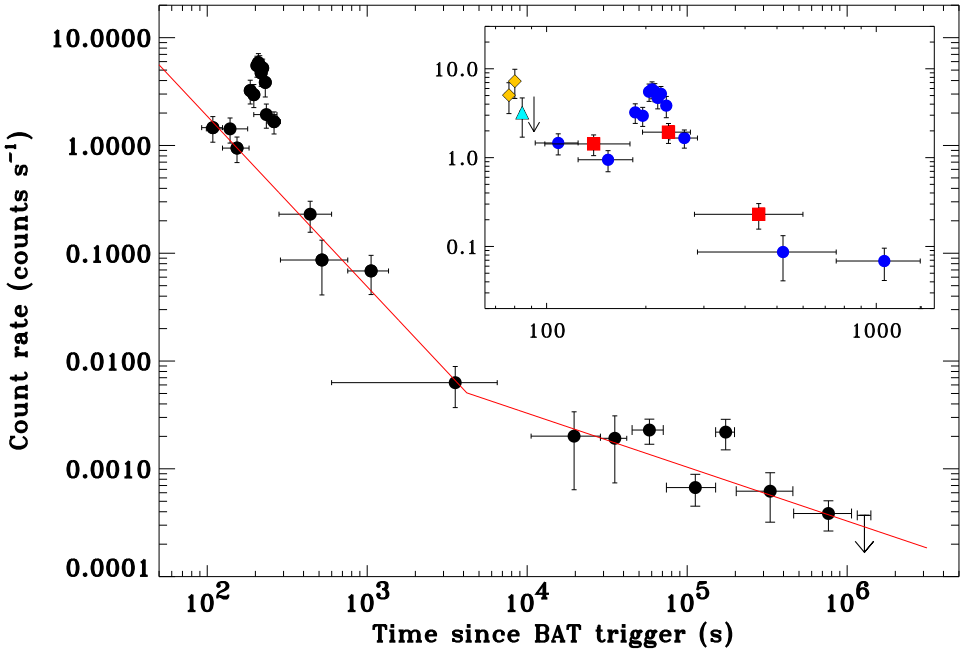

Figure 1. Background-subtracted X-ray light curve of GRB 050406 (0.2-10 keV). The red solid line shows the best-fit broken power-law model for the points excluding the flare at about 210 s. The inset shows details of the first 1000 s. Yellow diamonds are data taken in Photodiode (PD) mode, the cyan triangle is from the Image (IM) mode frame, the blue circles are from Windowed Timing (WT) mode data, and the red squares are Photon-Counting (PC) mode (see Hill et al., 2004). For details of the data processing and analysis, see Romano et al. (2005).

bands to allow a search for spectral variations. Figure 2 shows the light curve in soft and hard bands, as well as the ratio of the hard to soft bands. The flare begins in the hard band, softening significantly as it decays. This is similar to the behavior typically seen in the prompt gamma-ray emission from GRBs, and in particular, seen in the prompt emission from this burst.

To reiterate, the key features seen in this flare are:

- Underlying afterglow consistent with a single slope before and after the flare.
- Flare increases by factor of 6.
- $\delta t/t \ll 1$ for both the rising and falling sides of the flare.
- Flare softens as it progresses.

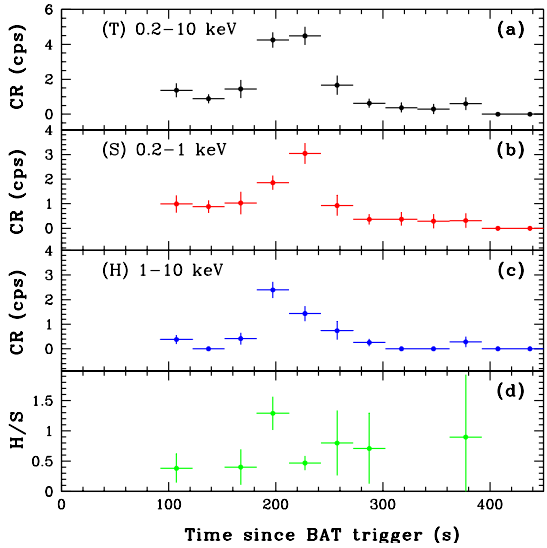

Figure 2. Background-subtracted X-ray light curves of the GRB 050406 flare. (a) Total intensity (0.2-10 keV). (b) Soft band (0.2-1.0 keV). (c) Hard band (1.0-10 keV). (d) Band ratio (H/S). Note that the hard band peaks before the soft band; this is also reflected in the band ratio, which is quite hard at the onset of the flare. For details of the data processing and analysis, see Romano et al. (2005).

3. GRB 050421

The XRT observations of GRB 050421 show a large flare and a small flare superposed on a single power-law decay with a decay index of 3.1 ± 0.1 (Figure 3). Although not as well sampled as GRB 050406, primarily due to the extremely rapid rise and fall of this flare, the X-ray light curve can be well-modelled as a single power-law decay with two Gaussian flares superposed. The stronger flare peaks at $111 \pm 2s$ and has an extremely steep rise and

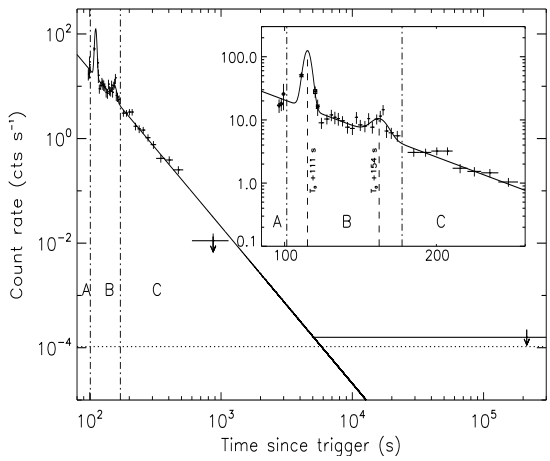

Figure 3. Background-subtracted X-ray light curve of GRB 050421 (0.3-10 keV). The solid line shows the best fit model, consisting of a power-law plus two Gaussian flares centered at 110 and 154 seconds post-burst. Data during time period A are in Photodiode (PD) mode (diamonds). Time period B has data in PD mode (square and star), and WT mode. Data in interval C are in PC mode. For details of the data processing and analysis, see Godet et al. (2005).

fall, with $\delta t/t \sim 0.07$ for both the rise and fall times, and increases by a factor of 4 above the underlying power-law decay (Godet et al., 2005).

Salient features of GRB 050421 include:

- Underlying afterglow consistent with a single slope before and after the flare.
- Flare increases by factor of ~ 4.
- $\delta t/t \ll 1$ for both the rising and falling sides of the flare.

4. GRB 050502B

The largest flare seen to date occurred in the light curve of GRB 050502B (Falcone et al., 2005; Burrows et al., 2005b). The X-ray light curve of this burst is shown in Figure 4. The light curve has an enormous flare peaking at about 650 s post-burst, with late-time bumps at about 30,000 s and 700,000 s. The main flare is shown in more detail in Figure 5, where the underlying afterglow is indicated by a solid line, as are power-law fits to the rising and falling parts of the flare, which are extremely steep, with power-law indices of about 9.5. The fluence of the giant X-ray flare, $\sim 9 \times 10^{-7} \mathrm{ergs\ cm^{-2}}$, actually exceeds the fluence ($\sim 8 \times 10^{-7} \mathrm{ergs\ cm^{-2}}$) of the prompt gamma-ray burst detected by the Swift Burst Alert Telescope (Barthelmy et al., 2005a).

As in the case of GRB 050406, we have generated light curves in two energy bands for this burst, shown in Fig-

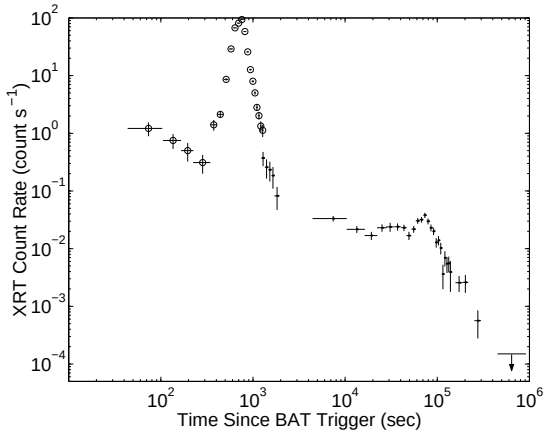

Figure 4. Background-subtracted X-ray light curve of GRB 050502B (0.2-10 keV). Open circles represent WT mode data and dots represent PC mode data. The latter were corrected for pile-up where necessary. For details of the data processing and analysis, see Falcone et al. (2005).

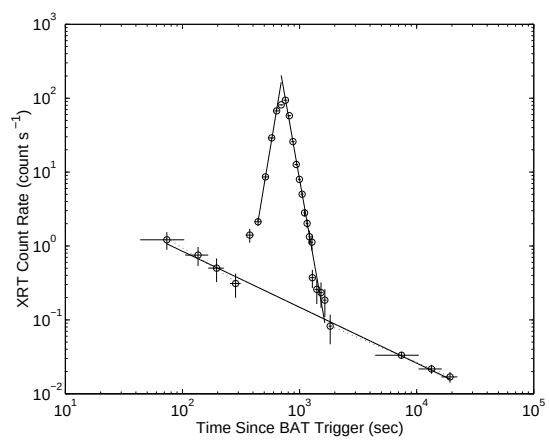

Figure 5. Background-subtracted X-ray light curve of the GRB 050502B flare (0.2-10 keV). The solid lines indicate the underlying afterglow (decay index of 0.8) and fits to the flare rise and decay. For details of the data processing and analysis, see Falcone et al. (2005).

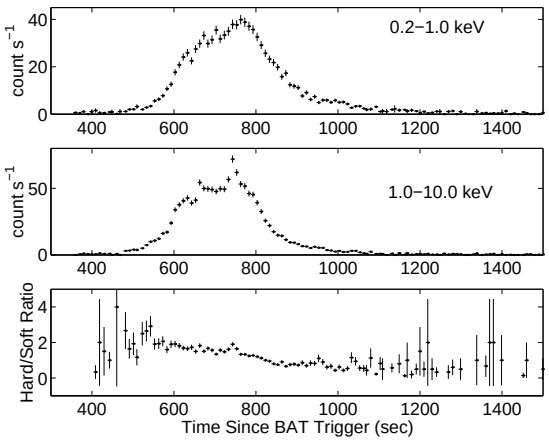

Figure 6. Background-subtracted X-ray light curves of the GRB 050502B flare. Top: Soft band (0.2-1.0 keV). Middle: Hard band (1.0 - 10 keV). Bottom: H/S band ratio. Like GRB 050406, the beginning of the flare is significantly harder than the preceeding afterflow, and the flare softens as it evolves, eventually ending up with a band ratio similar to the pre- and post-flare afterglow. For details of the data processing and analysis, see Falcone et al. (2005).

ure 6. The flare is significantly harder than the pre- or post-flare afterglow, and softens gradually as it evolves, with the hard band decaying much faster than the soft band. We note that there is rapid variability in the hard band at about 750 s.

The key features of this flare are:

- Underlying afterglow consistent with a single slope before and after the flare.
- Flare increases by factor of 500.
- $\delta t/t < 1$ for both the rising and falling sides of the flare.
- $\delta t/t \ll 1$ for the spike at the peak of the hard band.
- Flare softens as it progresses.

5. GRB 050607

The X-ray light curve of GRB 050607 is shown in Figure 7. Two flares are superposed on an underlying power-law decay (index 0.58 ± 0.07 until about 12 ks post-burst) in the first 500 s post-burst. In this case, we do not measure the afterglow intensity before the first flare, which may already be in progress when the XRT begins collecting data. The BAT data points have been extrapolated into the XRT band using two different spectral models, showing that they are at least roughly consistent with the XRT flux at about 100 s.

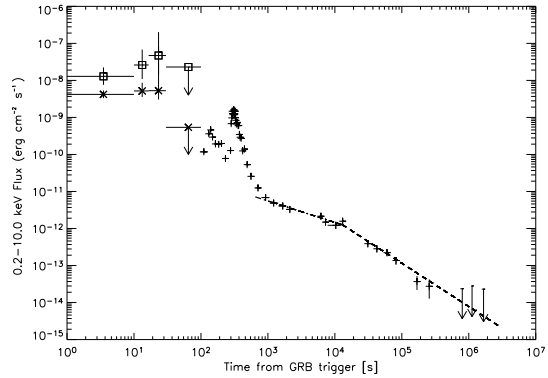

Figure 7. Background-subtracted X-ray light curve of GRB 050607 (0.2-10 keV). This light curve includes two different extrapolations of BAT data points into the XRT energy band (points before 100 s). The points after 100 s are XRT data, corrected for pile-up where necessary. The best-fit broken power-law is shown by the dashed and dash-dot lines. This light curve has two early flares. For details of the data processing and analysis, see Pagani et al. (2005).

The main flare, which peaks at about 310 s, has a total fluence about 16% of the BAT prompt fluence. The rising portion of this flare is extremely steep, with a power-law slope of about 16 when referred to the BAT trigger, or about 2.5 when referred to the beginning of the flare itself, and $\delta t/t \sim 0.2$. The decay following the flare is less steep; this flare is less symmetrical than the other examples presented here.

We have produced light curves in two energy bands to examine spectral variations during the flare (Figure 8). As in previous cases, the hard band rises faster than the soft band and also decays faster, resulting in an increase in hardness ratio at the beginning of the flare and a gradual decrease as the flare evolves and decays. Note that these statements are true for *both* flares.

Salient features of these flares include:

- Two flares in first 500 s.
- Main flare increases by factor of ~ 20.
- $\delta t/t \ll 1$ for the rising side of the flares.
- $\delta t/t < 1$ for the falling side of the flares.
- Both flares soften as they progress.

6. GRB 050730

This remarkable light curve (Figure 9) shows at least three successive flares of comparable magnitude (factor of 3–4) and durations ($\sim 200\ s$). Furthermore, substantial flaring and variability continue in this light curve out to times of at least 35 ks in the observer's frame.

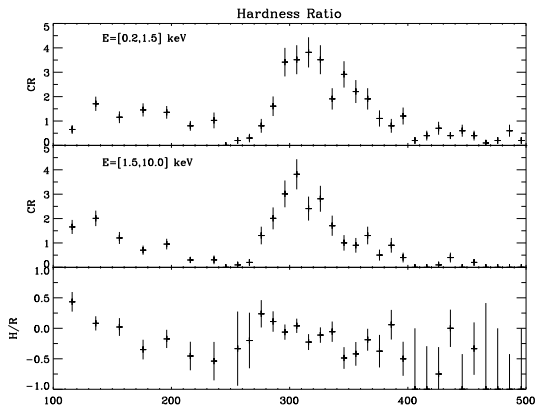

Figure 8. Background-subtracted X-ray light curves of GRB 050607. The top panel shows the soft (S) band light curve (0.2-1.5 keV in this case), the middle panel shows the hard (H) band (1.5 - 10 keV), and the bottom panel shows the hardness ratio, defined as (H-S)/(H+S). For details of the data processing and analysis, see Pagani et al. (2005).

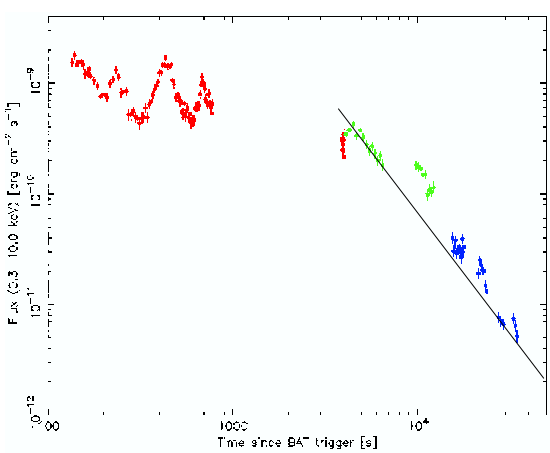

Figure 9. Background-subtracted X-ray light curve of GRB 050730 (0.3-10 keV). A possible underlying power-law decay after the first hour is indicated by the solid line. However, the variability throughout this light curve is so large that it is difficult (or impossible) to establish the level or slope of the afterglow contribution with certainty.

7. DISCUSSION

The flares discussed in the preceding sections have several features in common, which collectively point to an emission mechanism associated with internal shocks in the GRB jet:

- Rapid rise and fall times, with $\delta t/t_{peak} \ll 1$. It is very difficult to obtain rapid variability in the external shock, since the radiation physics of the shock results in decay time constants no faster than $\delta t/t_{peak} \sim 1$ (Ioka et al., 2005). Possible mechanisms associated with the internal shocks and jet for these rapid variations include extended central engine activity, anisotropic jets, or a jet comprised of many "mini-jets" (Ioka et al., 2005).
- Many light curves have evidence for the same afterglow intensity and slope before and after the flares (see Osborne et al., 2005, for a counterexample). This argues against energy injection into the external shock by the flare, as would be expected if the flare were associated with the external shock.
- Multiple early flares (at least 3 for GRB 050730) argue against one-shot explanations like the beginning of the afterglow.
- Large flux increases (factors of tens to hundreds) are incompatible with origins related to the Synchrotron Self-Compton mechanism in the reverse shock (Kobayashi et al., 2005).
- Flares typically soften as they progress. This is very reminiscent of the behavior of the prompt emission.

Our conclusion is that the most likely explanation, which seems to account for all of these observed features of the x-ray flares, is that they are caused by internal shocks similar to those that produce the prompt emission, but with lower resultant photon energies. The lower energies are a natural consequence of the late times (and corresponding large radii) at which these flares are observed.

This conclusion requires extended activity by the central engine at times long after the cessation of the prompt gamma-ray emission. This points in turn to a mechanism like fall-back of material into the new black hole whose formation caused the GRB, as discussed by MacFadyen, Woosley, & Heger (2001) and King et al. (2005).

More extensive discussions can be found in Nousek et al. (2005), Zhang et al. (2005), and Panaitescu et al. (2005).

8. GRB 050904

We now consider the case of GRB 050904, the highest redshift GRB found to date. The X-ray lightcurve of this burst is shown in Figure 10. The XRT light curve shows

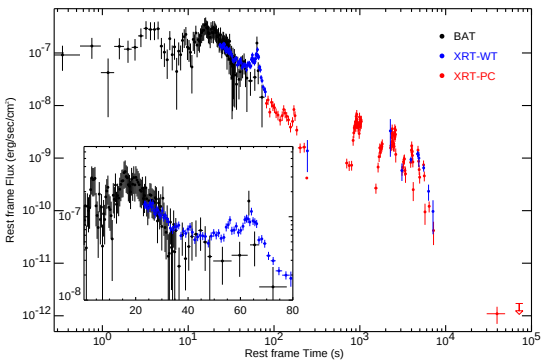

Figure 10. Background-subtracted X-ray light curve of GRB 050904, transformed into the rest frame for z=6.29. The plot shows the BAT light curve, extrapolated into the XRT energy range (black points, from 0-75 s) superposed on the XRT light curve (20-10,000 s). There is substantial overlap in this case between the BAT and XRT data points, which agree fairly well. For details of the data processing and analysis, see Cusumano et al. (2005).

a spiky flare at about 65 s, with substantial fluctuations in count rate extending out to nearly 10 ks in the rest frame of the burst.

Soft and hard band light curves for GRB 050904 are shown in Figure 11. Unlike previous examples, the band ratio declines steadily during the first 80 s of the XRT data, but then remains low during the late-time variability, when the XRT count rate is varying by an order of magnitude or more.

This light curve exhibits several differences to those discussed in previous sections:

- Flaring seems to occur predominantly at much later times (thousands rather than hundreds of seconds).
- The late flares exhibit no spectral variability, in stark contrast to the flares discussed above.

It is not clear at this time whether the differences between the flaring activity in GRB 050904 and the bursts discussed above is related to the high redshift of GRB 050904, although it seems quite premature to suggest this on the basis of a single example. Observations of additional flares, including additional high redshift cases, will undoubtedly shed light on this over the next year.

9. GRB 050724

We conclude by briefly mentioning the short GRB 050724 (Figure 12). Unlike the short GRBs 050509B (Gehrels et al., 2005) and 050813 (Fox et al., 2005), which were very faint in X-rays and exhibited power-law decays until they disappeared, the X-ray light curve of GRB 050724 is bright, complex, and has several

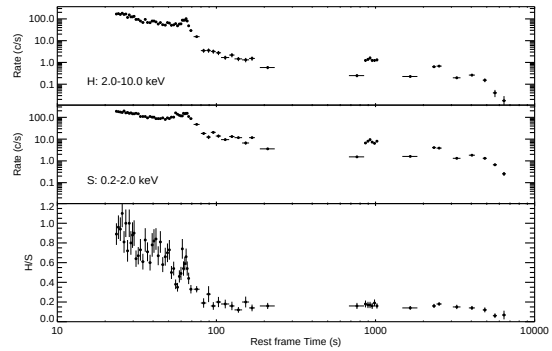

Figure 11. Background-subtracted X-ray light curves of GRB 050904, transformed into the rest frame for z=6.29. The upper panel shows the hard (H) band (2-10 keV in this case), the middle panel shows the soft (S) band (0.2-2 keV), and the lower panel shows the band ratio (H/S). For details of the data processing and analysis, see Cusumano et al. (2005).

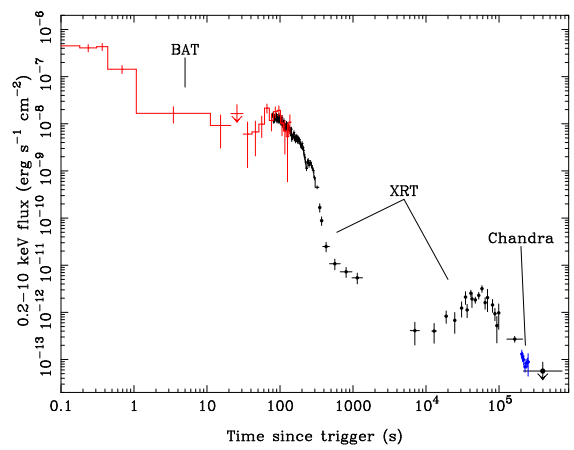

Figure 12. Background-subtracted X-ray light curve of GRB 050724, showing BAT data extrapolated into the XRT band, XRT data, and Chandra data. For details of the data processing and analysis, see Barthelmy et al. (2005b).

flare-like features. The optical and X-ray afterglows of this burst are clearly associated with an elliptical galaxy (Barthelmy et al., 2005b), making it very likely that the GRB was the result of a compact object merger. How then, in the rarified environment of a compact binary system in the outskirts of an elliptical galaxy, can the central engine produce flares and bumps at the late times seen in this light curve? One possibility is a neutron star-black hole merger. It is possible in such a system, given the right initial conditions, for the black hole to shred the neutron star, resulting in a lengthy period of in-fall into the black hole from the shredded remnants of the neutron star.

10. CONCLUSIONS

Observations of GRBs by the Swift XRT have shown that flaring is very common in X-ray light curves of GRBs and their afterglows. It seems likely that these flares result from extended central engine activity, pointing toward a much longer period of activity than expected on the basis of gamma-ray observations of prompt emission. Further progress in this area will undoubtedly result from statistical studies now underway of the properties of flares as an ensemble. Ultimately, we expect these observational results to lead to improved theoretical models of black hole formation and GRB central engines.

ACKNOWLEDGMENTS

This work is supported at Penn State by NASA contract NAS5-00136; at the University of Leicester by the Particle Physics and Astronomy Research Council under grant numbers PPA/G/S/00524 and PPA/Z/S/2003/00507; and at OAB by funding from ASI under grant number I/R/039/04.

REFERENCES

Barthelmy, S., et al. 2005a, Space Science Rev., in press (astro-ph/0507410)

Barthelmy, S., et al. 2005b, Nature, in press

Burrows, D. N., et al. 2005a, Space Science Rev., in press (astro-ph/0508071)

Burrows, D. N., et al. 2005b, Science, 309, 1833

Cusumano, G., et al. 2005, Nature, submitted (astro-ph/0509737)

Falcone, A., et al. 2005, ApJ, submitted

Fox, D., et al. 2005, in preparation

Gehrels, N., et al. 2004, ApJ, 611, 1005

Gehrels, N., et al. 2005, Nature, 437, 851

Goad, M., et al. 2005, A&A, submitted

Godet, O., et al. 2005, A&A, submitted

Hill, J. E., et al. 2004, Proc. SPIE, 5165, 217

Ioka, K., Kobayashi, S., & Zhang, B. 2005, ApJ, 631, 429

King, A., ApJ, 630, L113

Kobayashi, S., Zhang, B., Mészáros, P., & Burrows, D. N. 2005, ApJ, submitted, (astro-ph/0506157)

MacFadyen, A. I., Woosley, S. E., & Heger, A., ApJ, 550, 410

Nousek, J. A., et al. 2005, ApJ, submitted (astro-ph/0508332)

Osborne, J. P., et al. 2005, in preparation

Pagani, C., et al. 2005, ApJ, submitted

Panaitescu, A., et al. 2005, MNRAS, submitted (astro-ph/0508340)

Piro, L., et al. 2005, ApJ, 623, 314

Romano, P., et al. 2005, A&A, submitted

Tagliaferri, G., et al. 2005, Nature, 436, 985

Zhang, B., et al. 2005, ApJ, submitted (astro-ph/0508321)

GRB 050505: A HIGH REDSHIFT BURST DISCOVERED BY *SWIFT*

C.P. Hurkett, J.P. Osborne, K.L. Page, E. Rol, M.R. Goad, P.T. O'Brien, A. Beardmore, and O. Godet, on behalf of the *Swift* team.

XROA Group, Dept. of Physics & Astronomy, University of Leicester, Leicester LE1 7RH, UK.

ABSTRACT

We report the discovery by the *Swift* satellite, and subsequent multi-wavelength afterglow behaviour, of the high redshift (z = 4.27) Gamma Ray Burst GRB 050505. This burst is the third most distant burst discovered after GRB 000131 (z = 4.50) and GRB 050904 (z = 6.29). GRB 050505 is a long GRB with a multipeaked γ-ray light curve of T_{90} = 63±2 s and an inferred isotropic release in γ-rays of $\sim 1.45\times10^{53}$ ergs, placing it at the lower end of the long burst E_{iso} distribution. The *Swift* X-Ray Telescope followed the afterglow for 14 days, detecting two breaks in the light curve at $7.4^{+1.5}_{-1.5}$ ks and $58.0^{+9.9}_{-15.4}$ ks after the burst trigger. The powerlaw decay slopes before, between and after these breaks were $0.25^{+0.16}_{-0.17}$, $1.17^{+0.08}_{-0.09}$ and $1.97^{+0.27}_{-0.28}$ respectively. The X-ray afterglow shows no spectral variation over the course of the *Swift* observations, being well fit with a single powerlaw of photon index ∼1.90. This behaviour is expected for the cessation of continued energisation of the ISM shock followed by either a jet break or a break caused by the presence of a structured jet. Neither break is consistent with a cooling break. There is significant absorption in excess of that due to our Galaxy.

Key words: gamma-rays: bursts; gamma-rays: observations; galaxies: high redshift; galaxies: ISM.

1. INTRODUCTION

Gamma Ray Bursts (GRBs) are expected to be visible over a large range of redshifts with a potential upper limit of z ∼15-20 (Lamb & Reichart 2000). The lowest recorded GRB redshift to date is GRB 980425 with z = 0.0085±0.0002 (Tinney et al. 1998), whilst the highest is GRB 050904 at z=6.29±0.01 (Kawai et al. 2005). Bursts at high redshift are potentially important since they can be powerful probes of the early Universe. They allow us to probe the intervening matter between the observer and GRB, and particularly the conditions of their host galaxies (e.g. Vreeswijk et al. 2004).

So far, only ∼50 bursts have a firm redshift determination, mostly obtained through spectroscopy of their optical afterglow. The record holder is GRB 050904, but this is so recent that data on it are still being collected. Previously the highest redshift burst was GRB 000131 (Andersen et al. 2000). Unfortunately *BATSE* detected GRB 000131 during a partial data gap (Kippen 2000) so its position was not localised until 56 hours after the trigger, thus its early time behaviour is unknown. No breaks were directly observed in the light curve for GRB 000131 but, based on the spectral index, an upper limit on the jet break time of <3.5 days has been hypothesised (Andersen et al. 2000). In contrast, the rapid position dissemination for GRB 050505 allowed a rapid redshift determination, and its automated follow-up program provided a well-covered X-ray afterglow light curve. Here we present the results from *Swift* (Gehrels et al. 2004) on GRB 050505, which is shown to be a relatively weak burst.

2. *SWIFT* OBSERVATIONS OF GRB 050505.

At 23:22:21 UT on the 5th of May 2005, the *Swift* Burst Alert Telescope (BAT; Barthelmy 2005) triggered and located GRB 050505 on-board (trigger ID 117504; Hurkett et al. 2005a). The BAT mask-weighted light curve (see Fig 1) shows a multi-peaked structure with a T_{90} (15-350 keV) of 63 ± 2 seconds.

The T_{90} 15-150 keV BAT spectrum was adequately fit by a single powerlaw with a photon index = 1.56 ± 0.12 (with χ^2/DOF = 48/56) and a mean flux over T_{90} of $(6.44^{+0.42}_{-1.54})\times10^{-8}$ ergs cm^{-2} s^{-1} in the 15-350 keV range and $(3.76^{+0.21}_{-0.69})\times10^{-8}$ ergs cm^{-2} s^{-1} in the 15-150 keV range. All errors in this paper are quoted at 90% confidence unless otherwise stated. Whilst fitting a cutoff powerlaw does not give a significantly better fit (χ^2/DOF = 45/55) it does provide us with an indication of the $E_{\rm peak}$ for this burst. We find a photon index = $1.02^{+0.51}_{-0.57}$ and a lower limit of $E_{\rm peak} > 52$ keV.

Swift executed an automated slew to the BAT position and the X-Ray Telescope (XRT; Burrows et al. 2005) began taking data ∼47 minutes after the burst trigger. The delay

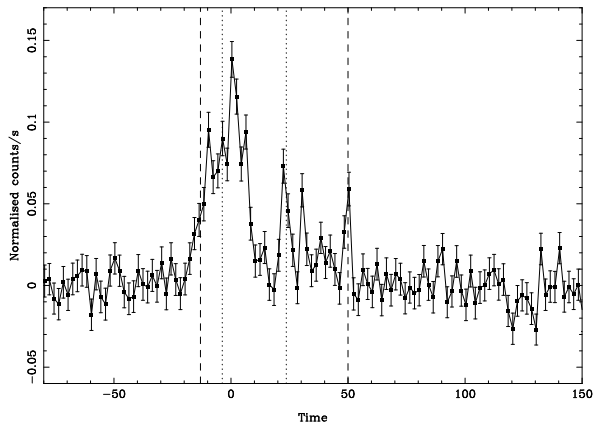

Figure 1. The BAT mask weighted light curve (15-350 keV), where T=0 is the trigger time. Vertical lines indicate the T_{90} (dashed) and T_{50} (dotted) intervals.

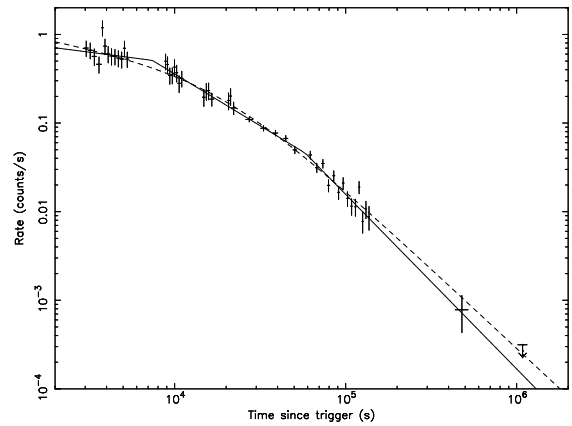

Figure 2. Light curve of GRB 050505 fit to a doubly broken powerlaw (solid line) and smoothly broken powerlaw (dashed line). Doubly broken powerlaw parameters (see §2.1): $\alpha_1 = 0.25^{+0.16}_{-0.17}$, $\alpha_2 = 1.17^{+0.08}_{-0.09}$ and $\alpha_3 = 1.97^{+0.27}_{-0.28}$, with breaks at $t_1 = 7.4^{+1.5}_{-1.5}$ ks (observer's frame) and $t_2 = 58^{+9.9}_{-15.4}$ ks. Smoothly broken powerlaw parameters: $\alpha_1 = 0.37^{+0.13}_{-0.15}$ and $\alpha_2 = 1.80^{+0.16}_{-0.16}$, which breaks at $t = 18.5^{+4.4}_{-3.2}$ ks (observer's frame), with a smoothing parameter = 1.0. It should be noted that the final point on the light curve is the upper limit to the detection of the afterglow at that time.

in the spacecraft slew was due to an Earth limb observing constraint. Ground processing revealed an uncatalogued X-ray source within the BAT error circle located at RA, Dec = 09:27:03.2, +30:16:21.5 (J2000) with an estimated uncertainty of 6 arcseconds radius (90% containment; Kennea et al. 2005).

Observations continued over the next 14 days, though the X-ray afterglow was not detected after the 6th day. Co-adding the final 8 days of observations produced a total of 58ks of data providing an upper limit of 3.5×10^{-4} counts s^{-1}, consistent with the extrapolated decay (see § 2.1).

The *Swift* Ultra-Violet/Optical Telescope (UVOT; Roming et al. 2005) observed the field starting at ∼47 minutes after the burst trigger. The initial data were limited to one 100 second exposure in each of the four filters. No new sources were found in the XRT error circle to limiting magnitudes (5σ in 6 arcsecond radius apertures) of $V > 17.7$, $U > 18.4$, $UVW1 > 18.9$ and $UVM2 > 19.7$. Additional co-added, deeper exposures (∼2000 s) with the UVOT also failed to detect an optical counterpart at the location of the GRB (Rosen et al. 2005). The deeper exposure in V placed a limiting magnitude for the source at > 20.35 (3σ confidence level) for a total exposure of 2527 s coadded from a series of short exposures over T+2807 s to T+28543 s.

2.1. X-ray Light curve and Spectral Analysis.

In PC mode the XRT suffers from pile-up when the count-rate is $\geq$ 0.8 counts/s (Vaughan et al. 2005). See Hurkett et al. (2005b) for details of the pile-up correction method.

The X-ray light curve of GRB 050505 is shown in Fig 2. We characterise the behaviour of the XRT flux in terms of the standard powerlaw indices $f \propto \nu^{-\beta} t^{-\alpha}$. A single powerlaw was rejected since it gave an unacceptable value of χ^2/DOF = 122.5/46.

'Broken' and 'doubly broken' powerlaws were also fitted to the data. These models consist of two or three (respectively) powerlaw sections whose slopes join but change instantaneously from α_i to α_{i+1} at the break times. A 'broken' powerlaw model is also a poor description of the lightcurve with χ^2/DOF = 58.0/44. A 'doubly broken' powerlaw provides a much better statistical fit to the data with χ^2/DOF = 38.7/42 (> 99.9% improvement over both the simple and the broken powerlaw). The model consists of $\alpha_1 = 0.25^{+0.16}_{-0.17}$, $\alpha_2 = 1.17^{+0.08}_{-0.09}$ and $\alpha_3 = 1.97^{+0.27}_{-0.28}$ with breaks at $t_1 = 7.4^{+1.5}_{-1.5}$ ks and $t_2 = 58^{+9.9}_{-15.4}$ ks.

The 'smoothly broken' powerlaw also consists of two powerlaw sections; however, the transition between these slopes is not instantaneous, but is spread out over several decades in time. This produces a smooth break rather than a sharp break as in the previous models. Typically the values of the smoothing parameter, S, reported in the literature range between 0.5-10, with a value of ∼1 being favoured both observationally and theoretically (Stanek et al. 2005; Beuerman et al. 1990). A larger value of the smoothing parameter gives a sharper break. The light curve of GRB 050505 is well fit by a smoothly broken powerlaw with χ^2/DOF of ∼1.0. Unfortunately there is degeneracy between the smoothing factor and the initial decay index, with any value between 0.5 and 3 producing a good fit to the data (limit of χ^2/DOF = 1.16). However, if we constrain the model parameters so that the intital emission must be decaying and that α_2 equals p, the electron spectral index [calculated from our spectral index, β, (Zhang & Meszaros 2004)], then we find that a smoothing

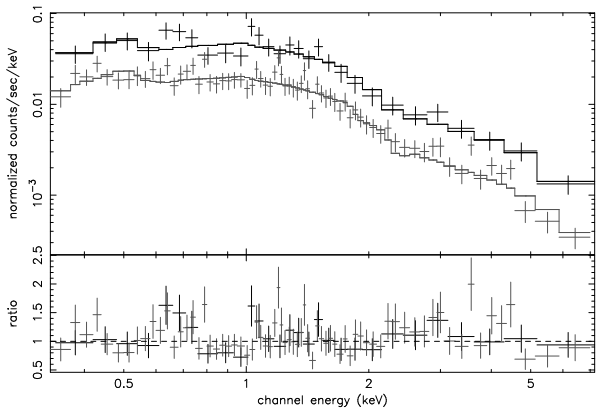

Figure 3. The summed 0.3-10.0 keV (observer's frame) spectrum of GRB 050505 from 'piled up' (black) and 'non piled up' (grey) data, which are consistent with a photon index of ∼1.90, Galactic absorption (2.1×10^{20} cm^{-2}) plus an excess absorption component from the host galaxy (128×10^{20} cm^{-2}).

parameter in the range of 0.5-2 is favoured. This range of smoothing factors produces $\alpha_1 \sim 0.5$; however, these values should be treated with caution. Restricting S to 1.0 we find $\alpha_1 = 0.37^{+0.13}_{-0.15}$, $\alpha_2 = 1.80^{+0.16}_{-0.16}$, $t_{\rm break} = 18.5^{+4.4}_{-3.2}$ ks and χ^2/DOF = 46.9/45 (see Fig 2).

Spectral fits were performed over 0.3-10.0 keV using grade 0-12 events (see Table 1). The spectra were fit with a power law model (see Fig 3) with the absorption, N_H, set at the Galactic column density, and with power law models with excess absorption (either in our Galaxy or the GRB host galaxy).

It is clear from Table 1 that there is no evidence for spectral change over the duration of the observations. It is also clear from the fit to the total data-set that there is significant excess absorption in this spectrum at >99.99% confidence. Statistically both Galactic and extra-galactic absorption fits appear equally likely, however, if the excess absorption were to be due to gas in our Galaxy alone then the value of the excess absorption is almost twice the column density quoted by Dickey and Lockman (1990). Therefore, we conclude that the bulk component of excess absorption must come from the host galaxy with a value of $N_H = 1.28^{+0.61}_{-0.58} \times 10^{22} {\rm cm}^{-2}$ assuming local ISM abundances in the GRB rest frame.

The photon index = $\beta + 1 = 1.90^{+0.08}_{-0.08}$, is typical of the photon indices seen in other GRBs (Preece et al. 2000). With a redshift of 4.27 (Berger et al. 2005) we are measuring the spectrum over a rest-frame range of 1.6-53 keV. The spectrum is well modelled up to such high energies in the rest frame of the GRB, and the photon index is comparable to the values found from low redshift bursts.

3. FOLLOW-UP DETECTIONS OF GRB 050505.

The first reported detection of an optical counterpart for GRB 050505 was made by Cenko et al. (2005a) observing from the Keck I telescope, quickly followed by a measurement of the redshift by the same collaboration (Berger et al. 2005). See Hurkett et al. (2005b) for a summary of all of the optical observations reported on the GCN network as well as data from Faulkes Telescope North, reported there for the first time.

Unfortunately the majority of robotic follow-up missions did not observe GRB 050505 promptly. The sparse nature of this combined data-set naturally limits the knowledge that can be obtained.

4. DISCUSSION

4.1. Physical Origin of the Light curve Break

A 'doubly broken' powerlaw fit contains breaks at $7.4^{+1.5}_{-1.5}$ ks and $58.0^{+9.9}_{-15.4}$ ks in the observer's frame, which translate to T+$1.4^{+0.3}_{-0.3}$ ks and T+$11.0^{+1.9}_{-2.9}$ ks in the rest frame of the burst. The amplitudes of these temporal breaks are $\Delta\alpha_{1-2} = 0.92 \pm 0.19$ and $\Delta\alpha_{2-3} = 0.80 \pm 0.29$.

Light curve breaks can be caused by the passage through the X-ray band of the cooling frequency, the ending of continued shock energization, the presence of a structured jet or jet deceleration causing the relativistic beaming to become broader than the jet angle. We examine these possibilities here.

We can immediately rule out the presence of a cooling break for either break as this would result in $\Delta\alpha$ = 0.5 and a change in spectral index (Sari et al. 1998).

The combined BAT and XRT light curve (shown in Fig 4) is consistent with the schematic diagram (fig 3 of Nousek. et al. 2005) of the canonical behaviour of *Swift* XRT early light curves. For GRB 050505 the decay of the BAT emission would comprise the first powerlaw segment identified by Nousek et al. (2005; hereafter N05), the early flat slope of the XRT decay (α_1) would comprise the second segment of canonical decay and the second slope of the doubly broken powerlaw fit (α_2) would comprise the third canonical segment. The BAT and XRT light curves are consistent with joining in the ∼47 minute gap that separates them (see O'Brien et al. 2005), though this behaviour cannot be confirmed with the data we have available.

It might be considered that either of the X-ray light curve breaks represent the end of the energy injection into the forward shock of the relativistic outflow (N05; Zhang et al. 2000), given the lack of spectral variation (and presuming the emission before the break was dominated by the forward shock). However, the temporal placement of

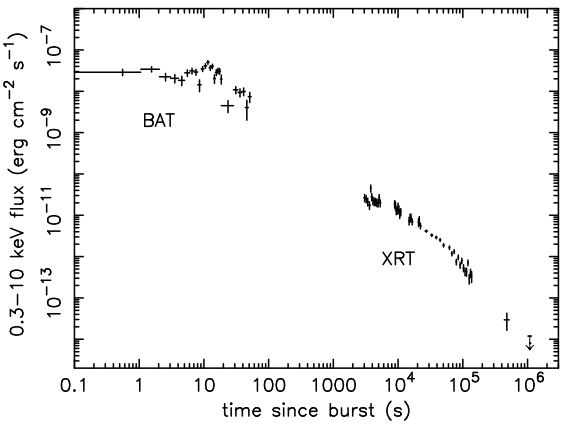

Figure 4. The combined BAT-XRT flux light curve, extrapolated into the 0.3-10.0 keV range. For the XRT section of the flux light curve, the countrate was converted into an unabsorbed flux using the best fit powerlaw model. The BAT data were extrapolated into the XRT band using the best fit powerlaw model derived from the BAT data alone.

the first break makes it the more favourable of the two for this interpretation.

N05 consider that a shallow flux decay is either caused by continous energy injection into the forward shock due to a decrease in the Lorentz factor of the outflow towards the end of the prompt emission or by long lasting central engine activity. The decreasing Lorentz factor (Γ) scenario requires that E($>\Gamma$) $\propto \Gamma^{1-s}$ with s $>$ 1, but N05 find, when modelling the light curve with a single broken powerlaw, that s = -16.7 ± 4.6 for this burst (see their table 3), thus disallowing this interpretation. However, our analysis shows that this scenario is valid for either of our breaks except when $\nu_{\rm c} < \nu_{\rm x} < \nu_{\rm m}$ for a wind medium.

The long-lasting central engine activity scenario requires that the source luminosity decays slowly with time, $L \propto t_{\rm lab}^{q}$ with q > -1. Our analysis shows that the long-lasting central engine activity scenario is valid, again for either of our breaks, as long as the X-ray frequency, $\nu_{\rm x}$, is above the cooling frequency, $\nu_{\rm c}$. We are unable to distinguish, in this case, whether a wind or homogenous cirumburst medium is favoured.

Another possible cause of either of the breaks in the light curve of GRB 050505 could be a structured jet outflow. In this case the ejecta energy over solid angle, $dE/d\Omega$, is not constant, but varies with the angle θ measured from the outflow symmetry axis (Meszaros et al. 1998). Panaitescu (2005) suggests that since afterglow light curves are power laws in time that $dE/d\Omega$ can be approximated as a power law in θ (see their eqn 13), with a power law index[1] of q. We assume a typical value of p (the electron spectral index) to be 2.2 and use the observed values of $\Delta\alpha$ to calculate q from eqns 14 and 15 of Panaitescu (2005). This relation only applies when q $<$ $\tilde{\rm q}$, where $\tilde{\rm q}$ = 8/(p+4) or 8/(p+3). For GRB 050505 the observed values of $\Delta\alpha$ give q significantly greater than $\tilde{\rm q}$ for both wind and uniform environments and for ν_x above or below ν_c.

For q $>$ $\tilde{\rm q}$, where $dE/d\Omega$ falls off sufficiently fast that the afterglow emission is dominated by the core of the jet, Panaitescu (2005) calculates $\Delta\alpha$ = 0.75 (homogenous environment) or 0.5 (wind environment). Thus a structured jet does not appear to be the origin of the first break but it appears to be consistent with the second break as long as the burst is surrounded by a homogenous environment.

The signatures of a jet break, where the relativistic outflow from the GRB slows sufficiently that $\Gamma \sim 1/\theta_j$ and the jet spreads laterally, are an achromatic temporal break with a typical amplitude of $\sim$1 (eg. see Rhoads 1999), no spectral variation (Piran 2005) and a post-break decay index equal to p (Rhoads 1999). There is no evidence for spectral variation during our observations (see Table 1). Unfortunately there were insufficent optical detections of this GRB pre- and post-break to confirm the presence of a jet break in other wavelengths at either epoch.

The temporal index of an X-ray light curve post-jet break should equal p. We calculate from our measured spectral index, β, that p = 1.8 and 2.8, assuming that $\nu_{\rm x}$ is above and below the cooling frequency, $\nu_{\rm c}$, respectively (Zhang & Meszaros 2004). We measure a value of $\alpha_2 = 1.17^{+0.08}_{-0.09}$, which is not compatable with either value of p, which rules out the first break being due to a jet break. However, $\alpha_3 = 1.97^{+0.27}_{-0.28}$ which agrees, within the limits, to the $\nu_{\rm x} > \nu_{\rm c}$ case (p = 1.8). With this value of p we can constrain the jet break parameters further and conclude that the amplitude of the second break is consistent with a jet break.

Having considered the various potential origins for the breaks in the light curve of GRB 050505 for the doubly broken model we conclude that the first break is due to the end of energy injection into the forward shock, i.e. that GRB 050505 fits with the canonical light curve model proposed by N05, and that the second break is either due to a structured jet or is a jet break.

The 'smoothly broken' powerlaw provides a good fit to the XRT light curve data; however, the large degree of smoothing involved produces a degeneracy between the smoothing parameter, the first decay index and the break time. If we take the example case for S = 1 (see Fig 2), then a break is observed at T+$18.5^{+4.4}_{-3.2}$ ks in the observer's frame. This translates to T+$3.5^{+0.8}_{-0.6}$ ks in the rest frame of the burst, with $\Delta\alpha$ = $1.43^{+0.21}_{-0.22}$.

The magnitude of this break allows use to rule out a cooling break, the presence of a structured jet or the end of continued energy injection into the forward shock. It is compatable with a jet break from optically thick synchrotron emission ($\Delta\alpha$ = 1.25, Rhoads 1999). However, a break this early requires an unreasonably large circumburst density to produce a value of E_γ, the true γ-ray energy released, that is comparable with the typical value seen thus far (Bloom et al. 2003). Thus the parameters of

[1]The q in this formulation is not the same as the q discussed by N05

Table 1. Spectral fits for GRB 050505. [a] *Spectral models: power-law (PL), Galactic absorption (Gal), which has been assumed to be 2.1×10^{20} cm^{-2} (Dickey & Lockman 1990), excess Galactic absorption (Abs) and excess absorption in the host galaxy (ZAbs).* $*$ *z fixed at 4.27.*

	Model[a]		
	PL+Gal	PL+Gal+Abs	PL+Gal+ZAbs*
Co-added data for T+3ks - T+17ks			
Photon index	$1.76^{+0.09}_{-0.09}$	$1.91^{+0.19}_{-0.18}$	$1.87^{+0.15}_{-0.14}$
Excess N_H (10^{20} cm^{-2})	-	< 7.74	113^{+123}_{-107}
χ^2/DOF	26.9 (27)	24.2 (26)	23.9 (26)
Co-added data for T+26ks - T+138 ks			
Photon index	$1.77^{+0.06}_{-0.06}$	$1.94^{+0.12}_{-0.11}$	$1.91^{+0.10}_{-0.09}$
Excess N_H (10^{20} cm^{-2})	-	$3.91^{+2.43}_{-2.14}$	133^{+73}_{-65}
χ^2/DOF	86.2 (69)	77.3 (68)	74.7 (68)
All data co-added			
Photon index	$1.76^{+0.05}_{-0.05}$	$1.93^{+0.10}_{-0.10}$	$1.90^{+0.08}_{-0.08}$
Excess N_H (10^{20} cm^{-2})	-	$3.81^{+2.09}_{-1.93}$	128^{+61}_{-58}
χ^2/DOF	133 (97)	102 (96)	99 (96)

the smoothly broken powerlaw model are not compatable with any theoretical framework put forward thus far.

4.2. Burst Properties

From the redshift of GRB 050505 (z = 4.27) we calculate an isotropic equivalent radiated energy, $E_{\rm iso}$, in the observed 15-350 keV energy range to be (1.45±0.14)×10^{53} ergs, using the standard cosmology: H_o = 71 km s^{-1} Mpc^{-1}, $(\Omega_M, \Omega_\Lambda)$ = (0.27, 0.73).

If we take the second break in the light curve to be a jet break we are then able to calculate the properties of GRB 050505. Using the formulation of Frail et al. (2001), and assuming that the efficiency of the fireball in converting the energy of the ejecta into γ-rays is ∼0.2, we obtain a range in $\theta_{\rm j}$ from 2.5$^{\rm o}$ (n = 1 cm^{-3}) to 4.4$^{\rm o}$ (n = 100 cm^{-3}).

From this we can calculate the beaming fraction, f_b, (Sari et al. 1999) to be between 9.4×10^{-4} (n = 1 cm^{-3}) and 3.0×10^{-3} (n = 100 cm^{-3}) and E_γ to be in the range of 1.37×10^{50} (n = 1 cm^{-3}) to 4.33×10^{50} ergs (n = 100 cm^{-3}). We note that the typical E_γ of bursts thus far is 1.33×10$^{51} h_{65}^{-2}$ ergs (Bloom et al. 2003) with a burst-to-burst variance about this value of ∼ 0.35 dex (or a factor of 2.2), thus this burst appears to be slightly weak in comparison.

Given that these values for E_γ are low compared to the mean value discovered so far we calculated $E_{\rm peak}$ from these values of E_γ via the Ghirlanda relation (Ghirlanda et al. 2004) and compared them to the observed lower limit of $E_{\rm peak,obs} > 52$ keV. We calculated that the Ghirlanda relation gave $E_{\rm peak}$ = 153^{+65}_{-63} keV (for n=1 cm^{-3}) and 341^{+138}_{-134} keV (for n=100 cm^{-3}), which both agree with the lower observed limit. We also calculated $E_{\rm peak}$ via the Amati correlation (Amati et al. 2002). Using equation 6 of Ghirlanda et al. (2005) for GRBs of known redshift gives $E_{\rm peak}$ = 112±6 keV, consistent with our observed limit.

5. CONCLUSIONS

We have presented multi-wavelength data for GRB 050505. The X-ray light curve of GRB 050505 (see Fig 2) can be adequately fit with either a 'smoothly broken' or 'doubly broken' powerlaw model.

The 'smoothly broken' powerlaw model favours a smoothing factor of 0.5-2 (highly smoothed transition). This produces an initially shallow decay with $\alpha_1 \sim 0.5$, which breaks over several decades in time to a steeper slope, α_2, of ∼1.8 (χ^2/DOF ∼ 1.04). However, the parameters of this fit are not compatable with any theoretical framework put forward thus far.

A 'doubly broken' powerlaw model consists of α_1) = $0.25^{+0.16}_{-0.17}$ (first detected at T+3 ks), $\alpha_2 = 1.17^{+0.08}_{-0.09}$ and α_3 = $1.97^{+0.27}_{-0.28}$ (which continues to at least T+1.05×10^3 ks) with breaks at $t_1 = 7.4^{+1.5}_{-1.5}$ ks and $t_2 = 58^{+9.9}_{-15.4}$ ks (χ^2/DOF = 38.7/42).

We see no change in the X-ray spectral properties during *Swift's* observations of this GRB. The best fit model parameters for the X-ray spectrum indicates that this burst has a typical photon index of $1.90^{+0.08}_{-0.08}$ and an excess absorption component from the host galaxy of $(1.28^{+0.61}_{-0.58})\times10^{22}$cm^{-2} ($\chi^2$/DOF = 99/96).

Having considered the temporal position and amplitude of the two breaks in the doubly broken light curve we conclude that the first break is due to end of energy injection into the forward shock (N05; Zhang et al. 2005), i.e. that GRB 050505 fits with the canonical light curve

model proposed by N05, and that the second break is either a jet break or a break caused by the presence of a structured jet.

The redshift of 4.27 allowed us to calculate the intrinsic parameters for this GRB, in conjunction with the second light curve break time observed in *Swift's* X-ray observations. Whilst the identification of this break with a jet break provides a value for E_γ that is slightly low with respect to previous GRBs, it is consistent with the Ghirlanda relation (Ghirlanda et al. 2004; 2005). It also suggests that GRB 050505 has a narrow beaming angle; however, this degree of beaming is not unexpected for GRBs at high redshift since GRBs with wider jets could potentially be too faint to be detected by any of the current γ-ray missions.

ACKNOWLEDGMENTS

This work is supported at the University of Leicester by the Particle Physics and Astronomy Research Council (PPARC). CPH gratefully acknowledges support from a PPARC studentship

REFERENCES

Amati L., et al., 2002, A&A, 390, 81.

Anders E. & Grevesse N. 1989, Geochim. Cosmochim. Acta. 53, 197.

Andersen M. I., et al. 2000, A&A, 364, L54.

Barthelmy S. D. 2005, Space Sci. Rev., in press (astro-ph/0507410).

Berger E., et al. 2005, GCN Circ. 3368.

Beuerman K., et al. 1990, A&A, 352, L26.

Bloom J. S., Frail D. A. & Kulkarni S. R. 2003, ApJ, 594, 674.

Burrows D. N., et al. 2005, Space Sci. Rev., in press (astro-ph/0508071).

Cenko S. B., et al. 2005a, GCN Circ. 3366.

Cenko S. B., et al. 2005b, GCN Circ. 3377.

Dickey & Lockman. 1990, ARAA, 28, 215.

Frail D. A. 2001, ApJ, 562, L55

Gehrels, N.; et al. 2004, ApJ, 611, 1005.

Ghirlanda G., Ghisellini G. & Lazzati D. 2004, ApJ, 616, 331.

Ghirlanda G., Ghisellini G. & Firmani C. 2005, MNRAS, 361, L10.

Hohman D., Henden A. & Price A. 2005, GCN Circ. 3370.

Homewood A., Hartmann D. H., & Wood M. 2005, GCN Circ. 3398.

Hurkett C. P., et al. 2005a, GCN Circ. 3360.

Hurkett C. P., et al. 2005b, in preparation.

Jelinek A. J. et al. 2005, GCN Circ. 3373.

Kawai, et al. 2005, GCN Circ. 3937.

Kennea J. A., et al. 2005, GCN Circ 3365.

Kippen R. M. 2000, GCN Circ. 530.

Klotz A., Boer M. & Atteia J. L. 2005, GCN Circ. 3403.

Lamb D. Q. & Reichart D. E. 2000, ApJ, 536, 1.

Meszaros P., Rees M. J. & Wijers R. 1998, ApJ, 499, 301.

Nousek J. A., et. al. 2005, ApJ, submitted.

O'Brien P. T. et al. 2005, in preparation.

Panaitescu A. 2005, MNRAS, 362, 921.

Piran T. 2005, Rev. Mod. Phys. 76, 1143.

Preece R. D, et al. 2000, ApJ, 126, 19.

Rhoads J. E. 1999, ApJ, 525, 737.

Rol E., et al. 2005, GCN Circ. 3372.

Roming P. W. A., et al. 2005, Space Sci. Rev., in press (astro-ph/0507413).

Rosen S., et al. 2005, GCN Circ. 3371.

Sari R., Piran T. & Narayan R. 1998, ApJ, 497, L17.

Sari R., Piran T. & Halpern J. P. 1999, ApJ, 519, L17.

Stanek K. Z., et al. 2005, ApJ, 626, 45.

Tinney C., et al. 1998, IAU Circ. 6896.

de Ugarte Postigo A., et al. 2005, GCN Circ. 3376.

Vaughan S., et al. 2005, ApJ in press (astro-ph/0510677).

Vreeswijk P. M., et al. 2004, A&A 419, 927.

Wilms J., Allen A., & McCray R. 2000, ApJ, 542, 914.

Zhang B. & Meszaros P. 2004, IJMPA, 19, 2385.

Zhang B., et al. 2005, in preparation.

NEW SOFT BATSE GRBS AND SPECTRA OF X-RAY RICH BURSTS

Yana Tikhomirova[1], **Boris Stern**[2,1], **Alexandra Kozyreva**[3], **and Juri Poutanen**[4]

[1]Astro Space Centre, P.N. Lebedev Physical Institute, Profsoyuznaya 84/32, 117997 Moscow, Russia
[2]Institute for Nuclear Research, Russian Academy of Sciences, Prospekt 60-letiya Oktyabrya 7a, 117312 Moscow
[3]Sternberg Astronomical Institute, Universitetskij pr. 13, 119992 Moscow, Russia
[4]Astronomy Division, P.O.Box 3000, FIN-90014 University of Oulu, Finland

ABSTRACT

A population of X-ray dominated gamma-ray bursts (GRBs) observed by Ginga, BeppoSAX and HETE-2 should be represented in the BATSE data as presumably soft bursts. We have performed a search for soft GRBs in the BATSE records in the 25–100 keV energy band. A softness of a burst spectrum can be a reason why it has been missed by the on-board procedure and previous searches for untriggered GRBs tuned to 50–300 keV range. We have found a surprisingly small number (~ 20 yr^{-1} down to 0.1 ph cm^{-2} s^{-1}) of soft GRBs where the count rate is dominated by 25–50 keV energy channel. This fact as well as the analysis of HETE-2 and common BeppoSAX/BATSE GRBs indicates that the majority of GRBs with a low $E_{\rm peak}$ has a relatively hard tail with the high-energy power-law photon index $\beta > -3$. An exponential cutoff in GRB spectra below 20 keV may be a distinguishing feature separating non-GRB events.

Key words: gamma-ray bursts; data analysis.

1. INTRODUCTION

Observations of the prompt gamma-ray bursts (GRBs) emission by different instruments show that their spectra can extend from several keV up to a few MeV (Wheaton et al., 1973; Trombka et al., 1974; Metzger et al., 1974) sometimes up to GeV range (Sommer et al., 1994). According to recent broadband observations by Ginga (Strohmayer et al., 1998), HETE-2 (Sakamoto et al., 2005) and combined results of BeppoSAX/BATSE (Kippen et al., 2003) and RXTE/IPN (Smith et al., 2002), most GRBs exhibit a peak in the EF_E spectrum at an energy $E_{\rm peak}$ in the 50–400 keV range. However, distribution of $E_{\rm peak}$ is broad and large part of events demonstrate significant X-ray (2–30 keV) emission (X-ray dominated GRBs, X-ray rich GRBs). At this moment study of broadband spectra is complicated because of insufficient statistics accumulated by broadband instruments and biases due to different instrument responses.

The BATSE (Paciesas et al., 1999) data of all-sky 9.1 years (1991–2000) continuous monitoring in γ-ray range give unique possibility for combined GRB analysis with X-ray observations. BATSE γ-ray detectors were the most sensitive instruments of this type over GRB history. Only recently launched Swift experiment (Gehrels et al., 2004) has a more sensitive γ-ray detector. However, during the next several years Swift cannot accumulate statistics comparable to that of the BATSE. BATSE detected about 2700 GRBs with fluxes down to ~ 0.3 ph cm^{-2} s^{-1} (Paciesas et al., 1999). In addition, the off-line scans of the BATSE continuous records almost doubled the number of observed GRBs with fluxes down to ~ 0.1 ph cm^{-2} s^{-1} (see Kommers et al. 2001; [1] Stern et al. 2001 [2])

The BATSE detectors were sensitive to photons from $\sim$25 keV up to $\sim$1 MeV. However, the on-board procedure and most off-line searches identified GRBs according to the signal in the 50–300 keV range while GRBs with a soft spectrum could be missed. These soft events can help to outline the place of the X-ray dominated bursts in the GRB variety.

The 25-50 keV range was inspected only in the off-line search of Kommers et al. (2001). Their scan have covered 6 out of 9.1 years of the BATSE data and yielded 50 unknown low-energy events some of which are probably soft GRBs. Even if all of them are GRBs, the number of these events is 50 times smaller than that found in the 50–300 keV range.

We performed a search for GRBs, inspecting the 25–50 keV range for time period not covered by the scan of Kommers et al. (2001) with a more careful and op-

[1]Non-triggered supplement to the BATSE GRB catalogs is available at http://space.mit.edu/BATSE/intro.html

[2]The uniform catalog of GRBs found in the continuous BATSE daily records is available at http://www.astro.su.se/groups/head/grb_archive.html

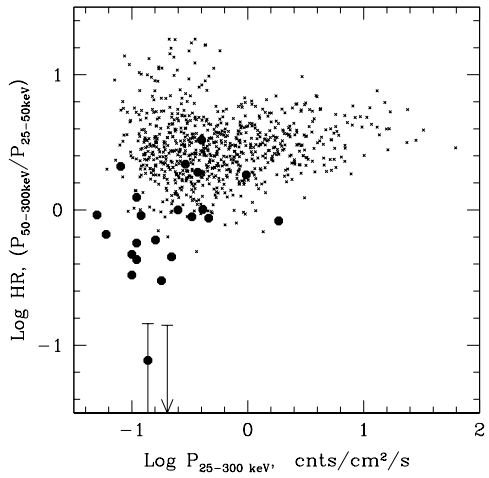

Figure 1. Hardness-intensity distribution of long (> 2s) GRBs found in the BATSE DISCLA records for the time period TJDs 11000-11699. Hardness is estimated as the ratio of peak count rates in 50–300 keV and 25–50 keV energy bands. Peak count rate is given in 25–300 keV band. GRBs from the scan of Stern et al. (2001) are marked by dots, GRBs found in the present scan in 25–100 keV are shown by circles, while two very soft events from the X-ray pulsar Vela X-1 are shown by symbols with errors bars.

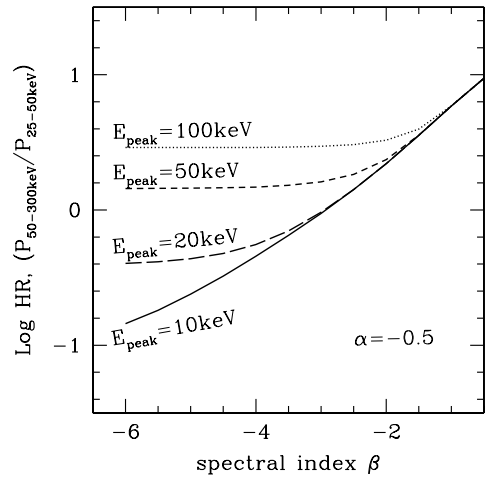

Figure 2. Hardness ratio of GRBs depending on different parameters of the simulated incident photon spectra. Spectra are approximated with the Band function (Band et al., 1993) and folded with the BATSE detector response matrix (Pendleton et al., 1999). α and β are low- and high-energy photon spectral indices, respectively.

timized for soft GRBs procedure. The continuous daily 1.024 s time resolution DISCLA records of count rate in 8 BATSE detectors in 4 energy channels (25–50, 50–100, 100–300 and 300–1000 keV) were used. We have applied the same technique and the same algorithm as in our scan of the BATSE DISCLA data in the 50–300 keV range (Stern et al., 2001) setting the trigger in the 25–100 keV range (i.e. in the 1st and 2nd energy channels).

We present the results of our search for soft BATSE GRBs in Section 2 and discuss new data together with the recent GRB observations by BeppoSAX and HETE-2 in Section 3.

2. SEARCH FOR SOFT GRBS IN THE BATSE RECORDS

We have performed the scan of BATSE DISCLA records available at FTP archive at Goddart Space Flight Center [3] for time period since July 6, 1998 till May 26, 2000 (TJDs 11000-11699, files for TJDs 11047, 11048, 11354, 11355-11359, 11519-11521 are missing). The applied algorithm and technique is described in Stern et al. (2001). Only the 25–100 keV range (1 and 2 channels) was checked. The 1024 ms time resolution DISCLA data are not suitable for studies of short (< 2 s) GRBs and we did not consider 1 bin events.

[3]FTP archive at the Goddart Space Flight Center is available at ftp://cossc.gsfc.nasa.gov/compton/data/batse/daily

This allows us to avoid scintillation from heavy nuclei and soft gamma-ray repeater (SGR) outbursts. We excluded also events with location in the vicinity of Galactic center, the Sun, four known SGRs and other persistent sources and events that appeared near and below Earth horizon. We recorded only new GRBs missing in the catalogs of Paciesas et al. (1999) and Stern et al. (2001).

We have found and classified as GRBs 21 new events. Table 1 present their time identificator, intensity, hardness, location and duration. In the previous scan in 50–300 keV (Stern et al., 2001) for the same time period we have detected about 800 long GRBs. Hardness-intensity diagram (Fig. 1) shows that although GRBs of a new sample are softer on average, the samples do overlap. Actually 13 out of 21 GRBs in a new sample (Table 1) and 23 of ∼800 long GRBs in the old sample (the catalog of Stern et al. (2001)) have the peak count rate in 25–50 keV higher than that in the 50–300 keV band. According to this somewhat arbitrary criterion we consider these 36 events as a sample of soft long (>2 s) BATSE GRBs.

These 36 soft GRBs have typical light curves, last up to about 100 s and do not demonstrate any significant anisotropy on the sky. Soft BATSE GRBs selected with the above criterion constitute about 5% of observed long GRB sample (about 20 per year with peak fluxes down to ~ 0.1 ph cm^{-2} s^{-1}).

Our scan (as well as an alternative scan Kommers et al. 2001) in the BATSE records in the 25–50 keV range has yielded surprisingly small number of new soft GRBs. Moreover, there are no events with hardness ratio (HR) below 0.3, while much softer events like outbursts of Vela X-1 can be confidently detected (see Fig. 1). We have considered sample of 50 events classified by Kommers et al. (2001) as unknown because of their softness.

Table 1. Long ($>$ 2 s) GRBs found in the present scan of the BATSE DISCLA records (TJD 11000-11699) in 25–100 keV band.

Date	Seconds of TJD	TJD	P_{50-300} keV cnt cm^{-2} s^{-1}	Hardness P_{50-300} keV/P_{25-50} keV	Location α, deg	δ, deg	Error box deg	T_{90} s
13 soft GRBs (P_{25-50} keV $>$ P_{50-300} keV)								
980726	63036	11020	0.11	0.57	255.8	−54.8	9.7	56
980804	50914	11029	0.46	0.87	173.3	−52.7	7.3	13
980927	6133	11083	0.33	0.89	9.6	−54.5	11.4	6
981225	76754	11172	0.22	0.45	161.9	−61.3	17.0	25
990304	77277	11241	1.85	0.83	31.6	−26.7	4.6	4
990513	2453	11311	0.18	0.30	236.4	−59.6	16.5	15
990610	20227	11339	0.11	0.43	234.8	16.6	17.3	80
990804	39065	11394	0.05	0.92	44.1	21.2	36.6	38
990907	75723	11428	0.06	0.66	301.0	−39.3	8.3	126
991003	30847	11454	0.16	0.60	253.8	33.2	21.1	13
991009	30691	11460	0.10	0.47	107.9	3.5	12.9	24
991106	59880	11488	0.10	0.33	284.7	−58.2	20.5	39
000107	8784	11550	0.12	0.91	74.9	−61.6	16.1	73
8 classic GRBs (P_{25-50} keV $<$ P_{50-300} keV)								
980707	9097	11001	0.40	3.29	79.0	40.4	9.9	6
980930	83166	11086	0.37	1.90	132.0	−70.9	6.7	38
981012	21270	11098	0.11	1.24	59.0	15.5	20.7	17
981019	69630	11105	0.29	2.18	208.9	−40.3	11.7	17
981221	18020	11168	0.97	1.82	71.9	3.6	15.4	9
990303	74922	11240	0.25	1.00	199.9	52.4	18.9	9
000324	36745	11627	0.08	2.10	58.7	26.4	18.8	36
000523	49912	11687	0.41	1.01	269.1	80.6	8.6	24

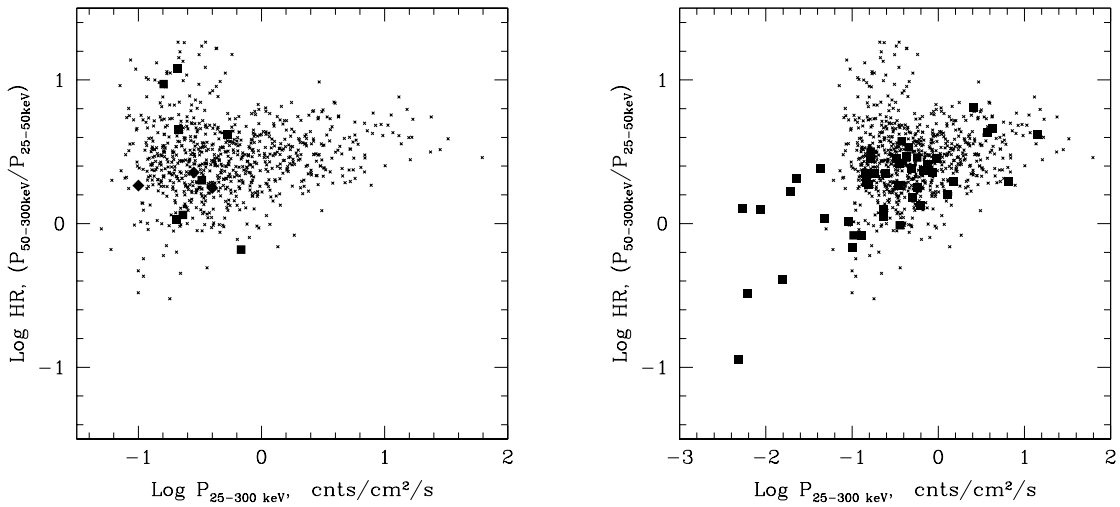

Figure 3. (a) Hardness-intensity distribution of of GRBs detected by BeppoSAX as seeing in the BATSE data. Squares show the events from Kippen et al. (2001) and diamonds are the events reported in in 't Zand et al. (2003). (b) Hardness-intensity distribution of the model BATSE counterparts of GRBs detected by HETE-2 (Sakamoto et al., 2005) (squares). In both panels, the dots represent the BATSE GRB sample from the time interval TJD 11000–11699.

When excluding short events they again have HR > 0.3 except two events from the direction to Vela X-1.

Why do not we see softer GRBs despite the fact that there exist X-ray dominated bursts with peak energy below the BATSE window? We calculated the BATSE detector response to estimate the dependence between the incident photon spectrum and the observed hardness ratio (see Fig. 2). We approximated GRB spectra with the Band function (Band et al., 1993) and folded them with the BATSE Detector Response Matrix (DRM) (Pendleton et al., 1999). The low hardness ratio (HR < 1) of our soft events is consistent with a wide variety of spectral parameters $E_{\rm peak}$, low energy and high energy spectral indices α and β, in particular, with $E_{\rm peak} < 20$ keV and $\beta < -3$ (see Fig. 1 and 2). It is also evident that the sufficient condition for a GRB to give HR > 1 and thus to look as a typical GRB in the BATSE data (with larger signal above 50 keV) is $\beta > -3$, independently on the $E_{\rm peak}$. A combination of a low $E_{\rm peak}$ and a very steep β would give the hardness ratio below 0.3 which we do not observe. The fact that all events with HR < 0.3 have evident non-GRB origin (solar flares, Vela X-1 pulsar, etc.) implies that a spectral cutoff below $\sim$15 keV may be a distinguishing feature to separate non-GRB sources.

3. GRB SPECTRA AS OBSERVED BY BATSE/BEPPOSAX/HETE-2

BeppoSAX observed 20 X-ray dominated GRBs which were detected by Wide Field Camera (2–26 keV), but did not activate the trigger of the Gamma-Ray Monitor (40–400 keV). Their counterparts were found in the BATSE records for almost all observable events (Kippen et al., 2001; in 't Zand et al., 2003). Most of them were detected earlier as classic GRBs by our scan of BATSE data in 50–300 keV band (Stern et al., 2001). It turns out that these events have a high hardness ratio similar to typical GRBs (see Fig. 3a). The hardness ratio 100–300/50–100 keV for common BeppoSAX/BATSE events shows a similar picture: 7 out of 8 events have a typical hardness for weak GRBs and one event is softer. Thus this distribution is also consistent with the extrapolated hardness-intensity trend for long GRBs (Kippen et al., 2001). These facts support our conclusion that most of the X-ray dominated GRBs should have a hard tail with $\beta > -3$ in the BATSE window 25–1000 keV (see Fig. 2).

HETE-2 observed 45 GRBs in the 2–400 keV band and their spectral fits are given in Sakamoto et al. (2005). In order to check how HETE-2 results are related to our data we folded HETE-2 spectra with the BATSE detector response matrix and obtained corresponding counts in BATSE channels (see Fig. 3b). The fraction of soft events in the HETE-2 sample is about 3 times larger than in the BATSE sample which can be explained by different instrument responses. But only 1 out of 45 HETE-2 events gives a lower hardness ratio than we see in the BATSE GRB sample. Nine out of 45 HETE-2 events are below the BATSE sensitivity threshold. The BATSE sample, however, represents probably the whole GRB spectral variety.

According to our results, the existence of GRBs with sharp spectral cutoff is questionable for events with low $E_{\rm peak}$. Indeed, the events with $E_{\rm peak}$ $\sim$10–20 keV would give a very low hardness ratio which we do not observe. Note that, as shown by Preece et al. (1999), only few percents of GRBs with high $E_{\rm peak}$ are better described by a power-law with the exponential cutoff rather than the Band function. If the dispersion in $E_{\rm peak}$ is due to variations in the redshift/blueshift in the source, then the spec-

tral shape would be stable and our conclusion could refer to all GRBs.

4. CONCLUSIONS

1. Despite the wealth of the X-ray dominated GRBs observed by Ginga, BeppoSAX and HETE-2 the number of soft GRBs in the BATSE data is relatively small. The fraction of events with the count rate in 25–50 keV higher than that above 50 keV is ∼5 per cent (20 per year with flux down to 0.1 ph cm^{-2} s^{-1}).

2. The hardness distribution of the X-ray dominated GRBs in the BATSE band is consistent with that of weak classic GRBs. In the case of a low $E_{\rm peak}$, the main fraction of GRBs should have a relatively hard high-energy tail with a power-law slope $\beta > -3$. Only a few per cent of the X-ray rich GRBs have a tail with $\beta < -3$, but still harder than the exponential one. This fact clarifies the deficiency of soft events in the BATSE data.

3. An exponential cutoff in the GRB spectra, if exists, is probably a rare phenomenon. Therefore, a spectral cutoff with the e-folding energy below ~ 20 keV may be a distinguishing feature to separate the non-GRB events.

ACKNOWLEDGMENTS

We are grateful to R.Preece and G.Pendleton for the code of the BATSE detector response matrix. We thank K.Hurley for providing us IPN data on our soft GRB sample. This research has made use of data obtained through the High Energy Astrophysics Science Archive Research Center Online Service, provided by the NASA/Goddard Space Flight Center. The work is supported by NORDITA Nordic project in high energy astrophysics in the INTEGRAL era, RFBR fellow 04-02-16987, and Russian Foundation for Science Support (Y.T.).

REFERENCES

Band D. , Matteson J., Ford L., et al. 1993, ApJ, 413, 281

Gehrels N., Chincarini G., Giommi P., Mason K. O., & Nousek J. A. 2004, ApJ, 611, 1005

in 't Zand J., Heise J., Kippen R., et al. 2003, in Piro L., Frontera F., Masetti N., Feroci M., eds, ASP Conf. Series 312, Third Rome workshop on gamma-ray bursts in the afterglow era, Astron. Soc. Pac., San Francisco, p. 18

Kippen R. M., Woods P. M., Heise J., et al. 2001, in Costa E., Frontera F., Hjorth J., eds, Gamma-Ray Bursts in the Afterglow Era. Berlin, Springer, p. 22

Kippen R. M., Woods P. M., Heise J., et al. 2003, in Ricker G.R., Vanderspek R., eds, Gamma-Ray Burst and Afterglow Astronomy 2001, AIP Conf.Proc. 662, AIP, New York, p. 244

Kommers J., Lewin W.H.G., Kouveliotou C.,. et al. 2001, ApJS, 134, 385

Metzger A. E., Parker R. H., Gilman D., Peterson L. E., & Trombka J. I. 1974, ApJ, 194, L19

Paciesas W.S., Meegan, C., Pendleton, G., et al. 1999, ApJS, 122, 465

Pendleton G.N., Briggs M., Kippen R., et al. 1999, ApJ, 512, 362

Preece R.D., Briggs M.S., Mallozzi R.S., et al. 2000, ApJS, 126, 19

Sakamoto T., Lamb D., Graziani C, et al. 2005, ApJ, 629, 311

Smith D.A., Levine A., Bradt H., et al. 2002, ApJS, 141, 415

Sommer M., Bertsch D., Dingus B., et al. 1994, ApJ, 422, L63

Stern B. E., Tikhomirova Y., Kompaneets D., Svensson R., & Poutanen J. 2001, ApJ, 563, 80

Strohmayer T. E., Fenimore E. E., Murakami T., & Yoshida A. 1998, ApJ, 500, 873

Trombka J. I., Eller E. L., Schmadebeck R. L., et al. 1974, ApJ, 194, L27

Wheaton Wm. A., Ulmer M. P., Baity W. A., Datlowe D. W., & Elcan M. J. 1973, ApJ, 185, L57

X-RAY FLARES IN THE EARLY *SWIFT* OBSERVATIONS OF THE POSSIBLE NAKED BURST GRB 050421

O. Godet [1], K.L. Page[1], M.R. Goad[1], A.P. Beardmore[1], P.T. O'Brien[1], J.P. Osborne[1], D.N. Burrows[2], M. Capalbi[3], J. Kennea[2], V. Mangano[4], A. Moretti[5], D. Morris[2]

[1] X-ray & Observational Astronomy Group, Dept of Physics & Astrophysics, University of Leicester, LE1 7RH, UK
[2] Dept of Astronomy & Astrophysics, 525 davey Lab, Pennsylvania State University, University Park, PA 16802, USA
[3] ASI Science Data Center, Via G. Galilei, I-00044 Frascati, Italy
[4] INAF-Istituto di Astrofica Spaziale e Fisica Cosmica Sezione di Palermo, Via U. La Malfa 153, 90146 Palermo, Italy
[5] INAF-Osservatorio Astronomico di Brera, Via E. Bianchi 46, 23807 Merate (LC), Italy)

ABSTRACT

We present the *Swift* observations of the faint burst GRB 050421. The X-ray light-curve shows two flares: the first flare peaking at $\sim$ 110 s after the BAT trigger (T_0) and the second one peaking at $\sim$ 154 s. We argue that the mechanism producing these flares is probably late internal shocks. The X-ray light-curve shows a rapid decline with a temporal index $\alpha \sim 3.1$. The X-ray source disappears completely less than 1 hour after the trigger. An X-ray spectral softening is also observed with time from $\beta \sim 0.1$ to ~ 1.2. A good joint fit to the BAT and XRT spectra indicates that the early X-ray and Gamma-ray emissions are produced by the same mechanism. The X-ray spectral softening is likely due to a shift down to lower energies of the peak of the prompt emission, and the rapid decline of the X-ray emission is probably the tail of the prompt emission. This suggests that the X-ray emission is completely dominated by high latitude radiation and the external shock, if any, is below the detection threshold.

Key words: Gamma-ray: bursts - Gamma-rays, X-rays: individual (GRB 050421).

1. INTRODUCTION

The *Swift* Gamma-Ray Burst (GRB) Explorer was launched on 20th November 2004 (Gehrels et al. 2004). It is a multi-wavelength observatory covering the Gamma-ray, X-ray and UV/optical bands. After the detection of a GRB by the Burst Alert Telescope (BAT, Barthelmy et al. 2005), the observatory slews automatically and rapidly to point the narrow field instruments: the X-ray Telescope (XRT, Burrows et al. 2005a), and the UV/Optical Telescope (UVOT, Roming et al. 2005). Due to its rapid pointing capability and high sensitivity, *Swift* is ideal for studying the properties of the early afterglow, in particular the transition between prompt and forward shock emissions.

We report here the *Swift* observations of the GRB discovered at 04:11:52 UT on 21st April 2005 by the BAT (Godet et al. 2005). The XRT started to observe 89 s after the BAT trigger (T_0) and observed an X-ray fading source at (J2000) RA=$20^{\rm h}29^{\rm m}02.44^{\rm s}$ and Dec= $+73^{\rm o}39'17.8''$ with a total uncertainty radius of 3.7 arc-seconds (90% containment). This XRT position is corrected for the effect of the boresight offset (Moretti et al. 2005). The UVOT started to observe 112 s after the BAT trigger, but detected no new source. No radio, infra-red or optical counterpart was detected by ground-based instruments (e.g. Bloom et al., Jelinek et al. 2005). By convention, we note the flux as $F_\nu \propto \nu^{-\beta} t^{-\alpha}$, where β is the energy spectral index and α is the temporal index.

2. SUMMARY OF THE MAIN SPECTRAL AND TEMPORAL RESULTS

- The BAT light-curve displays a FRED peak with a duration $T_{90} \sim 10.3$ s, a spectral slope of $\beta = 0.7 \pm 0.5$, and a tail extending to ~ 100 s after the trigger. A faint burst with a fluence of 1.1×10^{-7} erg cm^{-2} s^{-1} in the 15-150 keV band, it is in the bottom 10% of GRBs detected by the BAT.

- A rapid decline ($\alpha = 3.1 \pm 0.1$) of the XRT light-curve with 2 flares peaking at $T_0 + 110$ s and $T_0 + 154$ s (Fig. 1). The X-ray emission decayed from $\sim 10^{-9}$ erg cm^{-2} s^{-1} at $T_0 + 100$ s to $< 7 \times 10^{-13}$ erg cm^{-2} s^{-1} at $T_0 + 1000$ s, and was no longer detected beyond $T_0 + 1000$s.

- A spectral softening from the early $T_0 + 115 \rightarrow T_0 + 171$ s data with $\beta = 0.1 \pm 0.3$ to the later $\sim T_0 + 180 \rightarrow T_0 + 771$ s with $1.2^{+0.3}_{-0.1}$.

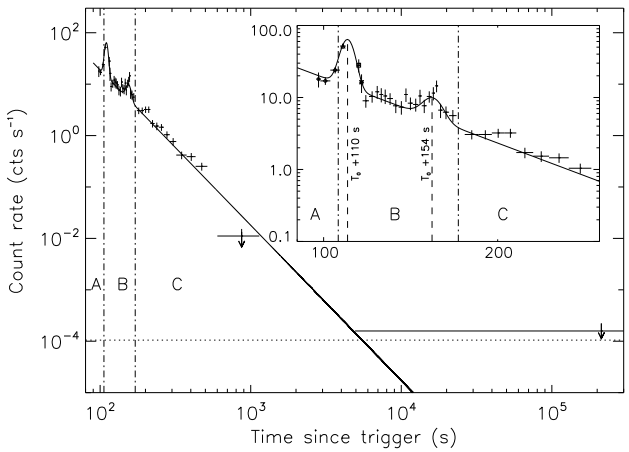

Figure 1. Background subtracted XRT light-curve of GRB 050421 over the energy band 0.3-10 keV: A) Low-rate Photo-Diode (LrPD) slew and settling data (diamonds); B) Image Mode (triangle), Piled-up Photo-Diode (PuPD) (square), LrPD (star) and Windowed Timing (WT) pointing data; C) Photon Counting (PC) pointing data. The best fit to the light-curve is plotted by the solid line. The dotted line corresponds to the background level in the PC data. The upper limits are 3 σ limits. The times of the two X-ray flares are also shown in the plot.

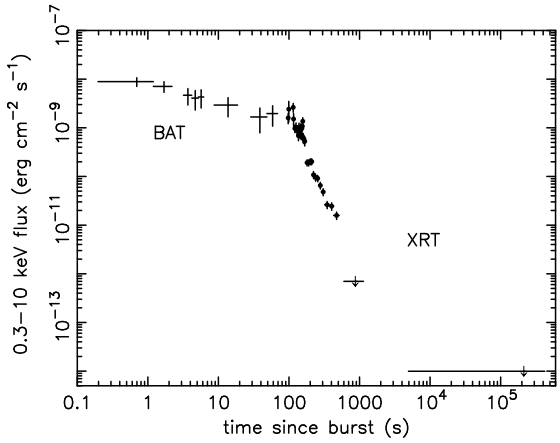

Figure 2. Combined light-curves of the BAT data (crosses) extrapolated in the 0.3-10 keV band and the XRT data (circles) in the 0.3-10 keV energy range. The unabsorbed fluxes are given in units of erg cm^{-2} s^{-1}. The BAT and XRT fluxes were derived from the spectral slopes given in Section 2.

- The joint fit of the BAT and early XRT data shows that they are likely produced by the same mechanism which is consistent with an absorbed power-law with a slope $\beta = 0.2 \pm 0.2$. Fig. 2 shows the combined light-curves of the BAT data extrapolated in the 0.3-10 keV band and the XRT data in the same band.

- Excess absorption $\Delta N_H(z = 0) \sim 4.4 \times 10^{21}$ cm^{-2}, over that due to the Galaxy is seen in the XRT spectra. No variation in absorption with time is seen.

3. DISCUSSION & CONCLUSION

GRB 050421 was one of the faintest bursts observed by *Swift*. It showed a rapid temporal decline in X-rays on which were superposed at least two X-ray flares. The short rise and decay times and the amplitude of the flares indicate that the flares are probably produced by late internal shocks (e.g. Burrows et al. 2005b and Zhang et al. 2005). Simple kinematic arguments also support this interpretation (Ioka et al. 2005). The spectral softening seen in the XRT is likely due to the shift, in the XRT energy band, of the peak of the prompt spectrum with time (Ford et al. 1995). The temporal decline and the spectral results can not be explained by invoking the current afterglow models (e.g. Zhang et al. 2005). A natural explanation for the steep temporal decay and the spectral slopes seen in the previous section is then to invoke a "high latitude emission" model (e.g. Kumar & Panaitescu 2000). In this model, the tail of the prompt emission is produced at high angles relative to the observer line of sight (with angles $\theta > \Gamma^{-1}$ where Γ is the Lorentz factor).

GRB 050421 would then be the first burst for which the XRT slewed promptly, for which no forward shock emission was observed. Therefore, GRB 050421 would be the first "naked burst" (Kumar & Panaitescu 2000) discovered by *Swift*.

REFERENCES

Barthelmy et al. 2005, Space Sci. Rev., 120, astro-ph/0507410

Bloom et al., GCN Circular 3306 (2005)

Burrows et al. 2005, Space Sci. Rev., 120, astro-ph/0508071

Burrows et al. 2005, astro-ph/0506130

Ford et al. 1995, ApJ, 439, 307

Gehrels et al., 2004, ApJ, 611, 1005

Godet et al. 2005, submitted to A&A

Ioka et al. 2005, ApJ, 631, 429

Jelinek et al., GCN Circular 3298 (2005)

Kumar & Panaitescu 2000, ApJ, 541, 51

Moretti et al. 2005, submitted to A&A

Roming et al. 2005, Space Sci. Rev., 120, astro-ph/0507413

Zhang et al. 2005, astro-ph/0508321

SWIFT-XRT OBSERVATION OF THE AFTERGLOW OF GRB050319 AND XRF050416A

V. La Parola[1], G. Cusumano[1], V. Mangano[1], T. Mineo[1], D. N. Burrows[2], S. Campana[3], M. Capalbi[4], G. Chincarini[3,5], P. Giommi[4], M. R. Goad[6], J. E. Hill[2], A. Moretti[3], M. Perri[4], P. Romano[3], and G. Tagliaferri[3]

[1]INAF-IASF Pa, Via U. La Malfa 153, 90146 Palermo, Italy
[2]Dep. of Astronomy & Astrophysics, 525 Davey Lab., Pennsylvania State University, University Park, PA 16802, USA
[3]INAF – Osservatorio Astronomico di Brera, Via Bianchi 46, 23807 Merate, Italy
[4]ASI Science Data Center, via Galileo Galilei, 00044 Frascati, Italy
[5]Università degli studi di Milano-Bicocca, Dipartimento di Fisica, Piazza delle Scienze 3, I-20126 Milan, Italy
[6]Department of Physics and Astronomy, University of Leicester, Leicester LE1 7RH, UK

ABSTRACT

We report on the analysis of the X-ray afterglow of GRB050319 and XRF050416A, detected with Swift-BAT and observed with the Swift narrow field instruments 225s and 80s after the burst onset, respectively. The afterglow emission was monitored by the XRT up to 2 months after the burst. The light curves show three different phases characterized by distinct slopes, with a flattening between the two break times. The extrapolation of the BAT light curve to the XRT band suggests that the initial phase of the afterglow may be the low energy tail of the prompt emission, while the next two phases are suggestive of refreshed shocks followed by a standard fireball evolution.

Key words: Gamma rays: burst; X-rays, individual: GRB050319, XRF050416A.

1. THE TWO BURSTS

GRB0950319 was a 150 sec long GRB, with a redshift z=3.24 (Fynbo et al. , 2005). The burst showed a multi-peak structure, with a fluence 1.6×10^{-6} erg cm^{-2} in the 15-350 keV band. The afterglow emission was monitored from 225 sec up to 28 days after the burst. The afterglow shows a very steep initial decay, followed by a flat phase and a further slow decay (see Table 1 and Figure 1). It also shows spectral evolution between the first two phases, as reported in Table 2. A detailed analysis of the afterglow of GRB050319 is reported in Cusumano et al. (2005).

The prompt emission of XRF050416A lasted 2.4 sec, with two distinct peaks and a fluence 3.8×10^{-7} erg cm^{-2} in the 15-350 keV band (Sakamoto et al., 2005). This event is classified as an X-ray flash, as the fluence in the 15.-30. keV band is larger than that in the 30-400 keV band. Cenko & Fox (2005b) report a redshift z=0.65. The afterglow emission was monitored from 76 sec up to 74 days after the burst. It shows a moderately steep initial decay, followed by a flat phase and by a very slow fading (see Table 1 and Figure 1). The spectrum, that shows significant absorption in excess to the Galactic line of sight value, is variable, going from a softer phase, consistent with the BAT slope, to a harder phase (see Table 2 and Figure 2). A detailed analysis of this event is presented in Mangano et al. (2005).

Table 1. Light curve best fit parameters

	GRB050319	XRF050416A
Slope A	5.53 ± 0.67	2.6 ± 0.7
T_{break1}	384 ± 22	170 ± 40
Slope B	0.54 ± 0.04	0.44 ± 0.13
T_{break2}	$(2.6 \pm 0.7) \times 10^4$	1450 ± 20
Slope C	1.14 ± 0.2	0.87 ± 0.2

2. DISCUSSION

The two events show a very similar behaviour, with a light curve characterized by three distinct phases, in agreement with the standard model of the Swift afterglows, presented in Zhang et al. (2005) (see also Nousek et al., 2005; Chincarini et al. , 2005). In both cases, the very good agreement of the XRT phase A data points with the extrapolation at low energy of the BAT fluxes suggests that this phase is the low energy tail of the prompt emission. This seems to be confirmed by the spectral analysis, where the X-ray spectrum evolves from

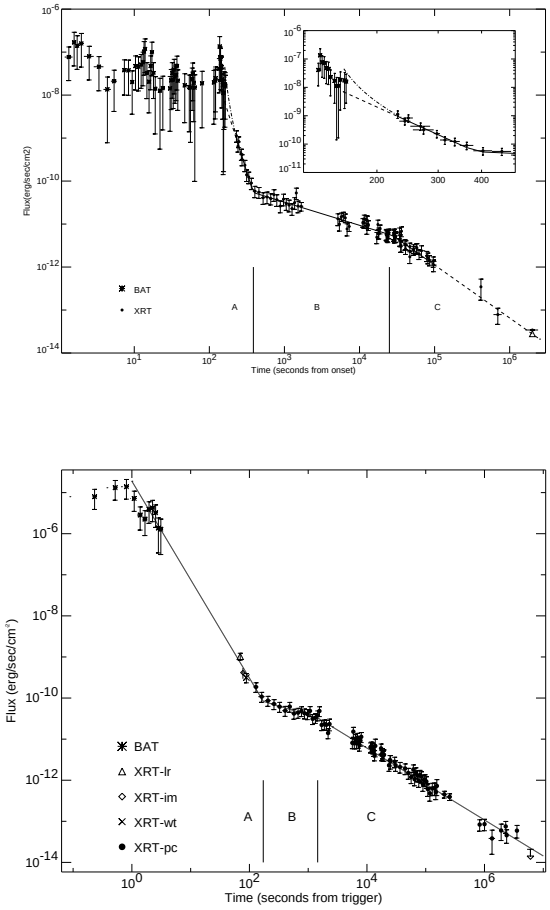

Figure 1. Top panel: GRB050319 light curve in the 0.2-10 keV band. The inset shows the good matching between the XRT and BAT light curves. Bottom panel: XRF050416A light curve in the 0.2-10 keV band. In both cases the BAT data are extrapolated into the XRT band using the best fit parameters derived from the spectral analysis

a steeper phase, with spectral index consistent with the BAT values, to a flatter phase. In this scenario, the flattening after the first break could be interpreted as the injection of additional energy from the central engine (refreshed shock). The last phase is consistent with a standard fireball evolution. The observed phenomenology suggests that XRFs and GRBs may share the same physical origin.

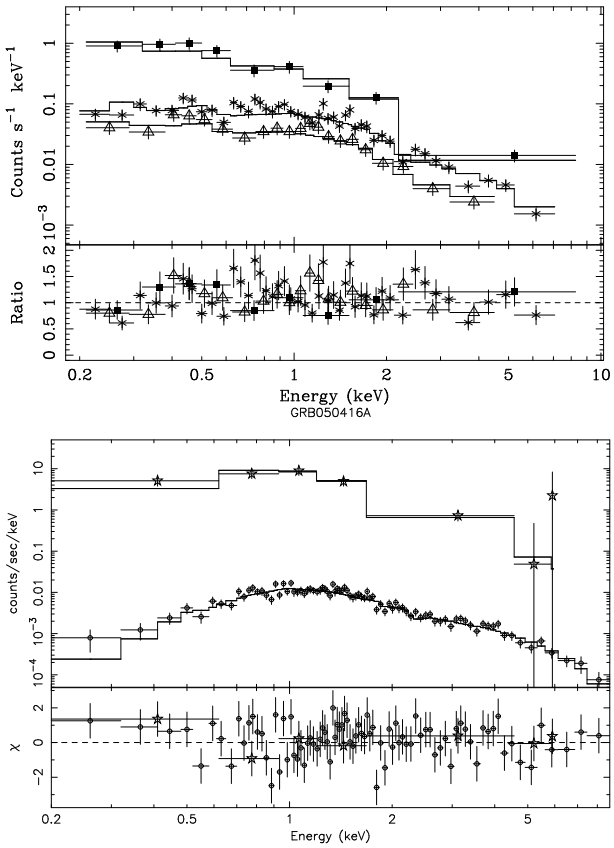

Figure 2. Top panel: GRB050319 XRT spectra and residuals of phases A (squares), B (stars) and C (triangles). Bottom panel: XRF050416A XRT spectra and residuals of phase A (stars) and B+C (circles)

Table 2. Spectrum best fit parameters

		GRB050319		XRF050416A
N_H(Gal.)		1.13×10^{20}		0.21×10^{21}
N_H(Intr.)		...		$(6.8 \pm 1.1) \times 10^{21}$
Γ_{BAT}		2.1 ± 0.2		2.9 ± 0.2
Γ_{XRT}	A	2.60 ± 0.22	A	3.0 ± 0.4
	B	1.69 ± 0.06	B+C	2.04 ± 0.11
	C	1.8 ± 0.08		

REFERENCES

Cenko, S.B., Fox D.B., Gal-Yam A., 2005, GCN 3269

Chincarini G. et al., 2005, ApJ, submitted, astro-ph/0506453

Cusumano G. et al., 2005, ApJ, in press, astro-ph/0509689

Fynbo, J.P.U., et al. 2005, GCN 3136

Mangano V. et al., 2005, in preparation

Nousek J. et al., 2005, ApJ, submitted, astro-ph/0508332

Sakamoto T. et al., 2005, GCN 3273

Zhang B. et al., 2005, ApJ, submitted, astro-ph/0508321

INTEGRAL AND *XMM-NEWTON* OBSERVATIONS OF THE LOW-LUMINOSITY AND X–RAY RICH BURST GRB 040223

S. McBreen[1], S. McGlynn[2], S. Foley[2], B. McBreen[2], and L. Hanlon[2]

[1]Astrophysics Mission Division, RSSD of ESA, ESTEC, Noordwijk, the Netherlands
[2]School of Physics, University College Dublin, Dublin 4, Ireland

ABSTRACT

We present gamma–ray and X–ray analysis of GRB 040223, which was observed by *INTEGRAL* and *XMM-Newton*. GRB 040223 has a peak flux of (1.60 $\pm$0.13) $\times$ 10^{-8} ergs cm^{-2} s^{-1}, a fluence of (4.4 $\pm$ 0.4) $\times$ 10^{-7} ergs cm^{-2} and a steep photon power law index of -2.3 $\pm$ 0.2, in the energy range 20–200 keV. The steep spectrum implies that it is an X–ray rich GRB with emission up to 200 keV and $E_{\rm peak} < 20$ keV. If $E_{\rm peak} < 10$ keV, it would qualify as an X-ray flash with high energy emission. The X-ray afterglow has a spectral index β_x = -1.7 $\pm$ 0.2, a temporal decay of t$^{-0.75\pm0.25}$ and a large column density of 1.8 $\times 10^{22}$ cm^{-2}. The luminosity-lag relationship was used to obtain a redshift $z = 0.10^{+0.04}_{-0.02}$. The isotropic energy radiated in γ–rays and the X–ray luminosity after 10 hours are both orders of magnitude less than classical GRBs. GRB 040223 is consistent with the extrapolation of the Amati relation into the region that includes XRF 030723 and XRF 020903.

Key words: gamma rays: bursts, gamma rays: observations, X–rays.

1. INTRODUCTION

The prompt emission from GRBs and their afterglows give valuable information on the radiation processes and the environment. In addition to GRBs, X–ray flashes (XRF) have been identified as a class of soft bursts that are very similar to GRBs. There seems to be a continuum of spectral properties for XRFs, X–ray rich GRBs and classical GRBs and it is probable that they have a similar origin (Sakamoto et al., 2004).

ESA's International Gamma-Ray Astrophysics Laboratory *INTEGRAL* (Winkler et al., 2003) is composed of two main coded-mask telescopes; an imager IBIS (Ubertini et al., 2003) and a spectrometer SPI (Vedrenne et al., 2003) with a combined energy range of 15 keV to 8 MeV. *INTEGRAL* has detected and localised 32 GRBs so far. The EPIC cameras on *XMM-Newton* (Turner et al., 2001) have been used to obtain X–ray afterglows of 6 of the GRBs. We report here observations of the prompt and afterglow emission from GRB 040223 and a detailed account is given elsewhere (McGlynn et al., 2005).

2. DATA ANALYSIS & RESULTS

GRB 040223 was detected by the INTEGRAL burst alert system IBAS (Mereghetti et al., 2003). The IBIS light curve is given in Fig. 1a and does not include two very weak pulses at about -80 s and -180 s. GRB 040223 is in the long duration class with a well resolved pulse. The IBIS light curve was denoised with a wavelet analysis (Quilligan et al., 2002) and the risetime, fall time and FWHM of the pulse are 19 s, 22 s, and 13 s respectively. The IBIS data was divided into two energy channels i.e. 25–50 keV and 100–300 keV. The cross-correlation analysis (Norris, 2002; Schaefer, 2004) was performed between the two channels and the lag was determined to be 2.2 $\pm$ 0.3 s which is longer than observed from most GRBs.

The IBIS spectral analysis was performed using the standard method (Moran et al., 2005). The IBIS data (20–200 keV) is well fit by a single power law with photon index -2.3 $\pm$ 0.2 with a reduced χ^2 of 1.01 for 20 degrees of freedom (dof). Errors are at the 90% confidence level (Fig. 1b). The peak flux is (1.60 $\pm$0.13)$\times$ 10^{-8} ergs cm^{-2} s^{-1} over the brightest second and the fluence is (4.4 $\pm$ 0.4) $\times$ 10^{-7} ergs cm^{-2}. The spectral results obtained with SPI are consistent with IBIS and γ-ray emission was significantly detected up to 200 keV.

XMM-Newton observed the location of the GRB for 42 ks starting 18 ks after the burst and a fading X–ray source was detected within the IBAS error circle. The temporal decay of the X–ray afterglow ($F_\nu(t) \propto t^{-\delta}$) was fit by a power law with index δ = -0.7 $\pm$ 0.25 by Gendre et al. (2004). Our analysis is consistent with this result. We obtained 3 afterglow spectra from the PN and MOS Cameras (0.2–10 keV) after standard data screening. The

spectra were well fit by a power law $F_\nu \propto \nu^{-\beta_x}$ where the spectral index $\beta_x = -1.7 \pm 0.2$ with reduced χ^2 of 1.29 for 111 dof (Fig. 1c). The absorption column density has a high value of $N_H = 1.8 \times 10^{22}$ cm^{-2}, exceeding the high galactic value in this direction of 6 $\times 10^{21}$cm^{-2}.

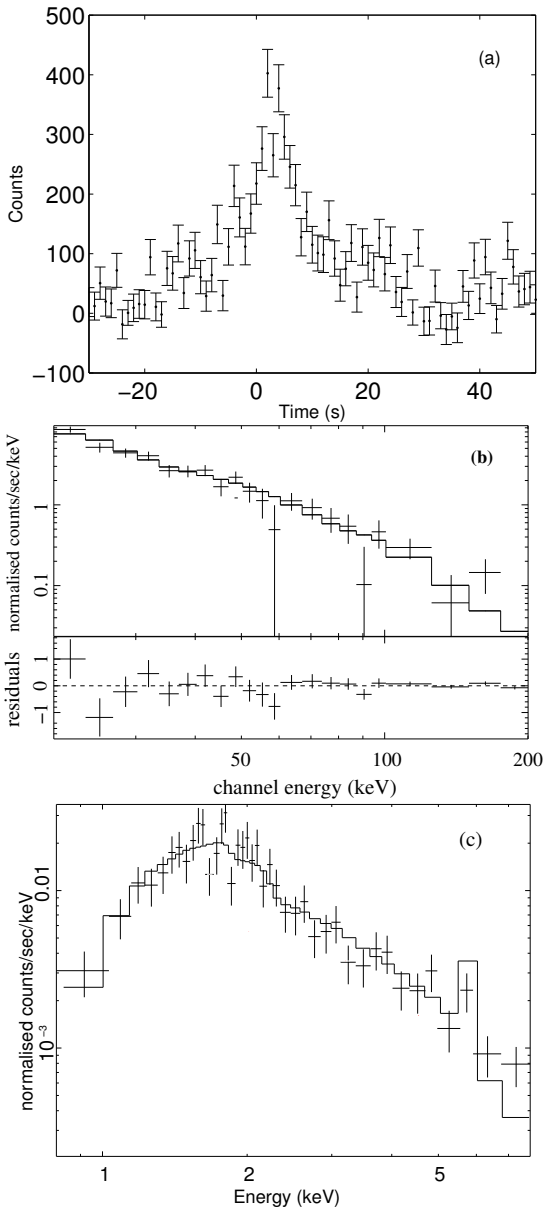

Figure 1. **a)** *IBIS lightcurve of GRB 040223 in the energy range 15–200 keV (zero time is the IBAS trigger at 13:28:10 UTC).* **b)** *IBIS spectrum of GRB 040223 fit by a power law model from 20–200 keV.* **c)** *EPIC spectrum of the GRB 040223 afterglow and its best fit absorbed power law model. The data points shown refer to the PN detector and agree with the MOS data.*

There are no direct measurements of the redshift to GRB 040223 so model dependent distance indicators were used. The luminosity-lag relationship (Norris, 2002) was used to calculate the peak luminosity of $3.8^{+3.8}_{-1.7} \times 10^{47}$ ergs s^{-1} (McGlynn et al., 2005). The redshift to the source is z = $0.10^{+0.04}_{-0.02}$ when the peak flux of (1.60 ± 0.13) $\times$ 10^{-8} ergs cm^{-2} s^{-1} is combined with the peak luminosity. The fluence gives a total isotropic γ–ray luminosity (E_{ISO}) of approximately 10^{49} ergs which is about three orders of magnitude less than classical GRBs. GRB 040223 is sub-luminous in γ–rays by a large factor. Using the Amati relation (Ghirlanda et al., 2004), the value of E_{ISO} is $< 2 \times 10^{50}$ ergs assuming that the rest frame value of E_{peak} is < 20 keV. GRB 040223 lies on or near the extrapolation of the Amati relation from classical GRBs to include XRF 030723 and XRF 020903.

The X–ray flux after 10 hours is $(2.4 \pm 0.4) \times 10^{-13}$ ergs cm^{-2} s^{-1} in the 2-10 keV region. The X–ray luminosity of GRB 040223 is 6×10^{42} ergs s^{-1} and is orders of magnitude fainter than observed from classical GRBs (Bloom et al., 2003). The X–ray and γ–ray luminosities of GRB 040223 and XRF 030723 are very comparable.

REFERENCES

Barraud, C., Olive, J.-F., Lestrade, J. P., et al. 2003, A&A, 400, 1021

Bloom, J. S., Frail, D. A., & Kulkarni, S. R. 2003, ApJ, 594, 674

Gendre B., Piro L., De Pasquale M.[astro-ph/0412302]

Ghirlanda, G., Ghisellini, G., & Lazzati, D. 2004, ApJ, 616, 331

McGlynn, S., McBreen, S., Hanlon, L., et al. 2005, [astro-ph/0505349]

Mereghetti, S., Götz, D., Borkowski, J., Walter, R., & Pedersen, H. 2003, A&A, 411, L291

Moran, L., Mereghetti, S., Götz, D., et al. 2005, A&A, 432, 467

Norris, J. P. 2002, ApJ, 579, 386

Quilligan, F., McBreen, B., Hanlon, L., et al. 2002, A&A, 385, 377

Sakamoto, T., Lamb, D. Q., Graziani, C., et al. 2004, ApJ, 602, 875

Schaefer, B. E. 2004, ApJ, 602, 306

Turner, M. J. L., Abbey, A., Arnaud, M., et al. 2001, A&A, 365, L27

Ubertini, P., Lebrun, F., Di Cocco, G., et al. 2003, A&A, 411, L131

Vedrenne, G., Roques J. P., Schönfelder V. et al. A&A, 441, L63

Winkler, C., Courvoisier, T. J.-L., Di Cocco, G., et al. 2003, A&A, 411, L1